

The Pennsylvania State University

The Graduate School

Department of Materials Science and Engineering

**FERROELECTRIC POLYMER THIN FILMS
WITH HIGH ENERGY DENSITY AND LOW LOSS**

A Dissertation in

Materials Science and Engineering

by

Paisan Khanchaitit

© 2012 Paisan Khanchaitit

Submitted in Partial Fulfillment
of the Requirements
for the Degree of

Doctor of Philosophy

May 2012

The Dissertation of Paisan Khanchaitit was reviewed and approved* by the following:

Qing Wang
Associate Professor of Materials Science and Engineering
Dissertation Advisor
Chair of Committee

Evangelos Manias
Professor of Materials Science and Engineering

Qiming Zhang
Distinguished Professor of Electrical Engineering and Materials Science
and Engineering

Michael Lanagan
Professor of Engineering Science and Mechanics

Joan Redwing
Professor of Materials Science and Engineering
Chair, Intercollege Graduate Degree Program in Materials Science and
Engineering

*Signatures are on file in the Graduate School

ABSTRACT

Dielectric materials with large electric energy density are actively pursued for many applications. Among commercially available polymer capacitor film, poly(vinylidene fluoride chlorotrifluoroethylene) P(VDF-CTFE) stands out due to its excellent capability to store electrical energy with relatively high efficiency. In this dissertation, we employed crosslinking approaches to improve energy density of the copolymer by concurrently reducing loss, enhancing permittivity, and improving breakdown strength of the copolymer. The fundamental idea of this effort is to introduce covalent bonding between the polymer chains to confine and destabilize the formation of ferroelectric domain. By carefully controlling of the process conditions and varying the polymer/crosslinking agents feeding ratios the copolymer structures were systematically tuned for optimized dielectric and electrical properties. The crosslinking method leads to the copolymer film with impressive 64% decreased of total loss, 24% improvement of polarization level (under 250 MV/m field) and 70 % improvement of breakdown strength compared to the pristine. All of above improvements have been synergized and consequently 315 % enhancement of energy density can be achieved in the crosslinked copolymers.

Table of Content

LIST OF FIGURES	vi
LIST OF TABLES	xi
LIST OF EQUATIONS	
ACKNOWLEDGEMENTS	xii
Chapter 1 Introduction	1
1.1 Research Theme	1
1.2 Capacitor Fundamentals	2
1.3 Polymer capacitors	13
1.4 Structure and Polymorphs of PVDF	18
1.4.1 Amorphous regions (disorder phase).....	19
1.4.2 Crystalline Phase of PVDF.....	21
1.5 Polarization Mechanism in Ferroelectric PVDF	24
1.6 Research Motivations and Goals	27
Chapter 2 Crosslinking of P(VDF-CTFE) with peroxides	32
2.1 Background.....	33
2.2 Peroxide crosslinking of PVDF-based copolymers.....	35
2.3 Experimental Procedure	40
a. Materials Fabrication	40
b. Characterization	41
2.4 Structural Analysis	43
a. Sol-gel Analysis	43
b. Fourier Transform Infrared Spectroscopy Analysis	45
c. X-rays diffraction analysis.....	47
d. DSC Analysis.....	54
2.5 Dielectric Characterization.....	56
a. Weak-Field Dielectric Properties.....	56
b. High Field Electric Displacement.....	61
2.6 Conductivity and Activation Energy	79
2.7 Thermally stimulated depolarization current (TSDC).....	82
2.8 Electrical Breakdown Strength.....	85

2.9 Mechanical Properties	91
Chapter 3 Thermally Processable crosslinking of P(VDF-CTFE)	96
a. Materials Fabrication	99
b. Characterization	101
a. Sol-gel analysis	102
b. Fourier Transform Infrared Spectroscopy Analysis	104
c. X-rays diffraction analysis	105
Chapter 4 Conclusions and Future Work.....	120
Appendix A Storage Energy Density of Pristine and crosslinked P(VDF-CTFE) copolymer	125
Appendix B Dielectric spectra of Pristine and crosslinked P(VDF-CTFE) copolymer	126
REFERENCES	127

LIST OF FIGURES

Figure 1 Ragone plot of energy storage technologies. [1]	2
Figure 2 (a) Empty capacitor, (b) polarization of dielectric and (c) capacitor filled with dielectric	3
Figure 3 Frequency dependence of the real and imaginary parts of the complex permittivity.	6
Figure 4 Schematic diagram of electric displacement versus electric field for (a) linear, (b) ferroelectric, and (c) antiferroelectric materials (shaded area represents energy density).	10
Figure 5 Schematic representation of unipolar electric displacement-electric field (D-E) hysteresis loops.....	13
Figure 6 Polymer capacitor.....	14
Figure 7 Different types of polarization as a function of frequency in polymers.	15
Figure 8 A polymer chain containing polar groups with (a) no applied field and (b) in the presence of an applied field	16
Figure 9 Temperature dependences of (a) the hysteresis electric displacement versus electric field (D-E loops) measured under 1/300 Hz triangular load and (b) the polarization current density versus electric field of as-prepared PVDF film[18].....	20
Figure 10 – Crystal phases of α , δ , γ and β forms of PVDF. [12, 19]	23
Figure 11 PVDF crystal phases processing routes. [19]	24
Figure 12 Schematic illustration of an electrically poled ferroelectric PVDF crystal sandwiched between two amorphous layers. The chain direction in the lamellar is perpendicular to the dipole moment or external electric field	27
Figure 13 Unipolar D-E loop of P(VDF-CTFE)(15 wt.% CTFE) at under application of (a) weak , (b) strong electric field. (c) and (d) represent the	

polarization mechanisms of PVDF-based polymer segment under weak and strong electric field respectively.....	30
Figure 14 Half-life of Vulcup® versus temperature in various polymers.	37
Figure 15 Schematic representation of probable crosslinking reaction mechanisms of the system proposed in this dissertation.	39
Figure 16 Hot-pressing process conditions for fabricating crosslinked P(VDF-CTFE) films using 1,4-bis(t-butyl peroxy) diisopropylbenzene (Vulcup®) triallylisocyanurate (TAIC)	41
Figure 17 Gel contents and average molecular weight between crosslinking sites as determined using Flory-Rehner swelling theories versus Vulcup® concentration with 1 wt.% TAIC (black) and 3wt.% TAIC (red).	44
Figure 18 ATR-FTIR spectra (top) and: tttt/tgtg ² fractions (bottom) of pristine and crosslinked P(VDF-CTFE) with different Vulcup® concentration (3wt.% TAIC).....	46
Figure 19 XRD patterns of pristine and crosslinked P(VDF-CTFE) using Vulcup® at 3 % wt. TAIC	49
Figure 20 Crystallinity versus Vulcup® concentration at 3 % wt. TAIC, determined by XRD patterns	50
Figure 21 α phase fraction versus the Vulcup® concentration at 3 % wt. TAIC.	50
Figure 22 Crystallinity and crystal size in (020) α and (110) α crystallographic planes versus average molecular weight between crosslinks, M_c	51
Figure 23 Crystal sizes of α phase crystals in all four crystallographic planes versus the Vulcup® concentration at 3 % wt. TAIC.	53
Figure 24 The α phase contents versus the Vulcup® concentration at 3 % wt. TAIC.	54
Figure 25 DSC thermographs of pristine and crosslinked P(VDF-CTFE). These DSC traces were collected with two (first (left) and second (right)) heating (top) and cooling (bottom) cycles with a ramp of 10 °C/min.....	56

Figure 26 Permittivity and dielectric losses ($\tan(\delta)$) versus frequency measured at 25 °C for pristine and crosslinked P(VDF-CTFE).	58
Figure 27 (a) Dielectric permittivity (ϵ') and of the dielectric losses ($\tan(\delta) = \epsilon''/\epsilon'$) versus temperature, at 100 Hz weak field with heating ramp of 10 °C/min, for the pristine and crosslinked P(VDF-CTFE).	59
Figure 28 Dielectric permittivity of the crosslinked P(VDF-CTFE) with 3 wt. % Vulcup® +3 wt. %TAIC compared to the pristine. The heating curves are assigned as closed symbols while the cooling as opened symbols.....	60
Figure 29 Electric displacement of pristine P(VDF-CTFE) under unipolar triangle load at 10 Hz.....	63
Figure 30 Electric displacement in crosslinked P(VDF-CTFE) using 1 wt. % Vulcup + 3 wt.% TAIC at 10 Hz.	63
Figure 31 Electric displacement in crosslinked P(VDF-CTFE) using 3 wt. % Vulcup + 3 wt.% TAIC at 10 Hz.	64
Figure 32 Electric displacement in crosslinked P(VDF-CTFE) using 5 wt. % Vulcup + 3 wt.% TAIC at 10 Hz.	64
Figure 33 A comparison of displacement-electric filed loops of pristine and crosslinked P(VDF-CTFE). The measurement was taken at 25 °C with a 10 Hz triangular unipolar signal with the maximum electric field of 250 MV/m.	65
Figure 34 Dielectric displacement at maximum load versus concentration of Vulcup® at 3 wt.% TAIC.....	68
Figure 35 Remnant displacement versus concentration of Vulcup® at 3 wt.% TAIC.....	68
Figure 36 Ration between Remnant displacement and displacement at maximum load versus concentration of Vulcup® at 3 wt.% TAIC.....	69
Figure 37 Electric field dependence of (top) discharge energy density and (bottom) energy loss of pristine and crosslinked P(VDF-CTFE) copolymers.	73
Figure 38 Bipolar D-E hysteresis loops of pristine and 3 wt.% Vulcup® + 3 wt.% TAIC crosslinked (PVDF-CTFE).....	76

Figure 39 Coercive Field versus the maximum electric field of pristine and 3 wt.% Vulcup [®] + 3 wt.% TAIC crosslinked (PVDF-CTFE).....	77
Figure 40 Energy loss of pristine and crosslinked P(VDF-CTFE) copolymers at 50°C and 70 °C	78
Figure 41 DC conductivity versus time of crosslinked and pristine P(VDF-CTFE) under different applied field at 25 °C.	80
Figure 42 Arrhenius plots of pristine and 3 wt.% Vulcup [®] + 3 wt.% TAIC crosslinked (PVDF-CTFE).....	81
Figure 43 Schematic of TSDC measurement technique	83
Figure 44 TSDC curves for pristine and 3 wt.% Vulcup [®] + 3wt. % TAIC crosslinked (PVDF-CTFE).....	84
Figure 45 Dielectric breakdown of high energy radiation crosslinked polyethylene [46].....	88
Figure 46 The Weibull analysis of breakdown strengths for the pristine and crosslinked P(VDF-CTFE).....	89
Figure 47 Storage moduli of the pristine and 3 wt.% Vulcup [®] + 3 wt.% TAIC crosslinked (PVDF-CTFE).....	94
Figure 48 Decomposition mechanism of 2,3-dimethyl-2,3-diphenylbutane (bicumene)	99
Figure 49 Hot-pressing process conditions for fabricating crosslinked P(VDF-CTFE) films using 1,4-bis(t-butyl peroxy) diisopropylbenzene (Vulcup [®]) triallylisocyanurate (TAIC)	101
Figure 50 Gel contents and average molecular between crosslinking sites as determined using Flory-Rehner swelling theories versus bicumene concentration with 1 wt. % TAIC (black), 3wt. % TAIC (red), and 5 wt.% TAIC (green).	103
Figure 51 ATR-FTIR spectra of pristine and crosslinked P(VDF-CTFE) with different bicumene concentration (3wt/% TAIC).....	104

Figure 52 XRD patterns of pristine and crosslinked P(VDF-CTFE) using bicumene at 3 % wt. TAIC.	106
Figure 53 Crystallinity versus bicumene concentration at 3 % wt. TAIC.	106
Figure 54 Crystal sizes of α phase crystals in all four crystallographic planes versus the bicumene concentration at 3 % wt. TAIC.	107
Figure 55 Permittivity and dielectric losses ($\tan(\delta)$) versus frequency measured at 25 °C for pristine and crosslinked P(VDF-CTFE) by bicumene and TAIC.	109
Figure 56 Electric displacement in crosslinked P(VDF-CTFE) using 1 wt. % Bicumyl + 3 wt.% TAIC at 10 Hz.	111
Figure 57 Electric displacement in crosslinked P(VDF-CTFE) using 3 wt. % Bicumene + 3 wt.% TAIC at 10 Hz.	111
Figure 58 Electric displacement in crosslinked P(VDF-CTFE) using 5 wt. % Bicumene + 3 wt.% TAIC at 10 Hz.	112
Figure 59 A comparison of displacement-electric field loops of pristine and bicumene crosslinked P(VDF-CTFE). The measurement was taken at 25 °C with a 10 Hz triangular unipolar signal with the maximum electric field of 250 MV/m.	113
Figure 60 Dielectric displacement at maximum load versus concentration of bicumene at 3 wt.% TAIC.	114
Figure 61 Remnant displacement versus concentration of bicumene at 3 wt.% TAIC.	114
Figure 62 Electric field dependence of discharge energy density and of pristine and bicumene crosslinked P(VDF-CTFE) copolymers.	116
Figure 63 Energy loss of pristine and bicumene crosslinked P(VDF-CTFE) copolymers.	117
Figure 64 The Weibull analysis of breakdown strengths for the pristine and bicumene crosslinked P(VDF-CTFE).	118

LIST OF TABLES

Table 1 Permittivity of some common polymers	16
Table 2 Weibull parameters of the pristine and crosslinked P(VDF-CTFE).....	90
Table 3 Predicted breakdown strength values from electromechanical breakdown model and measured values of the pristine and 3 wt.% Vulcup [®] + 3 wt.% TAIC crosslinked (PVDF-CTFE).....	95
Table 4 Weibull parameters of the pristine and bicumene crosslinked P(VDF-CTFE)	119

ACKNOWLEDGEMENTS

I would like to thank my advisor, Professor Qing Wang, for serving as my advisor and guiding me into the right direction. I also want to thank my group members Dr. Jason Claude, Dr. Kun Li, Dr. Yingying Lu, Dr. Bret Neese, Dr. Kui Xu, Dr. Jeishu Jin, Prof. Luis E. Norena-Franco, Siwei Liang,, Jilian Pan, Chalathorn (Jess) Chanthad, Ruixuan Han, Sunanta Nim Chuayprakong, Junjun Li, Matthew Robert Gadinski, Kuo Han and Wuttichai Reainthippayasakul for all their help in creating materials, characterizing them, and the helpful discussions for this dissertation. I also want to thank my committee members Professors Qiming Zhang, Mike Lanagan, and Evangelos Manias who will be the final judges of my worthiness for this degree.

I definitely thanks to my parents, who always believe in his son.

Chapter 1

Introduction

1.1 Research Theme

The ability to store electrical energy is essential in many applications. Many different physical phenomena can be used to obtain a charge storing effects. Capacitors, for example, are based on the hysteresis of charging and discharging of materials. A downside of this capacitor technology is that the energy stored in the device tends to lower than other class of energy storage devices. In power applications, polymers are often the materials of choice for many reasons including low cost and ease of manufacturing. However, the demands for increased performance from polymer dielectrics have prompted recent research into searching for new polymers. For power applications, the ideal dielectric material must have a high power and energy density, low electrical loss, and good reliability. A Ragone plot illustrating the various energy storage technologies is shown in *Figure 1*. Even though high speed charging-discharging of capacitors is extremely useful, low energy density such as this (about 1 J/cm³ for most of the commercially available polymers) is unsuitable for many applications.

The theme to the research presented here is to explore new polymer dielectrics with potential energy densities an order of magnitude higher than the current state of the art. Such an increase in energy density would make polymers more competitive in some applications.

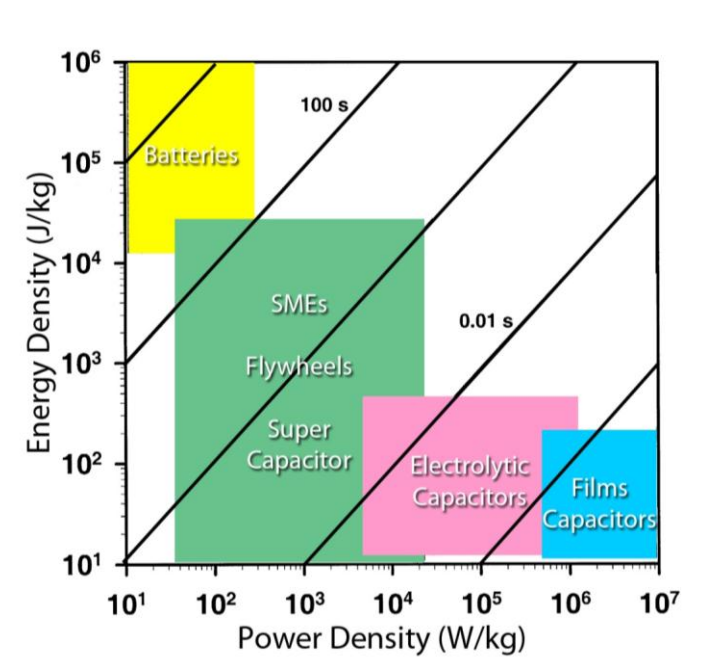


Figure 1 Ragone plot of energy storage technologies. [1]

1.2 Capacitor Fundamentals

A capacitor consists of two parallel conducting plates of area A separated by a dielectric thickness d . Applying a voltage V across the capacitor produces a charge Q on each plate. This charge is characteristic of charge storing ability of the dielectric and is quantified by capacitance, defined as

$$C = \frac{q}{v}$$

Equation 1

In vacuum (or free space), the capacitance C_0 is defined in terms of area and spacing between plate as $C_0 = \epsilon_0 \frac{A}{d}$. (ϵ_0 is the free space permittivity = 8.85×10^{-12} F/m). The electric field polarizes the dielectric, and the resulting surface charge density P on the dielectric produces an internal electric field that opposes the applied field, and also partly compensates the charge in the conducting plate. At the same voltage V more charge will be stored in the material, increasing capacitance to $C = \epsilon \frac{A}{d}$.

The relative permittivity is the factor most often used to describe the increasing of capacitance, charge, and stored energy compared to a free space and can be defined as

$$\epsilon_r = \frac{\epsilon}{\epsilon_0} = \frac{C}{C_0} = \frac{Q}{Q_0}$$

Equation 2

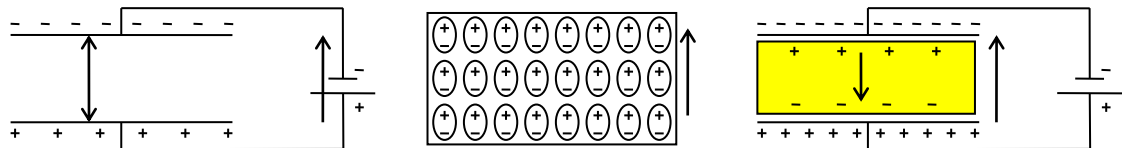


Figure 2 (a) Empty capacitor, (b) polarization of dielectric and (c) capacitor filled with dielectric

Under a bias, the dielectric experiences a polarization that decreases the applied electric field across the material. To compensate for the polarization, more charge accumulates on the electrodes until the circuit is balanced. Since the surface charge on

the dielectric equals to the increase in charge from both plates, $PA = Q' - Q = C'V - CV = CV(\epsilon_r - 1)$, the polarization \mathbf{P} can be expressed by substitute $C = \epsilon_0 A/d$ and $\mathbf{E} = V/d$:

$$\mathbf{P} = \epsilon_0 \mathbf{E}(\epsilon_r - 1) \quad \text{Equation 3}$$

The In macroscopic perspective, the electric displacement vector, \mathbf{D} , is defined as the sum of electric field in vacuum ($\epsilon_0 \mathbf{E}$) and the polarization of the dielectric material (\mathbf{P}).

$$\mathbf{D} = \epsilon_0 \mathbf{E} + \mathbf{P} = \epsilon_0 \epsilon_r \mathbf{E} \quad \text{Equation 4.}$$

Permittivity of a material is not a constant. It is a function of the magnitude and frequency of the applied electric field. Under alternating current (AC) conditions, capacitors serve to block direct currents but transmit alternating currents and offer a frequency dependence to their passage of alternating current. From

Equation 3, for an applying alternating electric field, $\mathbf{E} = \mathbf{E}_0 e^{-i\omega t}$, the alternating polarization is then produced.

$$\mathbf{P} = \epsilon_0 (\epsilon_r - 1) \mathbf{E}_0 e^{-i\omega t} \quad \text{Equation 5}$$

In the intermediate frequency region, according to Debye's model of orientational polarization, the polarization at time= t after application of the electric field is $\mathbf{P}(t) =$

$\mathbf{P}_0(1 - \exp(-t/\tau_r))$, where \mathbf{P}_0 is the equilibrium polarization for a given field and τ_r is the relaxation time. The Debye analysis can be used to predict the frequency-dependent permittivity resulting from polarization:

$$\varepsilon(\omega) = \frac{\varepsilon(0)}{1 - i\omega\tau_r} = \varepsilon' + i\varepsilon''$$

Equation 6 - Debye analysis of frequency-dependent permittivity. Where $\varepsilon(\omega)$ is the frequency-dependent contribution to the permittivity resulting from orientational polarization and $\varepsilon(0)$ is the DC ($\omega=0$) contribution.

From *Equation 6*, the $\varepsilon(\omega)$ is also known as complex permittivity, ε' is the real part of the complex permittivity, and ε'' is the imaginary part of the complex permittivity. The real part, or ε' , is traditionally referred to known as the dielectric constant and has been defined as the permittivity (ε) so far and will continue to be referred to as such. The dielectric constant is defined by the real part of the permittivity measured at relatively low frequency and electric field where this quantity has little variation. The imaginary part of the permittivity, ε'' , is related to the loss in the dielectric and will be discussed later. Both real and imaginary parts of the complex permittivity can be expressed in terms of relaxation time and frequency by *Equation 7*. Plotting of real and imaginary parts against frequency of the applied field are represented in Figure 3.

$$\varepsilon' = \frac{\varepsilon(0)}{1 + \omega^2\tau_r^2} \text{ and } \varepsilon'' = \frac{\varepsilon(0)}{1 + \omega^2\tau_r^2} \omega\tau_r$$

Equation 7 - Real and imaginary parts of the complex permittivity as a function of relaxation time and frequency.

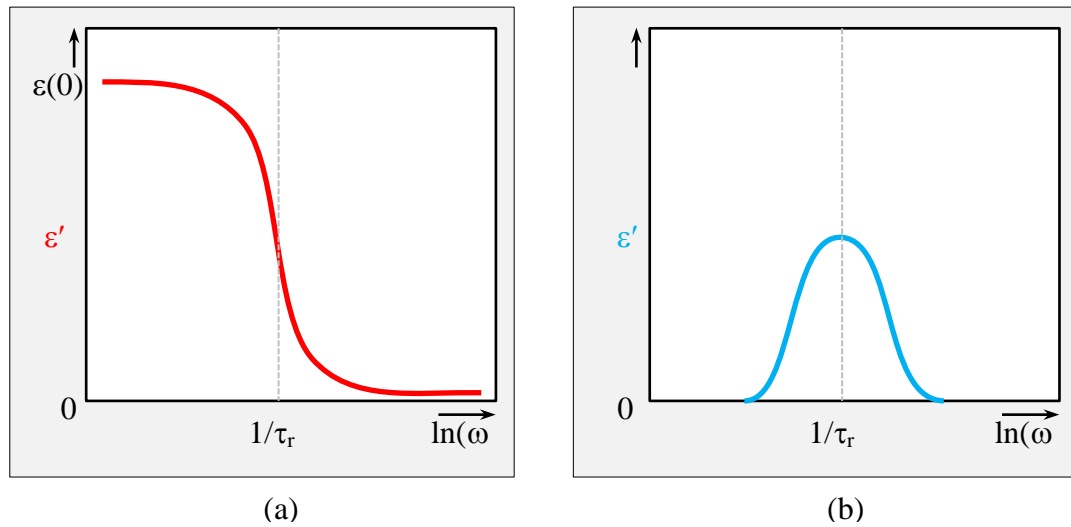


Figure 3 Frequency dependence of the real and imaginary parts of the complex permittivity.

As shown in Figure 3, the real part decreases gradually with increasing frequency from the DC static value $\varepsilon(0)$ to zero. The imaginary part is equal to zero when the applied frequencies are very low and very high but ε'' increase rapidly to a maximum value at frequency equal to $1/\tau_r$. This frequency region, where the dielectric has loss, the electrical energy dissipated in the other forms.

In dielectrics, there are five microscopic mechanisms of polarization: electronic, ionic, orientational (dipolar), ferroelectric, and interfacial. [2-4] Electronic polarization is

present in all materials and originates from the distortion of the electron cloud and nucleus at atomic level. Under an applied electric field, the electron cloud and nucleus are separated from their equilibrium position creating the displacement and therefore polarization. Ionic polarization is present in ionic materials. This polarization mechanism originates from the displacement of positive and negative ions from their equilibrium positions under bias. Dipolar polarization originates from the rotation of permanent dipoles usually present in organic materials under electrical bias. Ferroelectric polarization is unique to ferroelectric materials which have crystals with permanent dipoles. Under bias, polarization can originate from either ferroelectric domain wall motion in the crystals or rotation of the crystals themselves depending on the material. Finally, interfacial polarization originates from the long range motion of charged species that accumulate at interfaces in the materials such as crystalline-amorphous, grain, and phase boundaries. The total permittivity is then the combinations of these individual contributions of polarizations. Each mechanism plays different roles depending on the nature of the materials. More details on polarization response of polymer will be discussed later in this chapter.

From *Equation 5*, in a perfect capacitor where the polarization responds in phase to the applied electric field, the current density is the required charge flow in order to change the charge density P and can be defined as

$$J = \frac{dP}{dt} = -i\omega\epsilon_0(\epsilon - 1)E_0e^{-i\omega t}$$

Equation 8 - Current density in an ideal capacitor under AC applied field.

Therefore the conductivity of an ideal capacitor can be expressed by:

$$\frac{J}{E} = -i\omega\varepsilon_0(\varepsilon - 1)$$

Equation 9 - Conductivity of an ideal capacitor.

For an ideal capacitor, the current leads the field by $\pi/2$. Therefore there is no energy loss in the dielectric since the integration of the product J and E over one period is always equal to zero. This means the energy flows into and out of the dielectric reversibly. Therefore the ideal capacitor has only the real part. However, in a real dielectric, the polarization cannot remain in phase with rapidly changing in electric field. As the frequency of the field is increased the polarization will get lag, and the current will no longer $\pi/2$ out of phase with the applied field. Thus, in a real dielectric, the permittivity will eventually have an imaginary part. There is always a power loss in a real dielectric since the integration of the power, product J and E, over a cycle will not equal to zero. As the frequency of the field is increased, each polarization mechanism drops out as the frequency passes the response time of that mechanism. Eventually at high enough frequencies, all of the polarization mechanisms drop out and have no contribution to the permittivity with the capacitor behaving as though it was empty.

The loss in capacitor is usually reported as the loss tangent.

$$\tan\delta = \frac{\varepsilon''}{\varepsilon'}$$

Equation 10 – Loss tangent. Where the angle δ represents the lag angle between electric displacement and electric field.

In order to develop capacitors, volumetric efficiency and energy density are used as crucial parameters. The volumetric efficiency is usually used for filter capacitors and the energy density is for storage and pulse capacitors. The capacitance is divided by the dielectric volume. $(Vol)_d$ to give volumetric efficiency as shown in *Equation 11*.

$$\frac{C}{(Vol)_d} = \frac{\epsilon_0 \epsilon_r}{d^2}$$

Equation 11 – Definition of volumetric efficiency.

When considering a normal linear dielectric where electric displacement has a linear relationship with electric field as seen in *Figure 4(a)*, the stored energy density is equal to the area of shaded region and is defined as the energy per unit volume stored in capacitor, given by

$$U_e = \int E dD = \frac{1}{2} \epsilon_0 \epsilon_r E^2$$

Equation 12 - Definition of Energy density. Where electric field $E = V/d$.

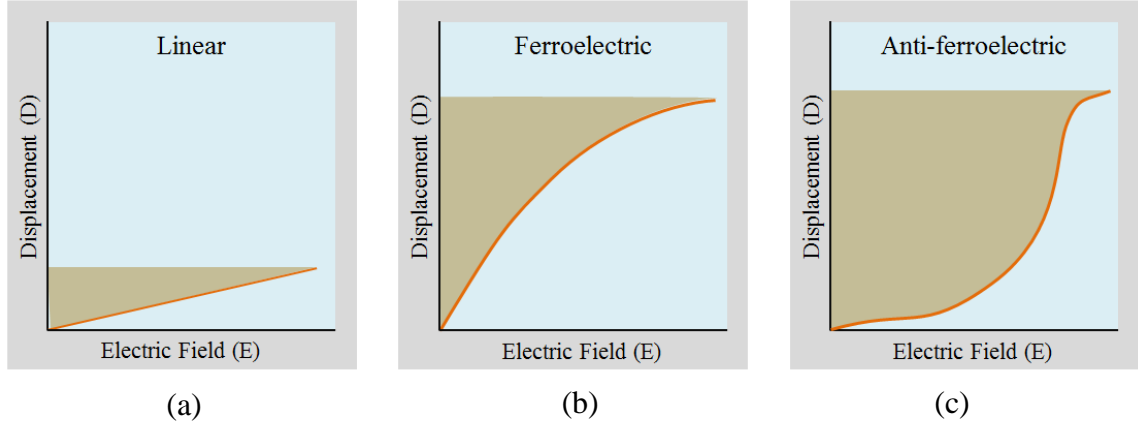


Figure 4 Schematic diagram of electric displacement versus electric field for (a) linear, (b) ferroelectric, and (c) antiferroelectric materials (shaded area represents energy density).

Electrical energy density is an extremely important parameter for a dielectric material using in capacitor because this parameter is a key to enable a reduction in capacitor size and weight which is critical for utilize in advancing technologies. The energy density is dependent on the permittivity of the dielectric and the applied electric field to the material. The applied electric field is limited by the electrical breakdown strength of the dielectric or the maximum field that can be applied before catastrophic degradation occurs. Since the energy density is proportional to the square of the electric field, any increase in this value leads to substantial increases in the energy density more so than an increase in permittivity. The electrical breakdown mechanisms of polymers have been wildly studied and found to relate to their thermal, mechanical, electrical, and microstructural properties. Linear dielectrics usually have low permittivity, which limits energy density capability. They, however, usually have a low dielectric loss which is

also necessary. For ferroelectric materials, the electric displacement is not a linear dependent on electric field as seen in *Figure 4(b)*. In contrast, ferroelectric materials typically have a high permittivity compared to linear dielectrics due to the ferroelectric polarization mechanism, which leads to large energy density. However, at high field the polarization is always suffered by saturation therefore subsequent increases in electric field will not influence in large increases in energy density. Another limit when compared with linear dielectrics is that ferroelectrics often have higher dielectric losses, especially at high frequencies, associated with slow response polarization. Anti-ferroelectric materials, *Figure 4(c)*, contain unit cells whose polarity points in opposite directions for adjacent atomic units resulting in zero net polarity. At low electric field, the low polarity leads to low permittivity. However, antiferroelectric materials possess a unique polarization behavior at a critical electric field where the polarization units experience switching and align in the direction of the field. The switching creates large increases in polarity at this field. This behavior allows the polarization to shift the saturation that may occur to a higher electrical field, resulting in larger energy densities.

In practice, a vital characteristic of dielectrics for electrical energy storage is energy losses associated with the charging and discharging of the capacitor. As mentioned above, loss of a dielectric contributes only to the imaginary part of the permittivity. Dipole relaxation under low applied field is often studied by broadband dielectric spectroscopy (e.g. see *Figure 7*). [3, 5]. At high electric fields (e.g., >30 MV/m), nearly all types of crystalline dipoles in polymers start to respond to the external field. With increasing in the electric field, the dipole relaxation will become faster and more crystalline dipoles can be polarized. Nonetheless, high-field dielectric spectroscopy

has not been widely used to characterize the dielectric loss upon charging/discharging cycle. Instead, dielectric behavior of polymers can be characterized by analyzing the electric displacement-electric field (D-E) hysteresis loop as shown in **Figure 5**. The loops are often hysteresis in the displacement upon charging and discharging. Integration of the electric field with respect to electric displacement can be performed for both the charging and discharging cycles to calculate the stored energy (U_{charge}) and released energy ($U_{\text{discharge}}$). The energy loss is calculated as a different between U_{charge} and $U_{\text{discharge}}$.

$$\text{Energy loss} = \int_0^{D_{\max}} E dD - \int_{D_{\max}}^{D_r} E dD = U_{\text{Charge}} - U_{\text{Discharge}}$$

Equation 13 – Dielectric energy loss, where D_{\max} is the electric displacement at maximum applied electric field and D_r is the remnant displacement.

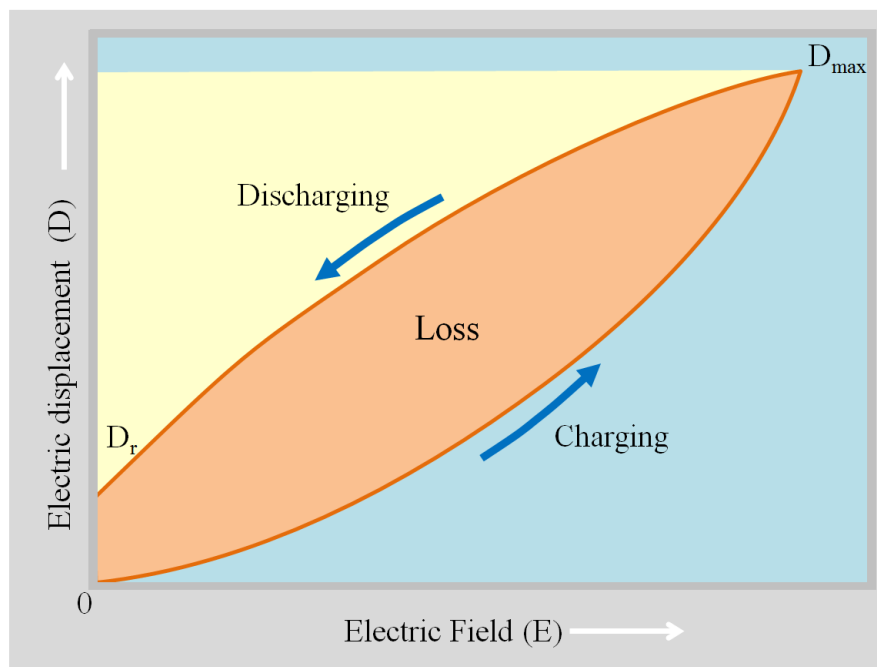


Figure 5 Schematic representation of unipolar electric displacement-electric field (D-E) hysteresis loops.

The energy losses associated with charging and discharging cycles of a dielectric originate from two main sources: conduction and dielectric losses. Energy loss due to conduction is occurred when small amount of charge carrier transports under applied electric field in the material causing conduction current. A portion of the electrical energy is not stored and can be dissipated into heat through Joule heating. Conduction loss can often be found at low frequency of the applied field. Dielectric energy losses resulted by orientational polarization and ferroelectric hysteresis of the dipoles. Upon apply and release electric field, the hysteresis from the orientation and de-orientation of polar species may occur in the dielectric due to phase lagging. The same manner can be found for the crystalline phase transformation between polar and non-polar phase in ferroelectric materials.

1.3 Polymer capacitors

Polymer capacitors are all found in dielectric thin film forms. Polymer thin film dielectrics are often more attractive than other materials for energy storage application due to their inherent high breakdown strength, flexible, light weight, self-healing capabilities and low cost.[6-10]. The polymer dielectric thin films are normally fabricated by extrusion, solution casting, or evaporation deposition. In most case the thickness of dielectric polymers using in capacitor is less than 10 microns. Polymer

capacitors are constructed in a parallel plate configuration with metal electrodes in contact with the dielectric. Evaporated aluminum is often the metal of choice, though metal foils or other evaporated or sputtered metals are also used. Since polymers are very flexible, they are typically rolled into cylinder configurations in actual devices.

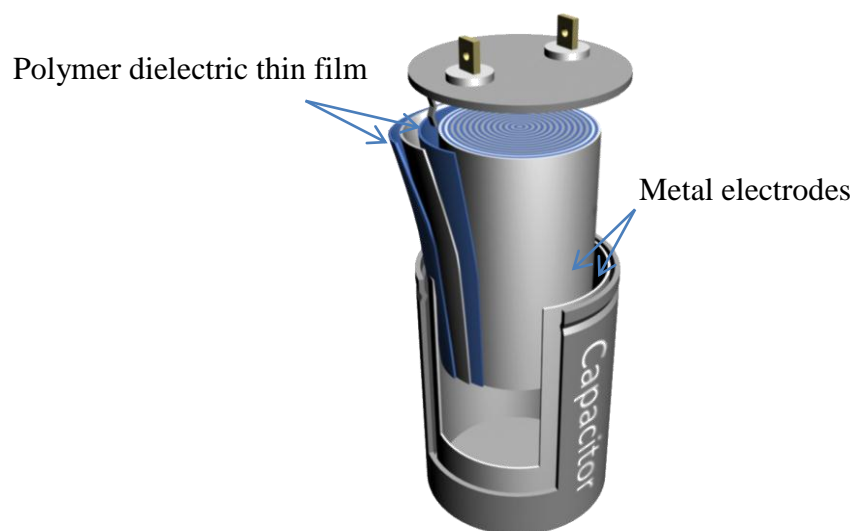


Figure 6 Polymer capacitor.

Permittivity of polymer is relatively low compared to the ceramic counterparts. As mentioned earlier, polymers also have five polarization mechanisms, i.e., electronic, atomic, orientational, ionic, and interfacial, as shown in **Figure 7**. Electronic and atomic polarizations in polymer originate from electron cloud and skeletal atom movements distorted away from the equilibrium position induced by an external field, and thus they occur at very high frequencies, i.e., in the infrared and optical range. These two types of polarization exist in all polymers, no matter they are polar or nonpolar, amorphous or

crystalline. These two types of polarization mechanism are predominated in typical non-polar polymers. For example in polypropylene, the dipole moment of the methyl group is very low , 0.4 Debye [11], therefore very small total polarization under electric field is expected. The most common polymers used as a dielectric layer are listed Table 1.

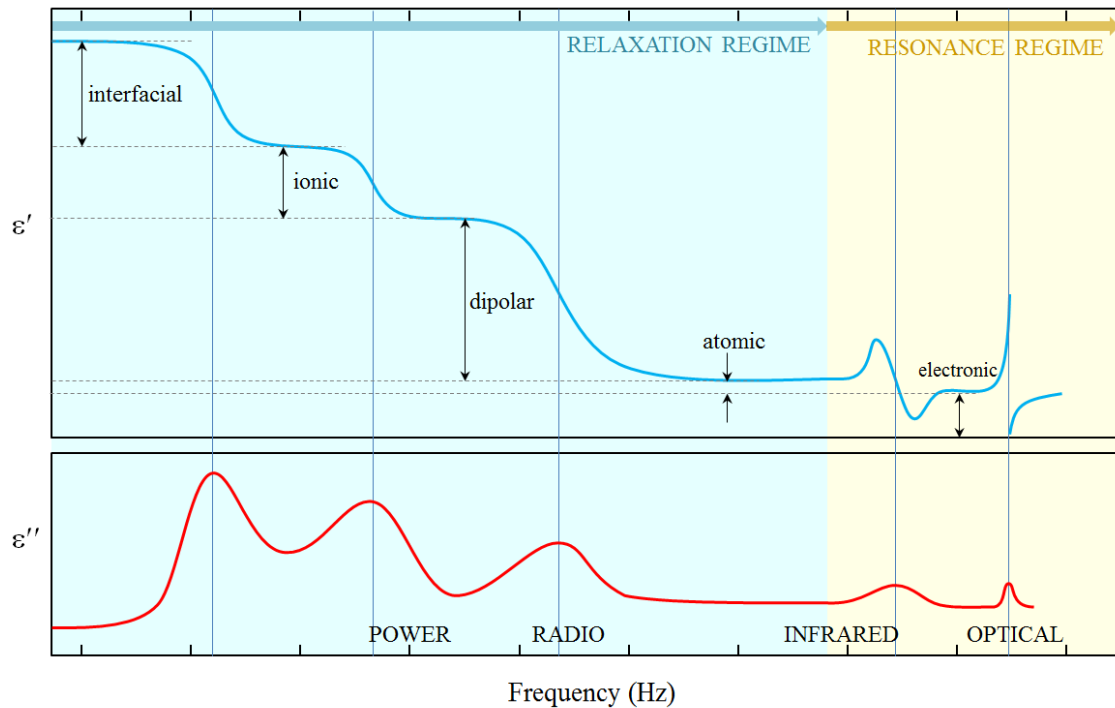


Figure 7 Different types of polarization as a function of frequency in polymers.

However, if a polymer has polar groups and contains permanent dipoles, these permanent dipoles may respond to the external field by rotation, resulting in orientational polarization in the polymer. In the absence of an applied field, these dipoles are randomly oriented and also restricted in their rotations by neighbor chains, as shown in

Figure 8(a). Under applied dc field, as in

Figure 8(b), some segmental rotation enables local dipolar orientation.

Depending on the nature of these dipoles, amorphous or crystalline, and temperature, this polarization mechanism relaxes in the frequency between 10 Hz to few gigahertz, covering the power and radio frequency ranges.

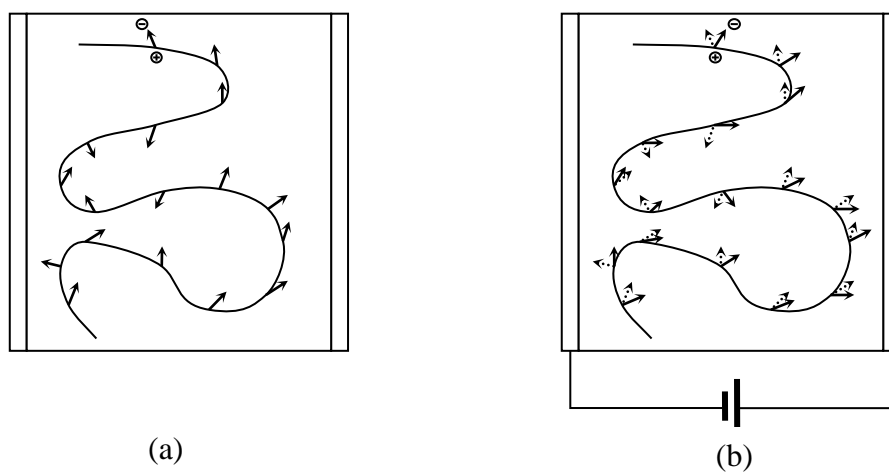
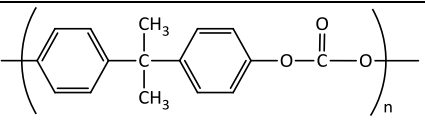
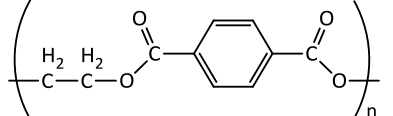


Figure 8 A polymer chain containing polar groups with (a) no applied field and (b) in the presence of an applied field .

Table 1 Permittivity of some common polymers

Polymer name	Structure	Permittivity
Polyethylene	$\left(\begin{array}{cc} \text{H} & \text{H} \\ & \\ -\text{C} & -\text{C}- \\ & \\ \text{H} & \text{H} \end{array} \right)_n$	2.2
Polypropylene	$\left(\begin{array}{cc} \text{H} & \text{H} \\ & \\ -\text{C} & -\text{C}- \\ & \\ \text{H} & \text{CH}_3 \end{array} \right)_n$	2.2
Polystyrene	$\left(\begin{array}{cc} \text{H} & \text{H} \\ & \\ -\text{C} & -\text{C}- \\ & \\ \text{H} & \text{C}_6\text{H}_5 \end{array} \right)_n$	2.8

Polycarbonate		2.9
Polyester		3.5

If a polymer contains ionic species, either impurity ions or ions in polymer electrolytes and polyelectrolytes, ionic polarization occurs below a few hundred Hertz. Finally, for a multicomponent polymer system, interfaces exist and interfacial polarization takes place due to the Maxwell-Wagner effect [3, 4]. The relaxation of these interfacial charges may take from minutes to hours or even years (e.g. charges trapped in electrets).

Obviously, for high voltage power and radio frequency applications, ionic and interfacial polarizations are not suitable due to their high losses. The rest type of polarization that we can utilize for high energy density and low loss dielectrics are electronic, atomic, and orientational polarizations. It is known that electronic polarization is high for conjugated polymers. Semiconducting polymers, however, are not suitable for high field application because of high conductivity at high applied electric fields. It is also difficult to enhance atomic polarization in polymer because atoms are covalently bonded. Orientational polarization in polymers is suitable for high energy and low loss application if the dipole relaxation happens above tens of megahertz.

Ferroelectric polarization is also possible for some polymers which can increase the permittivity an order of magnitude. However, ferroelectric polymers have higher

losses and limit their frequency responses into the megahertz region. Moreover, the permittivity and losses are found to be fluctuated around their Curie transition.

1.4 Structure and Polymorphs of PVDF

Like other semi-crystalline polymers, Poly(vinylidene fluoride), PVDF, and copolymers have very considerable potential for improving for specific purposes. It is also well-developed of many benefit features that could be drawn from PVDF e.g. good mechanical properties, chemical inertness, electrical endurance and processability. Chain structure of PVDF contains of $-\text{CH}_2\text{-CF}_2-$ repeating units. PVDF is commercially synthesized by free radical polymerization using suspension or emulsion processes [12]. This process provides very long linear structure. Long-chain molecules can exist in either one of two states. In disorder state, the individual chains adopt a random coil conformation. This state is commonly exhibits the characteristic long-range elasticity. The Crystalline or ordered state is one that is characterized by three-dimensional order over at least a portion of the chains. The chain axes are usually aligned parallel to each other. In contrast to the amorphous state, the crystalline state is relatively inelastic and rigid. There are also major differences in terms of thermodynamics. Hence it is possible to change properties by control of structure [13].

Since Fluorine is a strong electronegative the F1s binding energy was found to be 689.6 eV while the C1s was found to be 290.8 eV and 286.3 eV corresponded to $-\text{CF}_2$ and $-\text{CH}_2$ carbons respectively.[14] The polymer molecule is an alternating between carbon-fluorine and carbon-hydrogen bonds, each repeating unit provides strong dipole

moment of 7.6×10^{-30} C·m (2.3 Debye) [15] normal to the chain axis. Typically, PVDF is a semi-crystalline polymer with c.a. 50-60% crystallinity. It is known that PVDF exhibits polymorphism that contributes to its extraordinary electrical properties ranging from typical dielectrics to versatile ferroelectrics. Three of the four crystallographic configurations of PVDF unit cell usually have dipole moments; which are prerequisites for the formation of a ferroelectric structure. Crystallites (or their sections) can be considered as spontaneous polarization domains.[16] Another crystalline structure of PVDF is paraelectric phase which the chain confined into zero dipole moment. Details of crystallographic configurations are discussed later in this chapter.

1.4.1 Amorphous regions (disorder phase)

As mentioned earlier, PVDF and copolymers is semi-crystalline only 50 - 60% in PVDF is occupied by crystalline structures therefore the rest is filled by amorphous phase.

The unperturbed mean-square end-to-end distance, $\langle r^2 \rangle_0$, of PVDF molecules in dilute-solutions (θ -conditions) is $4.1(\pm 0.2) \times 10^{-17} \overline{M}_w \cdot \text{cm}^2$, i.e. the root-mean-square of end-to-end chain length, $\langle r^2 \rangle_0^{1/2}$, is around 65 nm for a molecule of 1,000,000 g/mol molecular weight [17]. Even though there is no order in this phase the experimental results are strongly confirmed that the amorphous phase makes a certain contribution to behavior of PVDF under electric field. However the role of this phase is yet entirely clear. For example, the evident of that the amorphous phase affects the electrical hysteresis characteristics of PVDF was reported by Furukawa et al [18] as shown in

Figure 9. Evidently, the D-E hysteresis loops Figure 9a was influenced by adjusting temperature even into below glass transition temperature ($T_g \approx -40^\circ\text{C}$) where chain sections are frozen.

At low temperatures, there are two peaks exist in the polarization current density curves in Figure 9b. The position of the lower-field peak (c.a. 50 MV/m), which is believed caused by the responding of polar crystalline structure, remains unchanged. While, it is obviously that the other peak (at higher field) that may be due to the responds of dipoles in amorphous phase, shifts to lower field as the temperature increases.

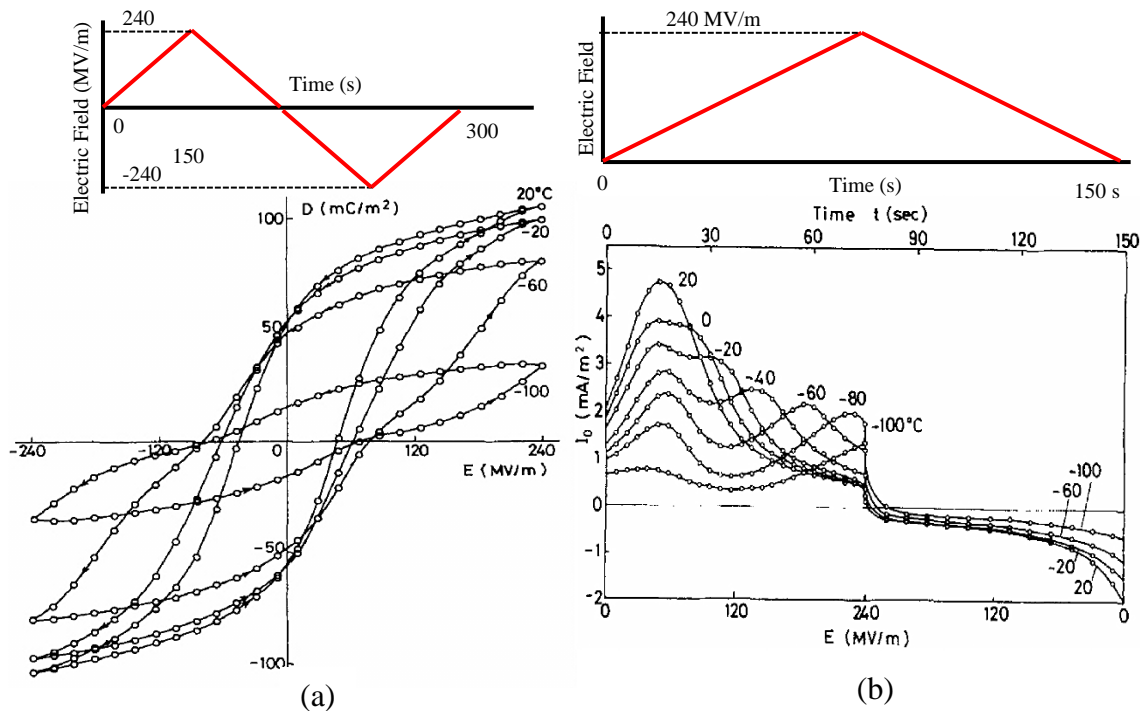


Figure 9 Temperature dependences of (a) the hysteresis electric displacement versus electric field (D-E loops) measured under 1/300 Hz triangular load and (b) the polarization current density versus electric field of as-prepared PVDF film[18]

1.4.2 Crystalline Phase of PVDF

In general, four major crystalline phases of PVDF are observed, i.e., α , δ , γ and β forms, as shown in *Figure 10*. Among them, the α form is paraelectric and δ , γ and β are ferroelectric. Both α and δ forms have exactly the same unit cell dimensions and the same TGTG' rational sequence; however, the dipole moments in α form are cancelled out but they point out to the same direction in the δ form. The α form of PVDF is the most common and easily produced through most processing methods. The δ form can be obtained by poling the α form sample under an electric field of 100-200 MV/m at room temperature [19]. However, this paraelectric-to-ferroelectric transition is not totally reversible; namely, the sample will largely stay in the δ form even after the applied field is removed. Because of the inclination of C-F dipoles at an angle to the molecular axis, the components of the dipole moment perpendicular and parallel to the chain axis are 1.20 and 1.02 Debye, respectively. The γ form has a TTTGTTTG' chain conformation and is often obtained by solution casting from polar solvents at temperature below 100 °C. While the α and β phases of P(VDF) were discovered fairly quickly, it took over a decade of debate before the structure of the γ phase was settled on. The difficulty in identifying the γ phase stemmed from two reasons. The first reason was the difficulty in producing a sample with a high amount of the crystal phase. The γ phase readily transforms to the β phase under mechanical stress necessitating careful handling of the sample. Pure samples of the gamma phase were produced by solution casting onto specific substrates. The second reason for the difficulty in identifying the γ phase lies in its similar x-ray diffraction peaks to the α and β phases. Early reports of the γ were

sometimes dismissed as mixtures of the α and β phases. Careful processing and collection of diffraction patterns eventually lead to the confirmation of the γ phase. Again, since the C-F dipoles are inclined, the component of the dipole moment are perpendicular and parallel to the chain axis and their values are similar to those from the α and δ phases. The β form is the highest polarity unit cell of PVDF. This form is often obtained by mechanical stretching or high field poling (400-500 MV/m) of α or γ form samples and has an all-trans conformation. The dipoles are perpendicular to the chain axis and have the dipole moment per chain per repeat unit, i.e., 2.10 Debye. Due to the large dipole moment, the β form has the highest spontaneous polarization. *Figure 11* illustrates the phases obtained in P(VDF) from various processing routes. However, it is difficult to get a complete phase conversion therefore resulting in a mixture of phases and resulting properties.

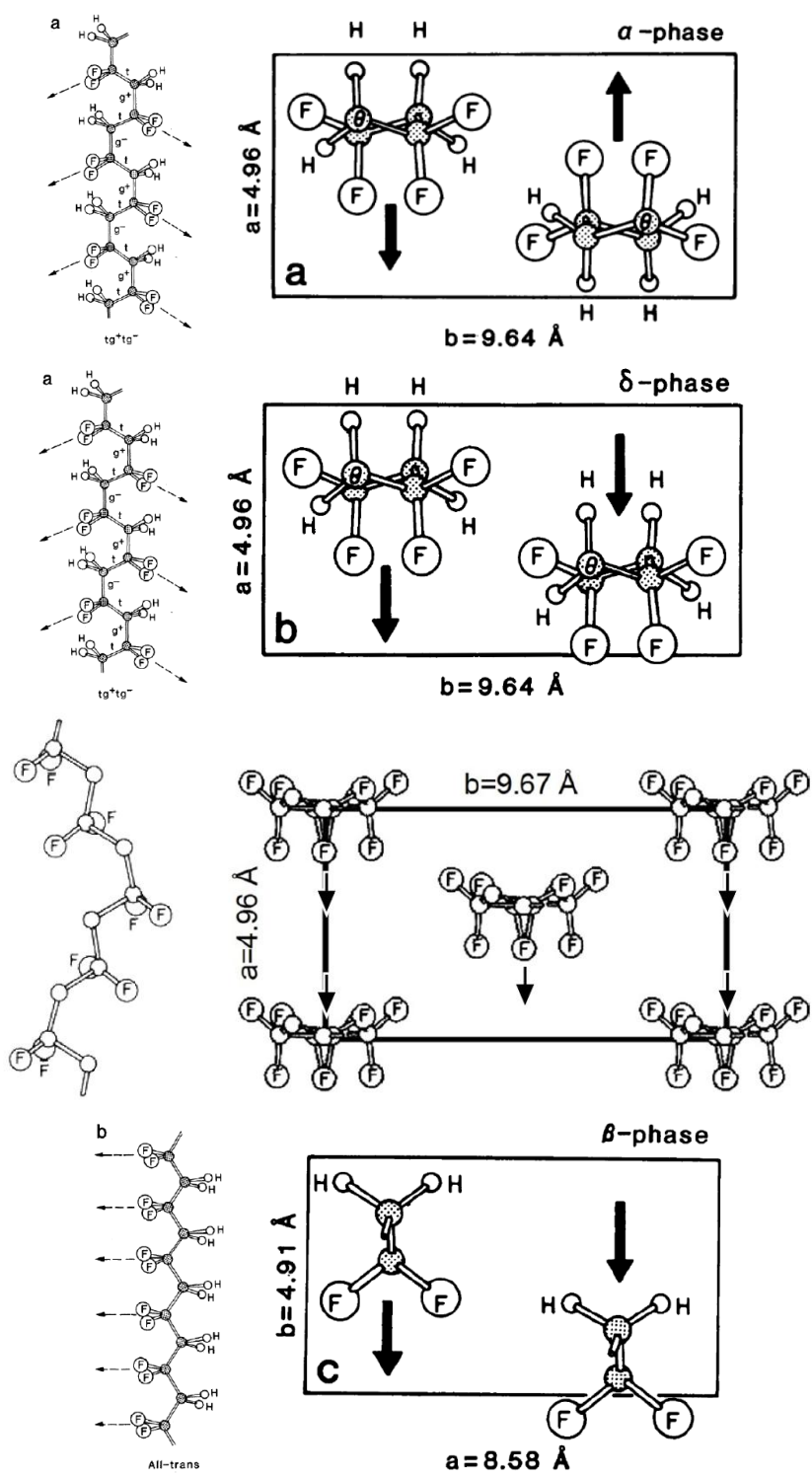


Figure 10 – Crystal phases of α , δ , γ and β forms of PVDF. [12, 19]

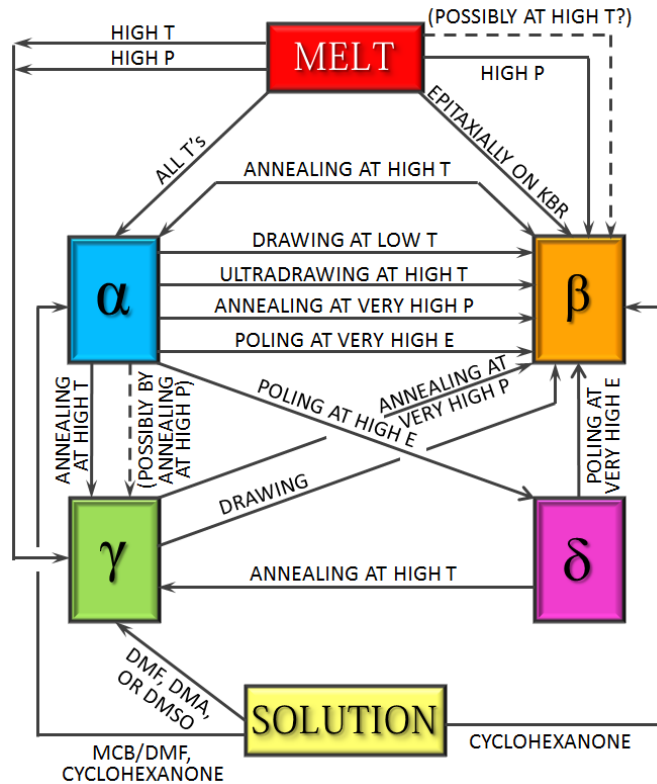


Figure 11 PVDF crystal phases processing routes. [19]

1.5 Polarization Mechanism in Ferroelectric PVDF

In order to describe the mechanism in the ferroelectric PVDF, a simple amorphous-crystal series model as shown in **Figure 12** are proposed. In this model a ferroelectric PVDF lamella is sandwiched between two amorphous layers. Electrodes are in direct contact to the amorphous layers. The chain direction is perpendicular to the external field. Upon application of an external field (E_0) the dipoles in amorphous phase

will be polarized first. This polarization is, however, usually small. As the external field increases, dipoles in the ferroelectric PVDF crystal will respond and orient along the field direction, thus creating a local depolarization field (E_{depol}) as shown in **Figure 12**. [4, 20]

$$E_{depol} = \frac{P_{in}}{\epsilon_0}$$

Equation 14 Local depolarization field, where P_{in} is the polarization inside the PVDF crystal induced by aligned dipoles

The polarization inside the PVDF crystal P_{in} will induce more polarization of the amorphous phase at the interfacial region, resulting in an enhanced compensation polarization (P_{comp}) outside the ferroelectric domain. The P_{comp} in amorphous phase is determined by the dipole density ($N_{0,am}$), the polarizability (α_{am}), and the local field ($E_{L,am}$) in the amorphous phase[4].

$$P_{comp} = N_{0,am} E_{L,am} \alpha_{am}$$

Equation 15 Compensation polarization

The P_{in} may not equal the P_{comp} , especially in a non-equilibrium state. Based on the model in **Figure 12**, the local polarization field for the crystal is imposed from the charges on the electrodes and can be defined as

$$E_{pol} = \frac{D}{\epsilon_0} = \frac{Q + P_{comp}}{\epsilon_0}$$

Equation 16 Local polarization field, where Q is the charge density induced in vacuum, i.e., $Q = \epsilon_0 E_0$.

Dipole switching depends on the local electric field in the crystal ($E_{L,cryst}$), which is contributed from at least three sources; (i) E_{pol} (positive) (ii) E_{pol} (negative) and (iii) other contribution from dipoles nearby. [4] However, the contribution (iii) may be neglected due to the random orientation. Then, the local field largely depends on the competition between E_{pol} and E_{depol} , which is determined by the relationship between P_{in} and $Q + P_{comp}$. Upon a forward poling, $Q + P_{comp} > P_{in}$ and thus $E_{pol} > E_{depol}$. Crystalline dipoles will be polarized along the external electric field. During a reverse polling process, two scenarios can take place. First, as both E_{depol} and E_{pol} decrease with decreasing the external field, at a certain point $P_{in} > Q + P_{comp}$ and then $E_{depol} > E_{pol}$. Fully aligned dipoles will become less stable than they are in a situation that some mobile (or reversible) dipoles revert to the opposite direction, resulting in a minimum (or even zero) remnant polarization. This behavior is so-called antiferroelectric-like behavior. Second, when $P_{in} < Q + P_{comp}$ as E_{depol} and E_{pol} decrease with the external field, the E_{depol} turns out to be always lower than the E_{pol} . Therefore, the normal ferroelectric behavior will be obtained. For the ferroelectric, the second scenario is commonly observed.

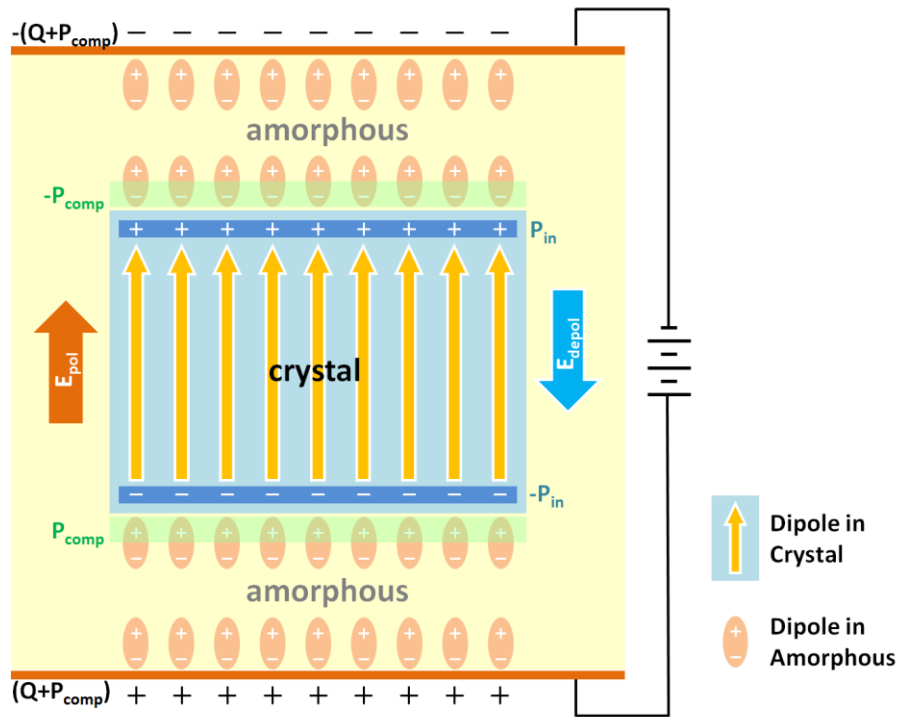


Figure 12 Schematic illustration of an electrically poled ferroelectric PVDF crystal sandwiched between two amorphous layers. The chain direction in the lamellar is perpendicular to the dipole moment or external electric field

1.6 Research Motivations and Goals

Among many polymer dielectrics, Poly(vinylidene fluoride-co-chlorotrifluoroethylene), P(VDF-CTFE), copolymer has strong potential in the polymer thin film capacitor industry. Due to the enormous capability to store electrical energy as high as 25 J/cm³ this copolymer is very promising over the commercialized BOPP (energy density around 1-2 J/cm³). However, in order to launch this polymer into industrial production there are some challenges that required to elucidate. One of the

most significant issues is the energy losses that arise during conduction (conduction losses) and/or phase-lagging transformation between non-polar phase and polar phase (α - and β - phase respectively). For example, the dielectric loss of 91/9 mol% uniaxially stretch P(VDF-CTFE) copolymer film as high as 40 % can be found. [21] This is showing us rooms for improvement.

As previously observed, the D-E hysteresis loop of β -phase containing PVDF is tended to be a square shape due to the polar phase was unrecoverable upon charging process. This is leading to a very large dielectric loss which is not desirable for capacitor applications. In contrast, the films prepared from P(VDF-CTFE) copolymer, which α -phase has stabilized, exhibited much smaller remnant polarization as compared to the PVDF homopolymer. For this reason, the α -phase is more suitable structure for energy storage applications. However, it seems there would be trade-off considerations in modification of molecular structure by this introduction of defects group into the main chain since the maximum polarization has been decreased. [22] In other words, this defect modification method sacrifices the ability to store charge while reducing dielectric loss. Moreover, the bulky Cl group impedes the crystallization process hence the overall crystallinity has been relatively reduced. Therefore this approach has some limitations and is leading to many adverse properties such as poor mechanical properties and thermal durability.

Although the energy losses of P(VDF-CTFE) is lower than PVDF homopolymer, it is challenged to further decrease this losses in P(VDF-CTFE) to enable this copolymer for high energy dielectric application. At fields of less than 150 MV/m, the polarization has an almost linear relationship with applied electric field in both charging and

discharging cycles. There is very small evident of hysteresis in the D-E loops as shown in *Figure 13a*. In this region, the polarization is mainly caused by dipolar polarization. The displacement of the dipole is a result from the Coulomb force which depends on the magnitude of dipoles and electric field. Hysteresis loops in this region are similar to those typical dielectric polymers such as polypropylene. However, as increasing of applied field to approximately 150 MV/m, the hysteresis loop is additionally affected by nonlinear responds due to the ferroelectric nature of the copolymer (*Figure 13b*). This behavior creates more ability to store larger amount of energy since the polarization increase more rapid. It is believed that the electric field induce nonlinear characteristics are affected by partially phase transformations from a non-polar phase (α) to polar phases (β and/or γ). Because of changing of configurations in chain segments large displacement can be achieved.

However, even though the phase transformation benefits the charge storage ability, this transformation seems to be stable and uneasy to recover back into their original non-polar state as evidenced in the upper bound of the loops in *Figure 13b*. Therefore the released energy density, which is the only useful energy, will be decreased by the amount of remnant polarizations. This so called ferroelectric loss is apparently undesirable for capacitor applications. In order to reduce this adverse effect of the ferroelectric switching the polar-phase must be destabilized.

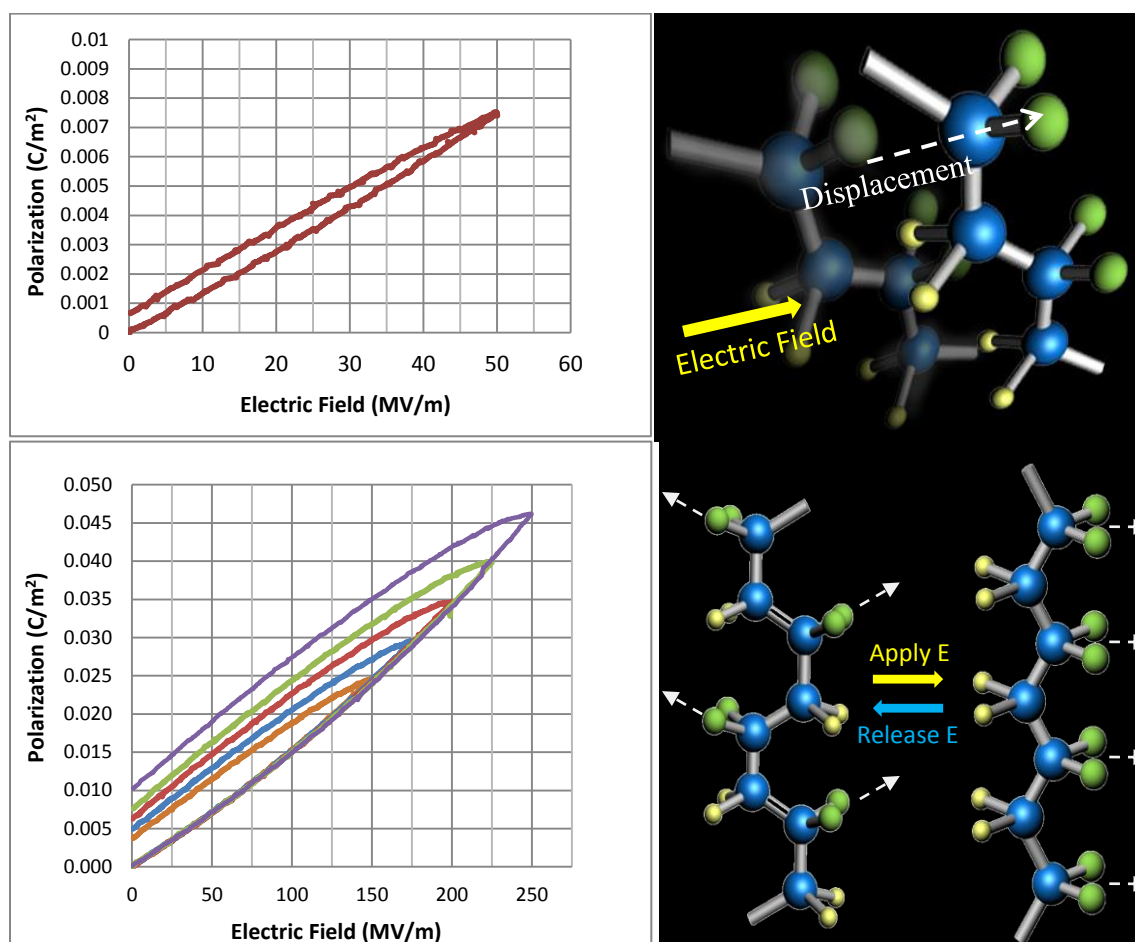


Figure 13 Unipolar D-E loop of P(VDF-CTFE)(15 wt.% CTFE) at under application of (a) weak , (b) strong electric field. (c) and (d) represent the polarization mechanisms of PVDF-based polymer segment under weak and strong electric field respectively.

In earlier works by several groups, the attempts to reduce dielectric losses of PVDF-based polymers using electron irradiation have been demonstrated. [23-25] The technique introduced defects to polymer structure by crosslinking via the generation of free radicals upon exposure to high energy electrons. After the irradiation, the reductions of losses have been obtained. However, the polarization level of the irradiated sample has

also been decreased due to the dropping of crystallinity as a result of crosslinking and chain scission. Therefore, less energy can be stored in the polymer by using this approach. Moreover, it is believed that the electron-induced transformation can introduce metastable chemical species into the polymer which may cause adverse effects under high temperature service.

To overcome these problems, we introduce chemically crosslinking approaches that can be triggered by thermal and photo-induced methods. These approaches together with precisely control of the process parameters are envisaged as a promising method to reduce losses without sacrificing the ability to store/discharge electrical energy of the copolymer. These techniques allow us to systematically control the crosslink content and density by varying feeding amounts of initiators and crosslinking-agents. Therefore the performance of the crosslinked copolymer can be optimized by controlling the morphologies. Introduction of covalent bonds between linear P(VDF-CTFE) copolymer chains will capitalize on reducing of crystallite size and favor the formation of the non-polar α phase. While crystallinity of the crosslinked copolymer can be maintained by carefully control the crosslink density.

In this research, we investigated a series of crosslink chemistries on P(VDF-CTFE). We also centered our effort on only commercially available initiators, co-agents and copolymer to create a venue of enabling future large-scale production. The majority part of this study covers processing-structure-property associations in crosslinked P(VDF-CTFE). We have explored the optimum formulation of initiator and crosslinking agent as well as process conditions based on their effects on dielectric performances.

Chapter 2

Crosslinking of P(VDF-CTFE) with peroxides

In this chapter we explore the structural modification of the poly(vinylidene chlorotrifluoroethylene) [(PVDF-CTFE)] copolymer by crosslinking using peroxides as reaction initiators. The reaction is triggered and manipulated by carefully control process condition, i.e. temperature, pressure, concentration and reaction time. The background section begins with a detailed review of crosslinking of fluoropolymers. Reaction chemistries between various initiators and fluoropolymers with roles of co-agents are then elaborated. The section then covers the effects of crosslinking on bulk material properties and its structures.

Next section in this chapter covers purposed materials and methodology of this research. An in-depth aspect in peroxide crosslinking of vinylidene fluoride-containing fluoropolymers is carried out in this section to assist in elucidating the proposed crosslinking reaction mechanisms and experimental design. We then review the experimental methodology section to clarify the sample fabrication parameters that consequently affect the structure-property relationship of the crosslinked copolymers. Hence this section also covers characterization techniques utilized in this research in order to analyze the material structures relate to properties and performances of the of the resultant crosslinked copolymers

The third section presents the results and discussion. The first part demonstrate the analysis of material structures effected by crosslinking based on various

characterization techniques, i.e. gel analysis, wide angle x-rays diffraction (WAXD), Fourier transform infrared spectroscopy (FTIR) and differential scanning calorimetry (DSC). The second part presents the results of mechanical and electrical properties of the crosslinked copolymers in comparison with the precursor. The mechanical properties are presented and discussed by means of dynamic mechanical analysis (DMA). The electrical properties are presented in order to examine the behavior of charge generated under applied electric fields through the performing measurement of conductivity and thermally stimulated discharge current. In order to evaluate the potential of crosslinking approach to P(VDF-CTFE) copolymers, the dielectric properties and performances are discussed based on the frequency-time dependence dielectric measurements and displacement-electric field hysteresis loop testing as well as the weibull analysis of breakdown strength. All results are elaborated and emphasized in terms of structure-property relationship for improving an understanding of the effects of microstructure on energy storage behavior of the materials.

2.1 Background

In general, crosslinking of fluoropolymers is not easy due to their chemical inertness. The high electronegativity fluorine atom forms a covalent bond with the carbon backbone giving a strong C-F bond with a dissociate energy of $485 \text{ kJ}\cdot\text{mol}^{-1}$. Furthermore these polymers also possess a strong hydrogen bonding between hydrogen and fluoride atoms resulting a small van der Waals radius (1.32 \AA)[26]. In this research, although we focus on vinylidene fluoride fluoropolymer that exhibits a slightly increased

in reactivity, the PVDF homopolymer is still not suitable for crosslinking due to their long linear macromolecular structure and high crystallinity. In contrast, the PVDF-based copolymers have been widely studied and successfully crosslinked using numbers of techniques over a half century [27-29]. As mentioned above, in this research, we are focusing our study on P(VDF-CTFE) copolymer due to its outstanding in low loss with the paraelectric-ferroelectric switchable property. However, another important feature that can be achieved from this particular copolymer is the fact that it is a halogen containing moiety in its structure as a side group. This halogenated (Cl) group insures the free radical attack from the reaction initiators.

Fluoropolymers are usually crosslinked by variety of methods. Reaction mechanisms of fluoropolymers with nucleophiles such as diamines or bisphenols or by organic peroxides have been introduced in the late 1950s [28-34]. Irradiating the fluoropolymers with high energy electrons [24, 25, 35] or gamma rays [36] are also known ways to crosslink PVDF-based polymers.

The diamine nucleophiles generally yield in relatively poor processability with ineligible safety issues. . The resulted crosslinked products from this system usually have poor physical properties such as low thermal and aging resistance and poor a compression set. In contrast, the processing and property advantages of bisphenol crosslinking system have led this nucleophile predominantly replaced diamines in early 1970. However, there are some drawbacks of this system such as the reaction mechanism eliminates some small molecules, i.e. methoxides and fluoride ion, resulting CF=CF double bonds. These double bonds presumably have ability to increase the number of charge transfer in bulk crosslinked polymer. This may cause an increasing in conduction

loss and suppress the breakdown strength of the device. Moreover, the bisphenol crosslinking system also generates excessive porosity and poor distribution of crosslinking due to volatiles produced by consequent reactions of the byproducts. Since the reliability and breakdown endurance of the capacitor are strongly affected by the quality of the dielectric film this system is inappropriate to use for fabricating the polymer film.

Bisphenol and diamine crosslinking systems have different reaction mechanisms from the peroxide systems. Diamines and bisphenols exhibit crosslink reactions via dehydrofluorination at the backbone of fluoropolymer chains. This step is followed by Michealson addition and substitution of fluorine atom from diamine and bisphenol systems respectively. In contrast, peroxide crosslinking system is a free radical attack of a special functional site monomer. As mention above, the P(VDF-CTFE) copolymer contains the active site that suite for this system. Therefore, in this dissertation, the peroxide system was chosen as a method to fabricate crosslinked film. The next section of this chapter presents some fundamentals and chemistries of peroxide crosslinking mechanisms.

2.2 Peroxide crosslinking of PVDF-based copolymers

Peroxides have been used as crosslinking agents for crosslinking wide range of polymer species since 1929. Since 1950s, peroxides have been used with triallylisocyanurates to enable the crosslinking of fluoropolymers through free radical mechanisms.

The reaction temperature of crosslinking via peroxide systems depends on the thermal properties of each component, i.e. polymer, peroxide and co-agent. At a specific temperature, peroxides with acid groups decompose into free radicals at higher rate than those alkyl- or aryl- peroxides. In general, the crosslinking rate of peroxide system is almost equivalent to the rate of thermal decomposition of the peroxide. The rate of crosslinking using peroxide, therefore, is dependent primarily on process temperature and is predicable for each polymer system. While the crosslinking yields of the crosslinking system is influenced by concentration of peroxide and the chemical properties of polymers. According to a previous study of vulcanization of fluoroelastomers with dicumyl peroxide [27], in order to obtain a good properties of crosslinked products with peroxide, the crosslinking reaction times should exceed 1 h at 160 °C.

Thus, crosslinking of a polymer with relatively high melting point such as P(VDF-CTFE), c.a. ~170 °C, requires a peroxide with high stability. However, there are very few crosslinking peroxides that available commercially. Therefore, in this study, we chose α,α' -bis(tert-butylperoxy) diisopropylbenzene (Vulcup®) with a half-life ($t_{1/2}$) of 1 h at 134 °C, see **Figure 14**, as crosslinking agent. This bisperoxide is highly efficient, scorch-resistant, low-odor peroxide with broad utility as a crosslinking agent for elastomers and plastics. Vulcup® decomposes thermally to form alkoxy radicals that readily to attack halogen atom in the polymer backbone, forming macromolecular radicals. Although the polymer radicals are readily to react to each other, the efficiency is relatively low due to the instability of the radicals. In contrast, a system that contained a radical trap co-agent was found to have more effective crosslinking. It is believed that the co-agent such as triallyl(iso)cyanurate (TAIC), known as a radical trap, gives a more

stable radical intermediate during the reaction taking place. From the previous studies on crosslinking of PVDF-propylene copolymer, it was found that the crosslink promoting effect of the TAIC is remarkable. A system with very low concentration of peroxide (2 phr) and TAIC (3phr) yielded gel content almost 95% [32]. From their results, the effect of peroxide level is insignificant when TAIC presents. The same result was also obtained from another research group who experimented the crosslinking system of P(VDF-HFP) with 2,5-bis-(t-butylperoxy)-2,5-dimethyl hexane in the presence of TAIC [33]. This research group found that the state of crosslinking is drastically influenced by the radical trap co-agent concentration than the peroxide concentration. However, the rate of crosslinking reaction is influenced by both TAIC and peroxide concentrations.

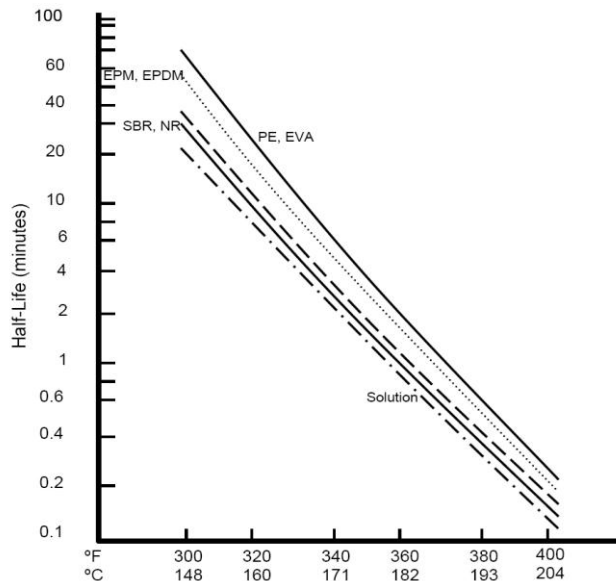


Figure 14 Half-life of Vulcup® versus temperature in various polymers.

Figure 15 presents the most probable reaction mechanisms taking place during the crosslinking of P(VDF-CTFE) with the α,α' -bis(tert-butylperoxy) diisopropylbenzene (Vulcup®) and triallyl(iso)cyanurate (TAIC).

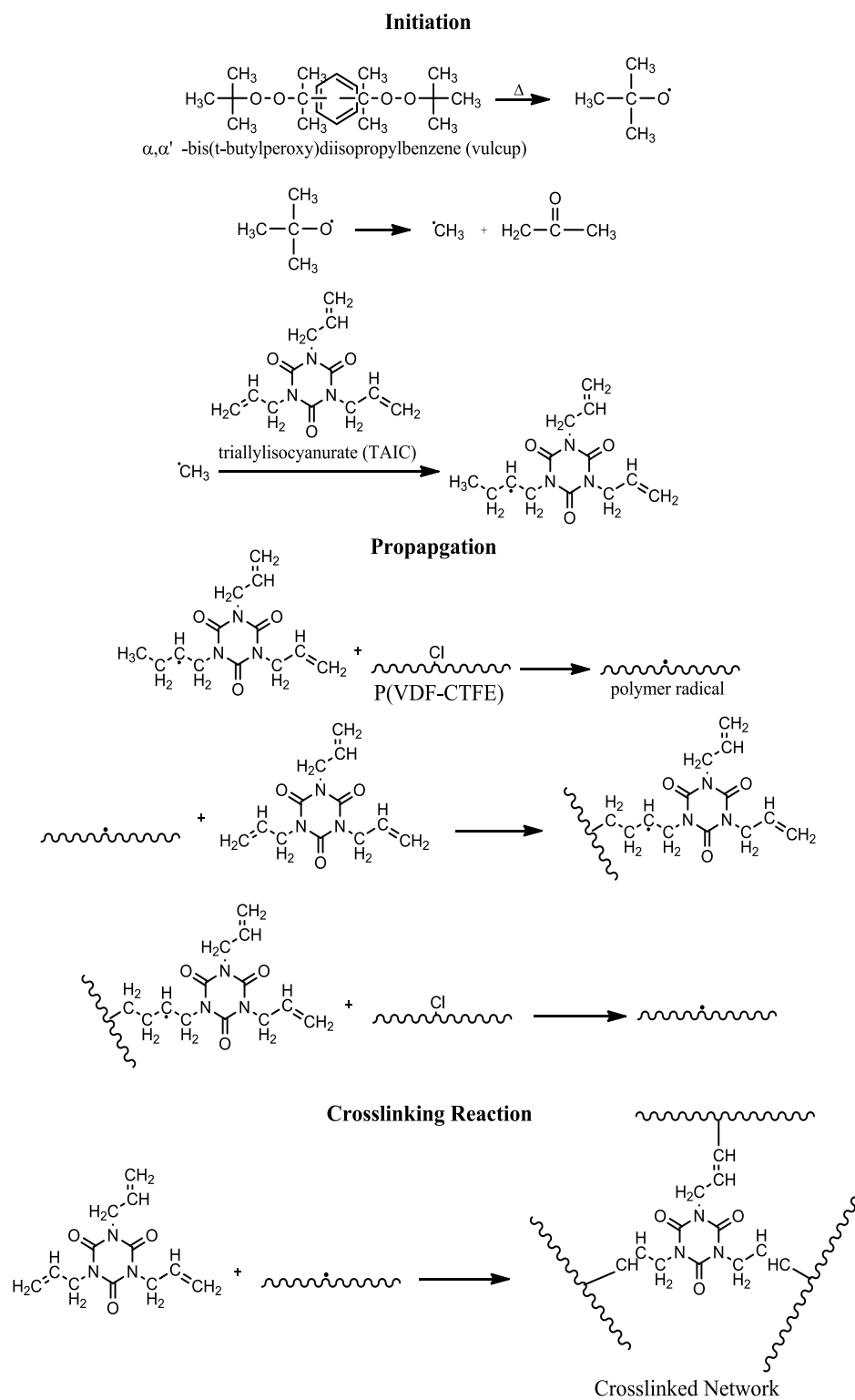


Figure 15 Schematic representation of probable crosslinking reaction mechanisms of the system proposed in this dissertation.

2.3 Experimental Procedure

a. Materials Fabrication

Poly(vinylidene fluoride-co-chlorotrifluoroethylene), referred hereafter as P(VDF-CTFE), is a random copolymer with 15wt.% CTFE monomer, in this study was supplied by Solvay (Solef 31508). The high thermal stability Vulcup[®] (1,4-bis(t-butyl peroxy) diisopropylbenzene, Hercules Inc.) initiator was used in this study to ensure effectively processing since the copolymer has a relatively high melting temperature (~165 °C). A polyfunctional crosslinking agent, triallyl isocyanurate (TAIC) was purchased from Aldrich. All materials were used as received without purification. The crosslinking reaction mechanism is outlined in *Figure 15*.

Pristine and crosslinked copolymers were made by hot-pressing method. The mixture compounds were prepared by vigorously shaking in controlled cryogenic atmosphere. The compounds were then hot-pressed using temperature and pressure as shown in *Figure 16*. At the beginning, the powder compound was placed into rapid heating and pressing to reach 150 °C under 2000 psi within 10 minutes. The temperature of the process was then held constantly while the pressure was gradually step-wise increased every 5 minutes until 4250 psi has been reached. The polymer film was further pressed rapidly to 5000 psi while the temperature was increased to 230 °C in 30 minutes. Finally, the polymer film was kept in high pressure and high temperature for 330 minutes to make sure the reaction is completed. The heat has then been cut off while pressure was maintained until the sample cooled down to room temperature. The resultant films were

then peeled off and dried in vacuum oven at 135 °C for 72 hours to remove any trace amount of impurities and by-products and also to anneal the copolymer at the same time. The copolymer films with thickness around 20 μm were obtained.

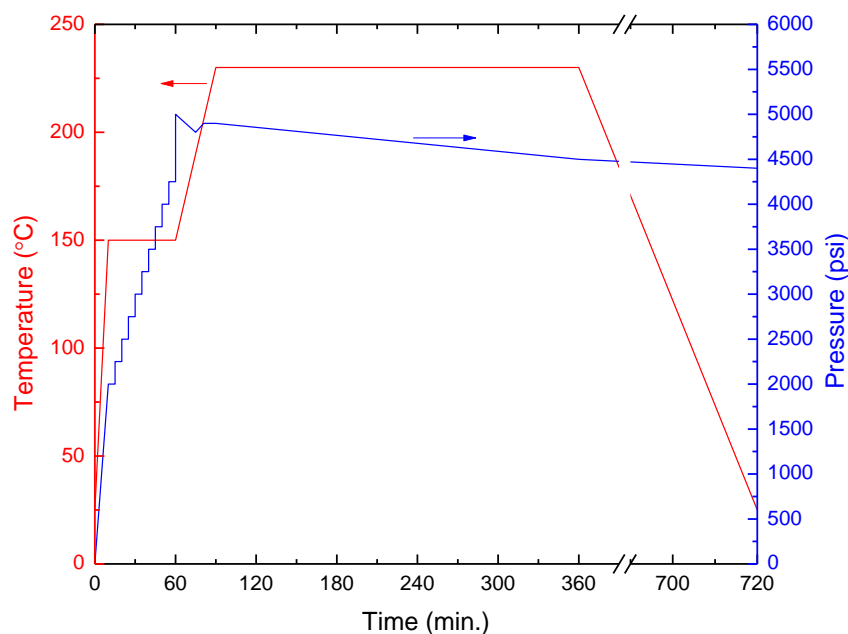


Figure 16 Hot-pressing process conditions for fabricating crosslinked P(VDF-CTFE) films using 1,4-bis(t-butyl peroxy) diisopropylbenzene (Vulcup[®]) triallylisocyanurate (TAIC)

b. Characterization

The gel contents and crosslink densities were examined using the ASTM D2765-01 standard procedure. The thermal transition data were obtained by TA Instruments Q100 differential scanning calorimeter (DSC) at a heating/cooling ramp of 10 °C/min in nitrogen atmosphere. Wide-angle X-ray diffraction (WAXD) studies were conducted

using a Scintag Cu-KR diffractometer with an X-ray wavelength of 1.54 Å. All data were deconvoluted using “Peakfit” software with a Gaussian-Lorentz superposition fitting functions. Fourier transform infrared spectroscopy (FT-IR) was carried out on Varian Digilab FTS-8010 spectrometer in room temperature. Spectrums were obtained in the attenuated total reflectance (ATR) mode using ZnSe crystal as a contact to the samples. Polarization hysteresis loops at room temperature were collected using a modified Sawyer-Tower circuit. The copolymer samples were subjected to a triangular unipolar wave with a frequency of 10 Hz. Dielectric properties were acquired using an Agilent LCR meter (E4980A) with 1.0 V bias. Temperature and frequency dependent of dielectric properties were measured using a Hewlett Packard 4284A LCR meter in conjunction with a Delta Design oven model 2300. Dielectric breakdown strength measurements were performed using the electrostatic pull-down method, with a 500 V/s ramp. Thermally stimulated discharge current (TSDC) was measured using Hewlett Packard 4140B pA meter with Kepco BOP1000M as a high voltage source and performed in a Delta Design oven model 2300. Gold electrodes of 2.6 mm diameter and typical thickness of 60 nm were sputtered on both sides of the samples for the electrical measurements.

2.4 Structural Analysis

a. Sol-gel Analysis

The sol–gel analysis was performed by solvent swelling and extraction of samples in cyclohexanone (boiling point 156°C) heated to reflux for 12 hours (ASTM D2765). The insoluble component was recovered and immediately weighed to give the weight of the swollen gel at solvent equilibrium. The gels were then dried at 70 °C in vacuum to provide the dry weight of the insoluble component. The gel contents were then simply a fraction of dry insoluble weight to the initial weight. The average molecular weight between two adjacent crosslinked sites was calculated using Flory-Rehner swelling theories (*Equation 17*). [37-39]

$$M_c = (\ln(1 - V_{pol}) + V_{pol} + \mu V_{pol}^2) / ((V_{pol}^{1/3} - V_{pol}/2) \rho_{pol} V_o)$$

Equation 17 - Flory-Rehner swelling theories

Where M_c is the average molecular weight between crosslinks; $V_{pol} = 1 / (1 + (f-1) * (\rho_{pol} / \rho_{sol}))$; f is the swelling factor = weight of the swollen gel / weight of the gel; ρ_{pol} is the density of P(VDF-CTFE) = 1.79 g/cm³; ρ_{sol} is the density of cyclohexanone = 0.97 g/cm³; μ is the Huggins solvent-polymer interaction parameters = - 0.3 for P(VDF-CTFE) and V_o is the molar volume of cyclohexanone = 139.3 cm³/mol. **Figure 17** demonstrates the influence of Vulcup[®] and TAIC concentration on the gel contents and M_c .

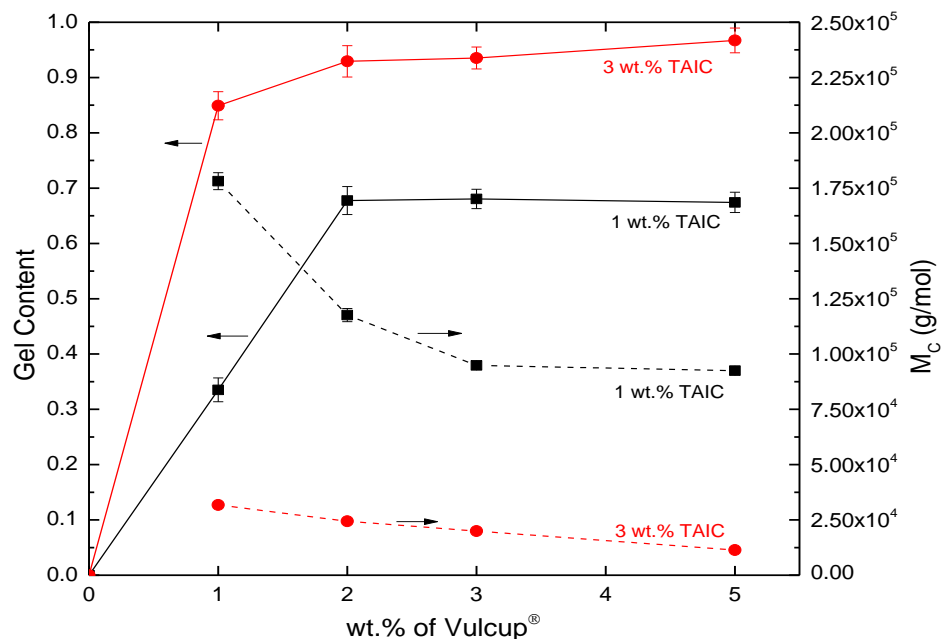


Figure 17 Gel contents and average molecular between crosslinking sites as determined using Flory-Rehner swelling theories versus Vulcup[®] concentration with 1 wt.% TAIC (black) and 3wt.%TAIC (red).

From this analysis it appears that the compounds with 3wt.% TAIC form denser crosslink networks compared to 1wt.% TAIC. The crosslinking efficiency increases with the concentration of Vulcup[®] and TAIC. By using 3wt.% of TAIC, the 85% gel content was obtained with only 1wt.% addition of Vulcup[®]. By further increasing amount of Vulcup[®] the gel content reached 95 % which is very high showing that the combination of Vulcup[®] and TAIC for crosslinking P(VDF-CTFE) is very effective.

b. Fourier Transform Infrared Spectroscopy Analysis

Infrared absorption spectra were collected using a Thermo Scientific Nicolet 6700 FTIR spectrometer in the range of 2000-400 cm^{-1} . A resolution of 2 cm^{-1} was used in the acquisition of all spectra, and 100 scans were signal-averaged. Peak heights were determined manually with normalization of the highest peak at 870 cm^{-1} . Baseline was determined by peak fit software. A dry atmosphere was maintained during collection of spectra for all materials.

Attenuated total reflectance FTIR spectra of the melt pressed copolymer samples of pristine and crosslinked with various Vulcup[®] concentrations with 3wt.% TAIC are shown in *Figure 18*. The peak at wave number 1685 cm^{-1} is assigned as the carbonyl group contained in TAIC that increased with the concentration of the Vulcup[®] feeding. This can be reflected that the increasing concentration of Vulcup[®] can generate more radical leading to higher crosslink density in the copolymers.

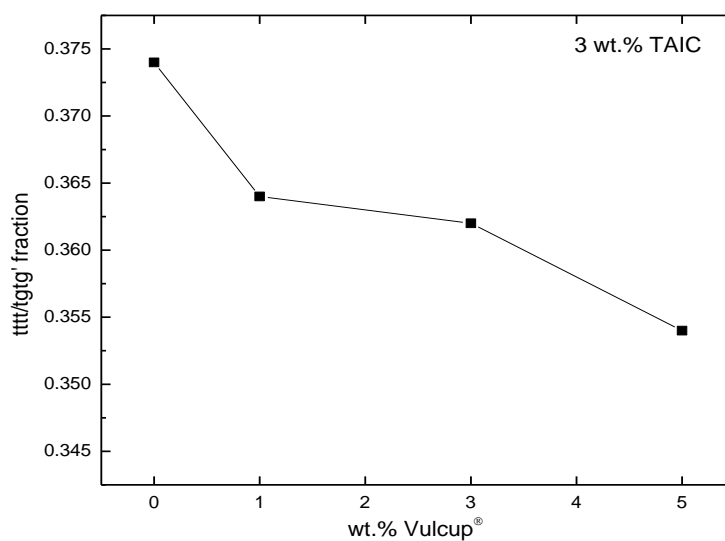
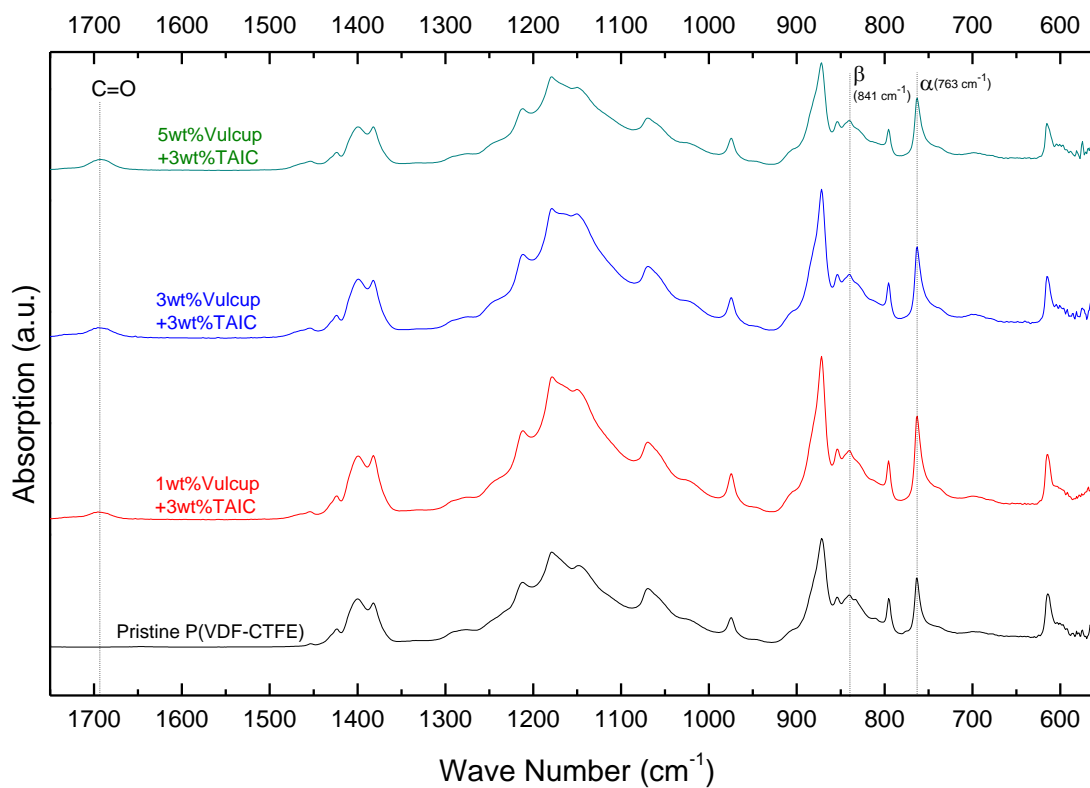


Figure 18 ATR-FTIR spectra (top) and: tttt/tgtg' fractions (bottom) of pristine and crosslinked P(VDF-CTFE) with different Vulcup[®] concentration (3wt.% TAIC).

The absorption intensities of peaks at wavenumbers of 763 cm⁻¹ and 841 cm⁻¹ can be used to determine the fraction of TTTT conformation to TGTG' conformation. [40, 41] The fraction of the β crystalline phase present in each sample was calculated by using

$$F(\beta) = \frac{X_{\beta}}{X_{\alpha} + X_{\beta}} = \frac{A_{\beta}}{1.26A_{\alpha} + X_{\beta}}$$

Equation 18 β crystalline phase fraction. Where X_{α} and X_{β} are the mass fractions of the α and β crystalline phases, A_{α} and A_{β} are the absorption bands (peak heights) at 763 cm⁻¹ and 841 cm⁻¹, and 1.26 is the ratio of absorption coefficients at 763 cm⁻¹ and 841 cm⁻¹.

As expected, these fractions are slightly decreased after crosslinking which indicating that the formation of 3D networks inhibits the formation of all-trans chain conformation. Therefore, it is plausible that the crosslinked copolymers should contain greater amount of the desirable paraelectric phase (non-polar α phase) than the pristine.

c. X-rays diffraction analysis

The XRD patterns of pristine melt pressed and crosslinked copolymers are shown in *Figure 19*. The patterns are characteristics of four α -phase crystallographic planes with very a small peak intensity of (110,200) β -phase. Even though these samples were cooling from molten under pressure, the crosslink structures and the post annealing seemed capable to inhibit the formation of polar phase. As discussed earlier, the large

amount of α -phase crystal gives benefits to the energy storage applications since the non-polar α -phase is more desirable for high energy density capacitor. All XRD data was deconvoluted using Gauss-Lorentz area functions, which allowing us to identify peak locations, integrate peak areas and calculate the full width at half maximum (FWHM). Since the copolymer is mostly comprised of vinylidene mer, the crystalline peaks were assigned based on PVDF polymorphs. The Peak fitting of the diffraction patterns showed clear changes in peak intensity. For instance, the peaks associated with the (100) α , (110) α and (021) α planes decrease in intensity as the Vulcup[®] concentration increased. Broaden haloes centered at 17° are assigned as distributed by the amorphous phase. The crystallinity of the samples can be calculated by integrations of the areas under each peak. As may be seen in **Figure 20**, the introduction of crosslinked network into polymer structure with this approach slightly decreases the crystallinity. This is due to the formation of 3D-network inhibits the orientation of polymer chain into lamellar structure. However, even with the highest crosslink density sample (3 wt.% Vulcup[®] + 3wt.% TAIC), the reduction of crystallinity is only about 2%. This may be due to the fact that the bulky Cl-atoms, which also have the same crystallization inhibition effect, may have been consumed as it is an active site during crosslinking reaction. As mentioned earlier, one major goal of crosslinking via this approach, in order to minimize dielectric loss, is to reduce the ferroelectric domain by reducing crystal size. However, the crystallinity of the resultant polymer should be maintained since the polarization mechanism taking place in PVDF predominantly stems from the ferroelectric polarization that occurs only in the crystal forms. Otherwise the total polarization will be decreased even though the reduction of loss has been successfully decreased. The α phase is the major component

in crystal structure of all samples. The content of this phase is increased after crosslinking. From **Figure 21**, the 3 % wt. Vulcup[®] + 3 % wt. TAIC system has the highest content of the α phase. This is most likely due to the structure modification by crosslinking prohibit the all trans conformation since the crosslink site has less mobility and requires large amount of energy and time to from the β phase.

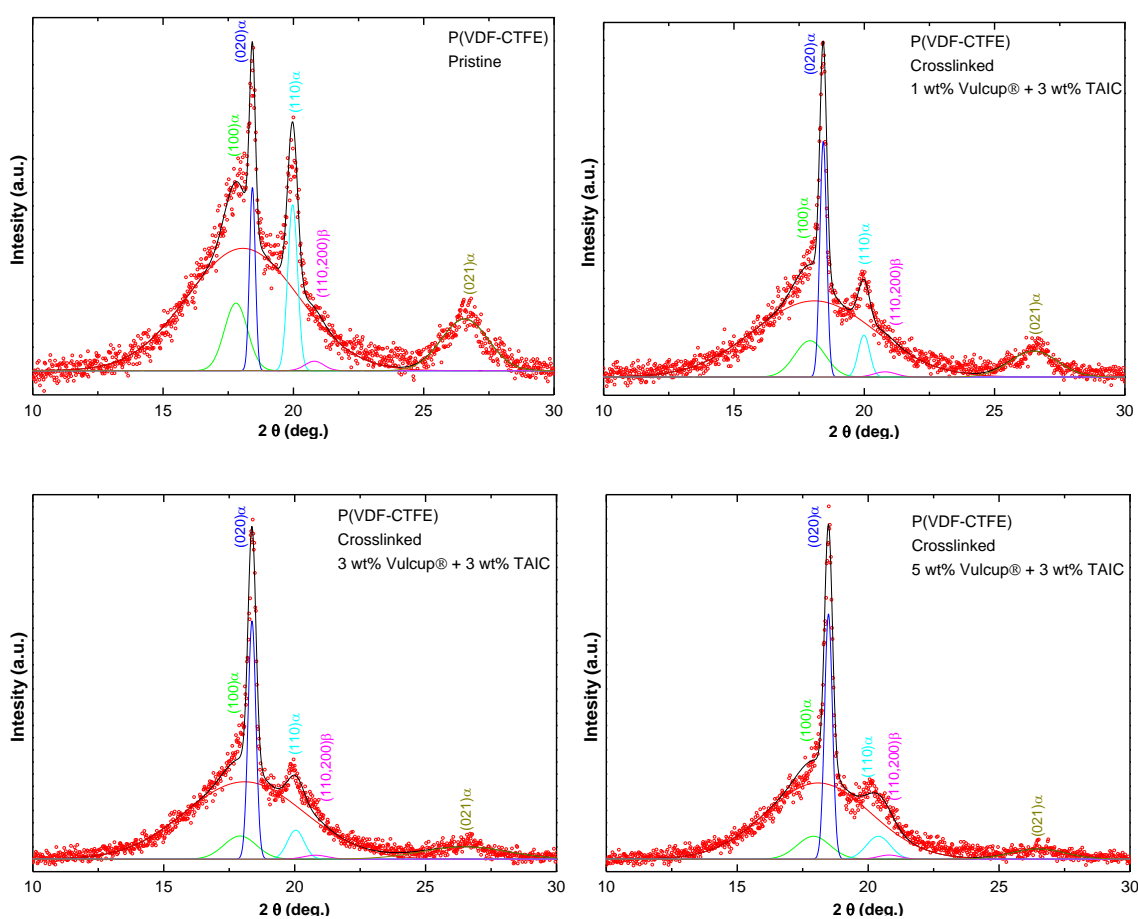


Figure 19 XRD patterns of pristine and crosslinked P(VDF-CTFE) using Vulcup[®] at 3 % wt. TAIC

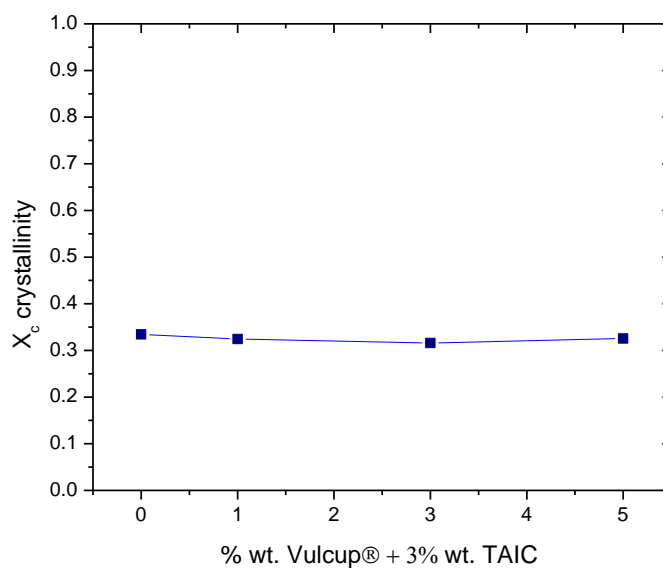


Figure 20 Crystallinity versus Vulcup® concentration at 3 % wt. TAIC, determined by XRD patterns

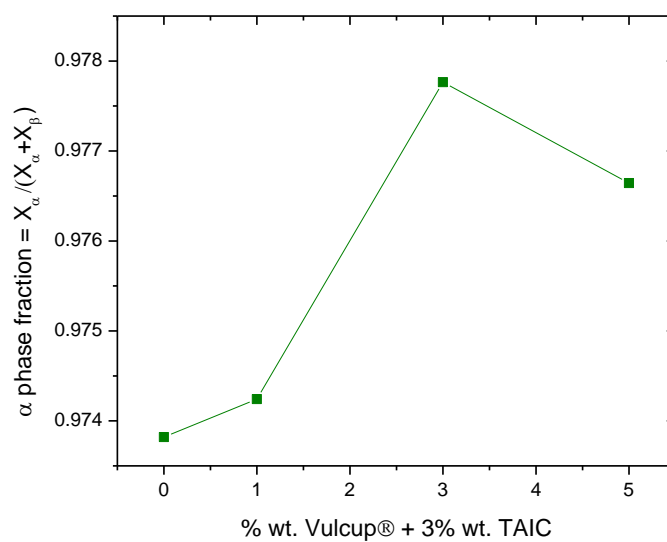


Figure 21 α phase fraction versus the Vulcup® concentration at 3 % wt. TAIC.

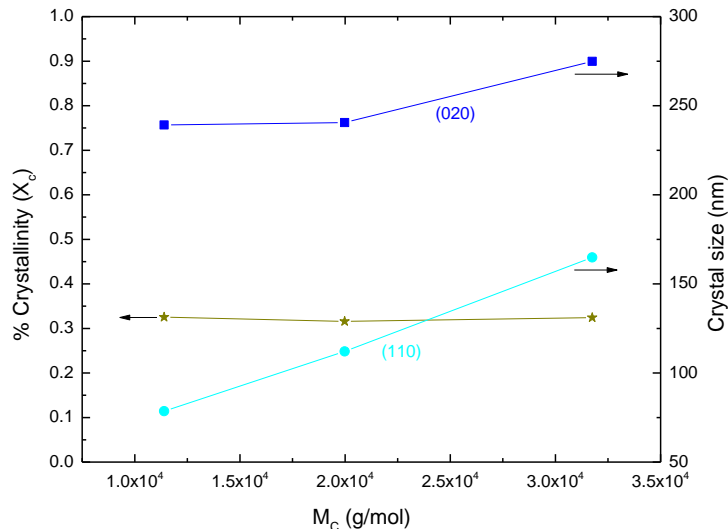


Figure 22 Crystallinity and crystal size in (020) α and (110) α crystallographic planes versus average molecular weight between crosslinks, M_c .

In order to verify the above hypothesis of reduction of crystallite size by crosslinking the indirect information of crystallite size was calculated. By using Scherrer's equation the crystallite size can be computed based on the assumption that there is no-strain in crystal. Crystallite size based on two major peaks, which are associated in the (110) and (020) planes, versus Vulcup[®] loads and average molecular weight between crosslink (M_c) are also represented in **Figure 22** to compared the effect of crosslink density on crystal size. As the concentration of Vulcup[®] increase, shorter chain section between crosslink sites, an enormous reduction in crystallite size has been observed. In **Figure 23**, by comparison to the pristine copolymer, the highest crosslink density sample (5 wt.% Vulcup[®] + 3wt.% TAIC) has all shown 29%, 26%, 59%, and 21% reduction of α phase crystallite size in (100), (020), (110) and (021) planes, respectively. This is probably caused by covalently bonding between chains restricts the

mobility of the chain section even in molten state. Since the crosslink junction cannot be incorporated in crystal lattice, the formation of ordered phase requires much more effort thus the crystal structures presumably prefer to take place in shorter chain sections between crosslink sites. Therefore the resultant crystal structures are became greatly smaller than free long linear chain precursor. Smaller crystallite is presumably cause reduction in ferroelectric domain size which benign the suffering due to the fact that larger domain lost more energy during polarization process [21, 25]. These results indicate that the proposed thermo-chemically crosslinking method is a promising approach to produce smaller crystallite structure without sacrificing the crystallinity of the P(VDF-CTFE) copolymer.

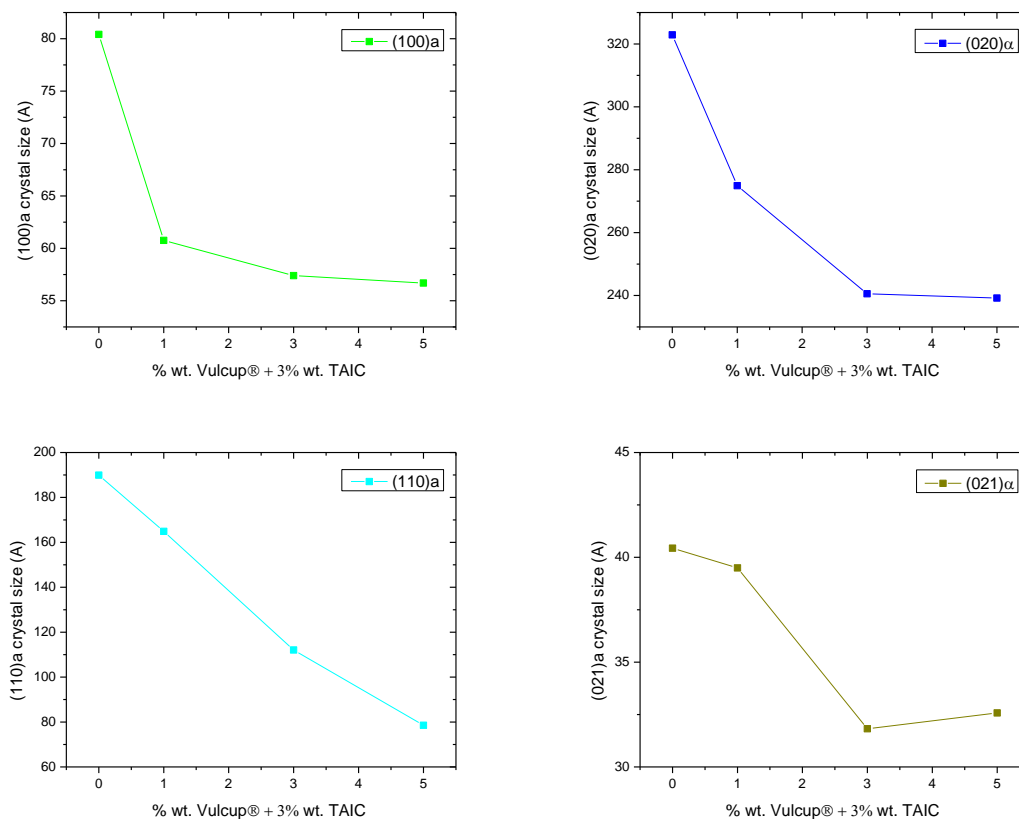


Figure 23 Crystal sizes of α phase crystals in all four crystallographic planes versus the Vulcup[®] concentration at 3 % wt. TAIC.

From XRD, it is also worth to consider the effect of crosslinking to the β phase crystal even though the fraction of this phase is very small due to the large amount of defects that prohibits the chain orientation in crystal, especially in all trans conformation. Based on our hypothesis, the α -phase crystal is preferred for high energy density storage and from XRD the 3% wt. Vulcup[®] + 3 % wt. TAIC system performs the best result in term of minimize formation of the polar β phase therefore maximize the content of α phase.

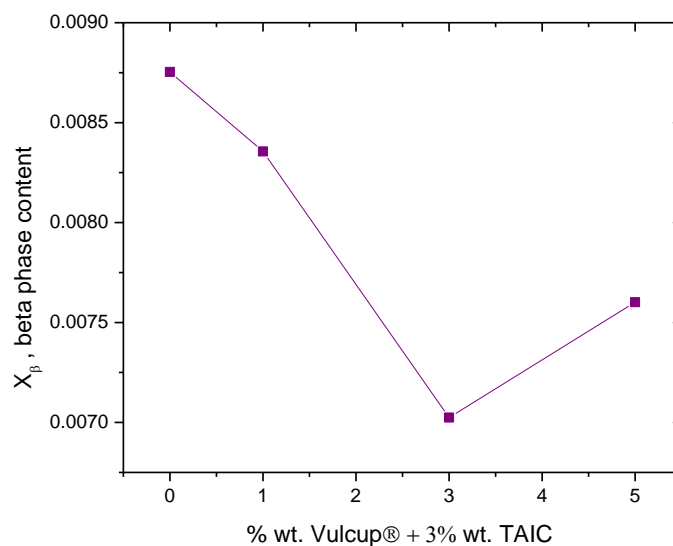


Figure 24 The α phase contents versus the Vulcup® concentration at 3 % wt. TAIC.

d. DSC Analysis

DSC thermographs (two heating/cooling cycles) of the crosslinked copolymers with different Vulcup® loads are compared with the pristine in **Figure 25**. The size of the crystallites that can be formed during crystallization process depends on how easily the polymer chains fill into the crystal structure. Polymers with crosslinked chains are less mobile thus only small and less stable crystals are produced at low temperature. Therefore these crystals have a low melting temperature. At first scan, the DSC endothermic peaks of crosslinked P(VDF-CTFE) display a slight melting temperature (T_m) depression which indicates the reductions of crystallite size. This is consistent with the XRD results described above. In addition, the crosslinked samples also have

narrower melting endotherms, which indicate a more uniform distribution of crystallite size was achieved.

Apart from strong endotherms, each curve also shows a minor peak at lower temperatures associated with the ferroelectric to paraelectric phase change of the Curie transition. [42] These results are in contrasted with the XRD where that polar crystal was undetectable. It is noteworthy to point that the DSC traces of the crosslinked samples show much weaker curie transition endotherms compared to the trace from the pristine. The intense, broad and merged to the T_m of curie transition endotherm in pristine also indicates the larger amount of ferroelectric phase in polymer structure. Moreover, this phase transition is still remained in the second heating scan of the pristine samples where the thermal memory of the samples has been erased. In contrast, there are no evident of phase transformation endotherms in the crosslinked samples in the second heating scan, these results reflect that the polar phase of P(VDF-CTFE) has been destabilized and cannot be reformed, in this cooling rate, by crosslinking. The cooling thermographs of both scan are almost identical. It is obviously to observe that the crystallization exotherms of crosslinked samples are much broader than the pristine. Again, this reflects the difficulty of crystal formation therefore the smaller crystallite structures were obtained by this crosslinking technique.

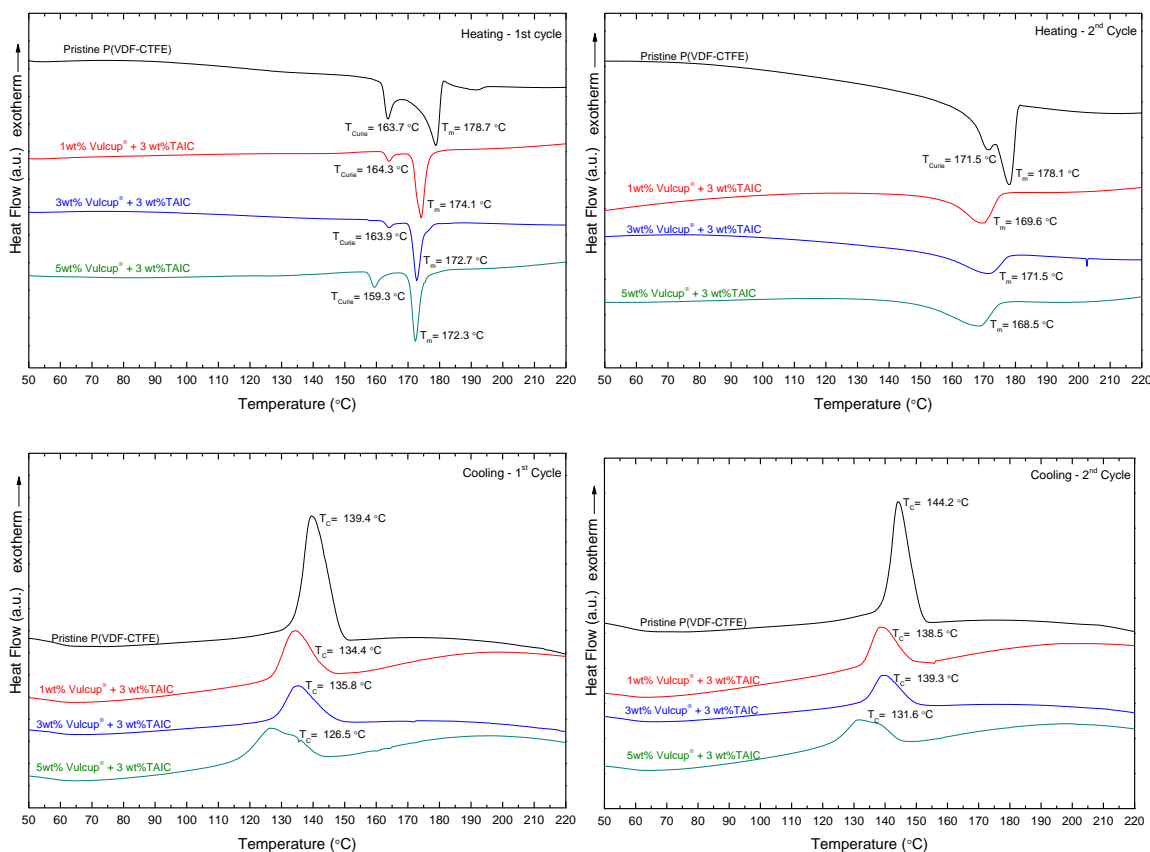


Figure 25 DSC thermographs of pristine and crosslinked P(VDF-CTFE). These DSC traces were collected with two (first (left) and second (right)) heating (top) and cooling (bottom) cycles with a ramp of 10 °C/min.

2.5 Dielectric Characterization

a. Weak-Field Dielectric Properties

The frequency dependence of the permittivity (ϵ') and of the dielectric losses ($\tan(\delta) = \epsilon''/\epsilon'$) for pristine and crosslinked P(VDF-CTFE) are shown **Figure 26**. The measurements were measured at 25 °C under an electric field approximately of 0.05

MV/m with the heating ramp of 10 °C/min. All crosslinked copolymers show a similar permittivity for entire range of frequency from 20 Hz to 1MHz, with significantly higher than the data from the pristine. This is probably affected by the polar-groups contained in the TAIC molecule that act as a 3D bridge between linear polymer chains. It is also believed that this permittivity rising is due to the increasing of polarization in amorphous-crystal interfacial region. Since the crystallite size has been decreased with minor change in crystallinity upon crosslinking, as shown by XRD, this interfacial region is expected to be greatly increased. Thus the total polarization should be increased. The losses of crosslinked copolymers are lower at low frequency range and remained the same level at frequency above 10 kHz compared to the pristine. This result suggests that the crosslink structure probably immobilizes the charge transportation and inhibits space charge formation which dominated at low frequency range.

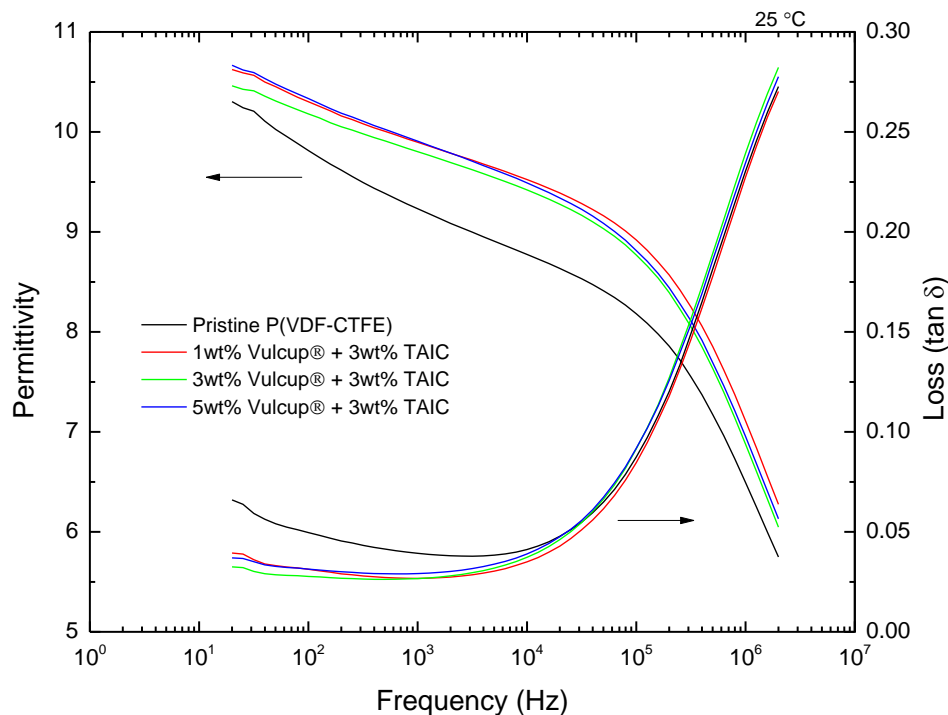


Figure 26 Permittivity and dielectric losses ($\tan(\delta)$) versus frequency measured at 25 °C for pristine and crosslinked P(VDF-CTFE).

The temperature dependence of the dielectric permittivity and of the dielectric loss tangent, at 100 Hz, is shown in **Figure 27** for pristine and crosslinked P(VDF-CTFE). All samples were tested with a heating/cooling ramp of ± 10 °C respectively. The increasing in dielectric permittivity and reducing in loss at room temperature are consistent with previous frequency-dependent results in **Figure 26**. A small peak associated in permittivity at approximately 50 °C is observed for all crosslinked samples. This peak is not recoverable upon the cooling ramp, see **Figure 28**. It is believed that this relaxation peak has been originated by the polarization of amorphous-crystallite interfacial region of the PVDF polymer. The orientation of dipolar in this region

significantly increases the permittivity response. Since the greatly reduction of crystallite size without significantly decrease in crystallinity, the amount of interfacial zone has been greatly increased by crosslinking. Therefore this relaxation behavior can be observed only in the crosslinked samples. It is also interesting to note that there is also a reduction of permittivity upon temperature rising to around 70 C has been observed only for the crosslinked samples. This behavior is probably caused by the recoil contraction of the polymer chain in amorphous phase.

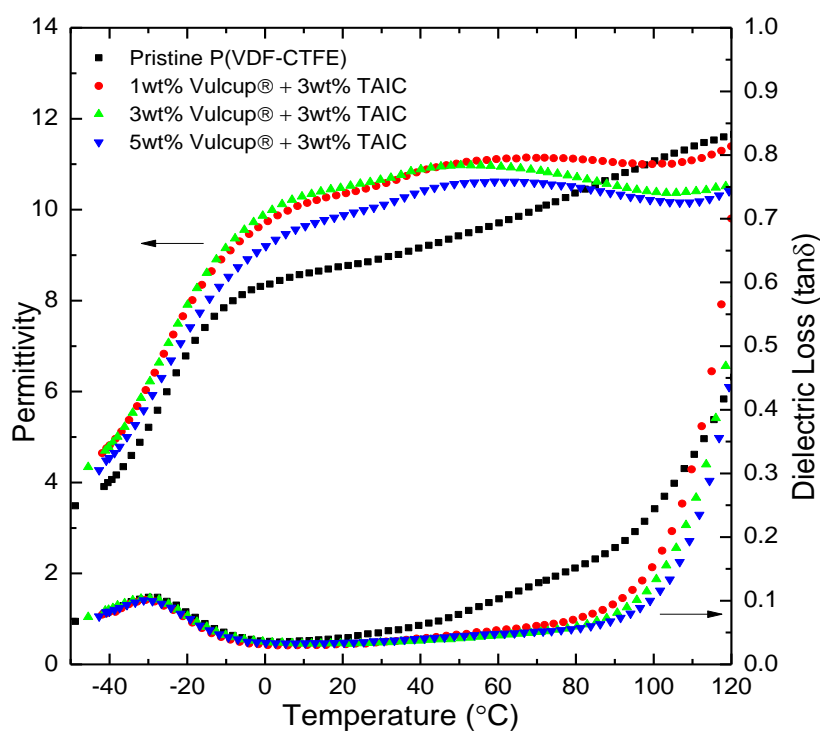


Figure 27 (a) Dielectric permittivity (ϵ') and of the dielectric losses ($\tan(\delta) = \epsilon''/\epsilon'$) versus temperature, at 100 Hz weak field with heating ramp of 10 °C/min, for the pristine and crosslinked P(VDF-CTFE).

The dielectric loss shows a major peak at about $-28\text{ }^{\circ}\text{C}$ which associate to the glass transition. Obviously, there is a greatly improvement of dielectric loss from temperature ranging from $10\text{ }^{\circ}\text{C}$ to $105\text{ }^{\circ}\text{C}$ upon introduction of crosslink structure compared to the pristine. For example, at $90\text{ }^{\circ}\text{C}$, the dielectric loss has been decreased up to 60% by the crosslinking process. As supported by the previous measurement at low frequency, these results indicate a reduction of space charge conduction in the crosslinked samples.

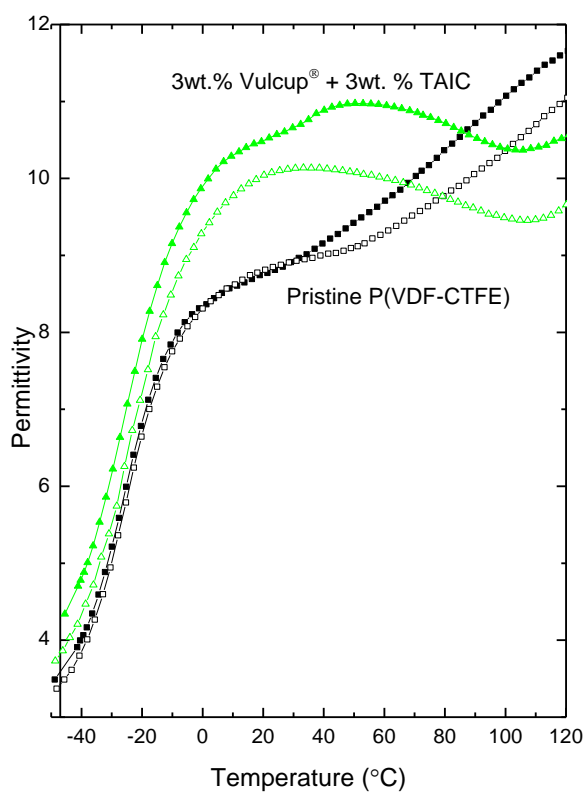


Figure 28 Dielectric permittivity of the crosslinked P(VDF-CTFE) with 3 wt. % Vulcup® + 3 wt. % TAIC compared to the pristine. The heating curves are assigned as closed symbols while the cooling as opened symbols.

b. High Field Electric Displacement

The high field performances of crosslinked and pristine P(VDF-CTFE) were examined by measuring a series of displacement-electric field loops (D-E loops) as an attempt to understand the behavior of the material during charge-discharge cycle. The electric displacement hysteresis loops for pristine and crosslinked P(VDF-CTFE) compared to the pristine are shown in *Figure 29* to *Figure 32* where the comparison of D-E filed loops of pristine and crosslinked P(VDF-CTFE) with the maximum electric field of 250 MV/m. *Figure 33*. The measurements were taken at 25 °C with a 10 Hz triangular unipolar signal.

It is clear that the crosslinked samples showed greatly improve in polarization. The crosslinked sample with 1 wt.% Vulcup[®] + 3wt. % TAIC showed the highest maximum displacement which is about 24 % higher than the value from the pristine. This marked improvement is consistent with the result from weak field analyses that showed the upward shifting of permittivity in crosslinked samples. However the polarizations are seemed to be systematically slightly decreased upon increase concentration of Vulcup[®]. The origin of these reductions of displacement can be described by the increasing of crosslink density which restricts the dipole orientation. However, it can be clearly seen that the D-E loops of crosslinked samples are much slimmer than the pristine. The 3 wt.% Vulcup[®] + 3wt. % TAIC sample showed the lowest remnant displacement which is only 40% of the value from the pristine. It is also worth to mention that the breakdown fields of crosslinked samples are greatly improved compared to the pristine because the crosslinked sample were able to endure the repeat charge-discharge cycles at higher field.

Although this D-E loops measurement technique is not a direct method to investigate the breakdown strength of materials, this increasing of breakdown endurance by crosslinking shows a significant promising feature of this crosslinked technique for elevating the service field of the capacitor.

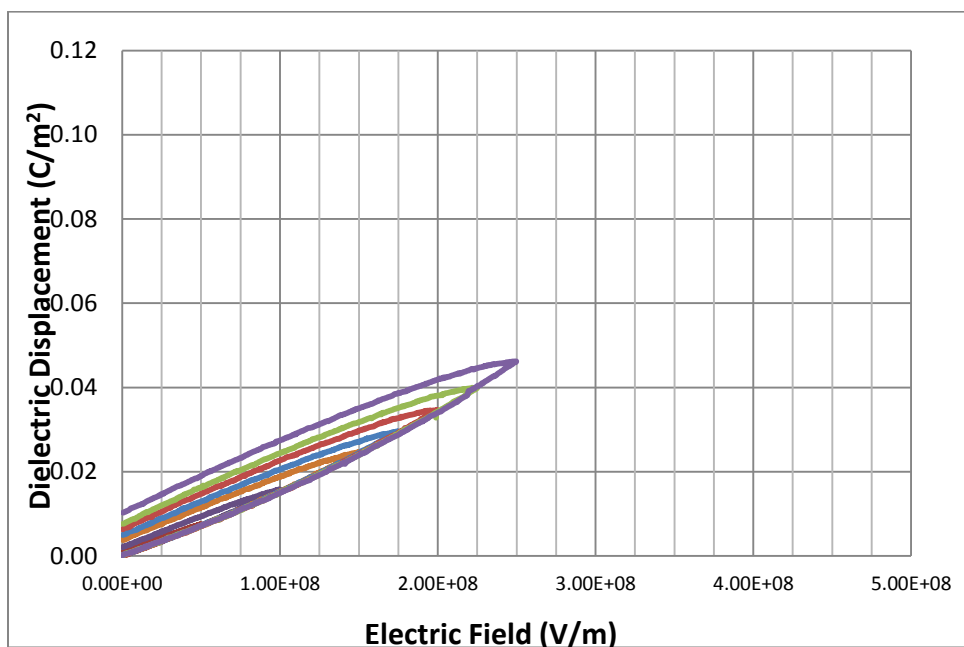


Figure 29 Electric displacement of pristine P(VDF-CTFE) under unipolar triangle load at 10 Hz.

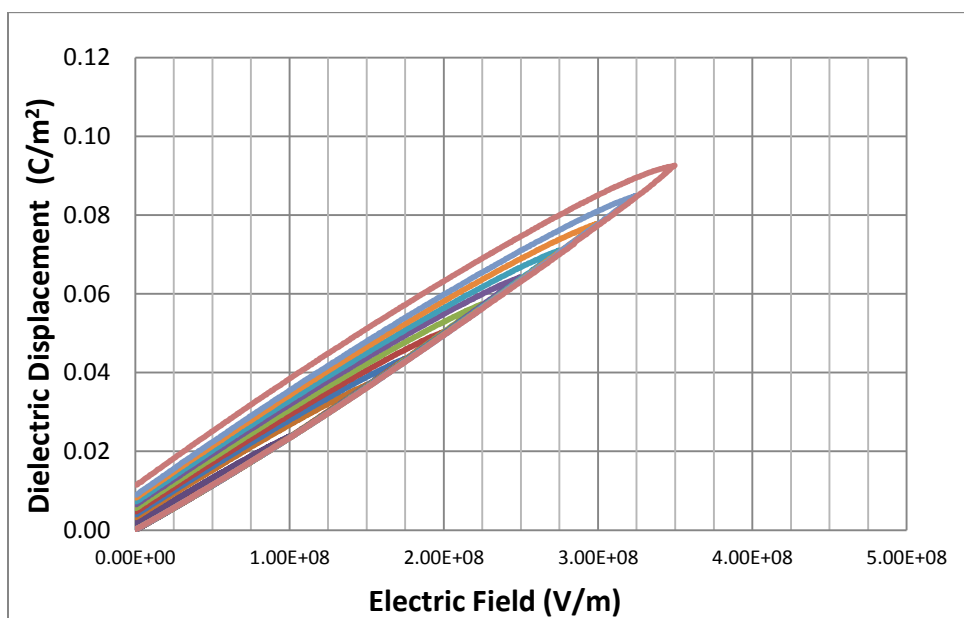


Figure 30 Electric displacement in crosslinked P(VDF-CTFE) using 1 wt. % Vulcup + 3 wt.% TAIC at 10 Hz.

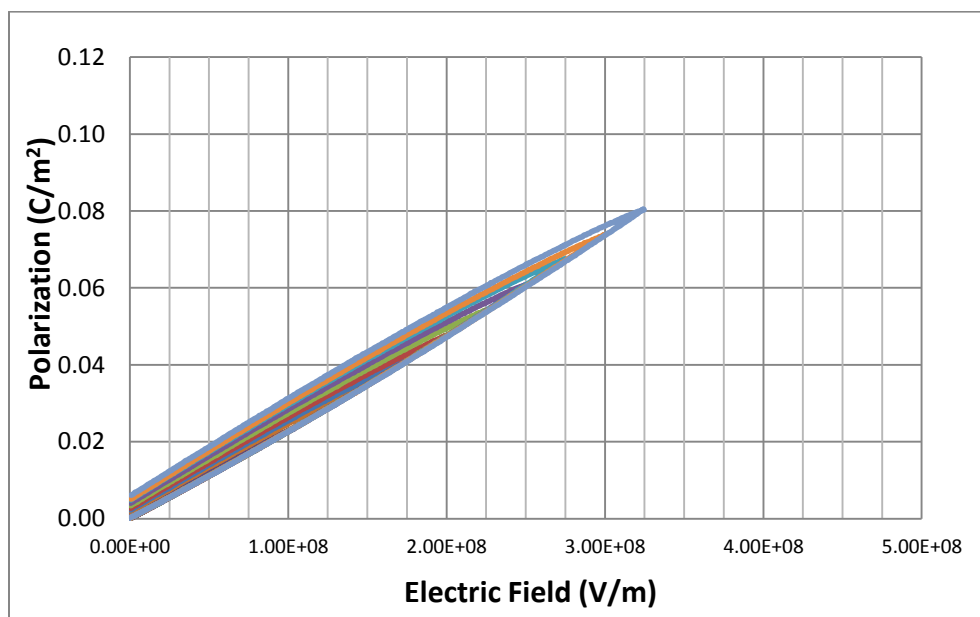


Figure 31 Electric displacement in crosslinked P(VDF-CTFE) using 3 wt. % Vulcup + 3 wt.% TAIC at 10 Hz.

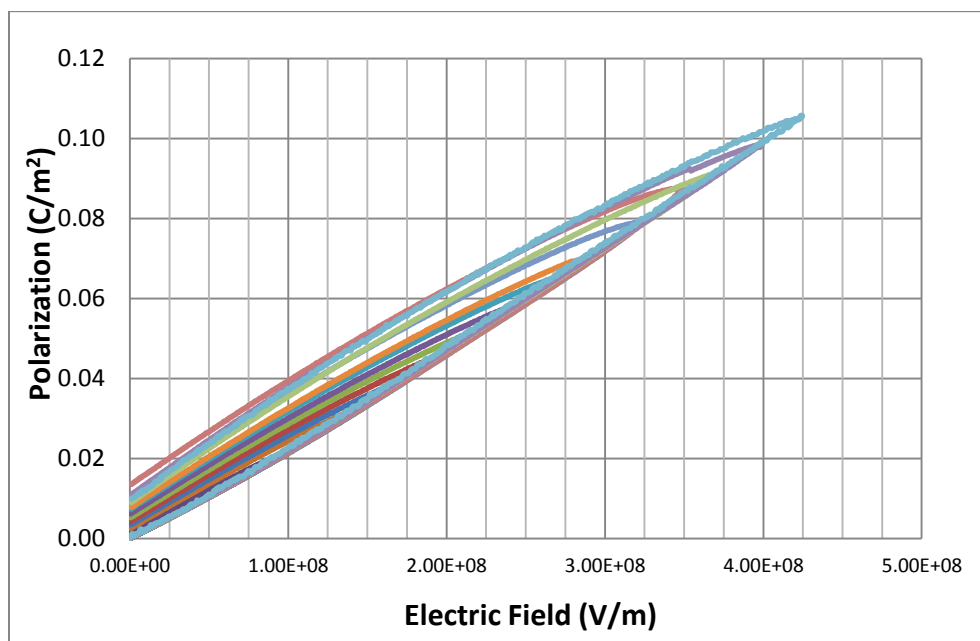


Figure 32 Electric displacement in crosslinked P(VDF-CTFE) using 5 wt. % Vulcup + 3 wt.% TAIC at 10 Hz.

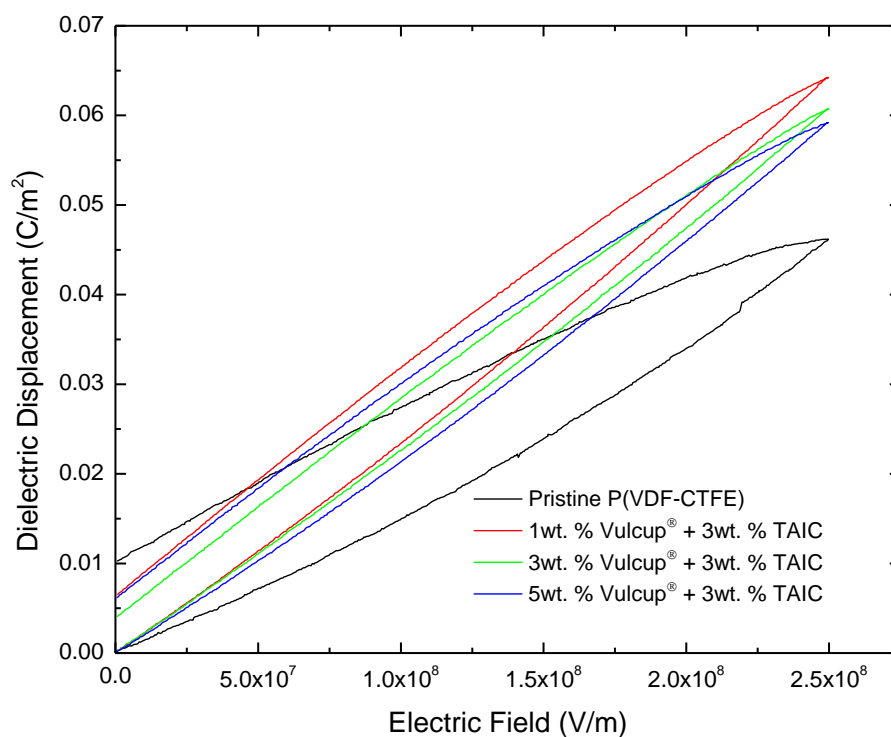


Figure 33 A comparison of displacement-electric field loops of pristine and crosslinked P(VDF-CTFE). The measurement was taken at 25 °C with a 10 Hz triangular unipolar signal with the maximum electric field of 250 MV/m.

Another benefit of D-E loops measurement is this technique allows us to calculate the energy density and loss associated with the charge-discharge process. The energy density at particular electric field can be obtained by integration of the area between the D-E loop curve and the corresponding ordinate. From **Figure 33**, the charge and discharge energy density can be calculated by the area between the lower and upper bound of the loop and the displacement axis respectively. Energy loss is then obtained by the area inside the loop, which is the difference between charge and discharge energy

densities. The electric field dependence of discharge energy density and energy loss of the crosslinked P(VDF-CTFE) copolymers compared to the pristine are shown in **Figure 37**. All crosslinked samples showed significant increase in the maximum discharge energy. Due to the fact that the pristine cannot endure electric field higher than 250 MV/m, only 4.8 J/cm^3 of energy density was obtained. While the crosslinked sample with 3wt.% Vulcup[®] + 3wt.% TAIC has energy density of 7.3 J/cm^3 which is 52% increase compared to the pristine at the same electric field applied. The higher breakdown strength of crosslinked samples leads their energy density reached up to 19.9 J/cm^3 for the crosslinked with 5 wt.% Vulcup[®] + 3wt. % TAIC at 400 MV/m. It is also interesting to compare this result to the high quality thin film of the same copolymer made by extrusion-blow molding reported in ref. [21], the crosslinked sample by our approach shows a very impressive ~60% improvement in energy density at 400 MV/m. However, more than 25 J/cm^3 of energy density can be achieved from the blown film due to their higher breakdown strength.

Hysteresis loops of all samples have a similar shape. In charging cycle, the changes of displacement versus the applied electric field are clearly nonlinear. The slopes of D-E loops of crosslinked sample are clearly higher than the pristine. This reflects that the effective permittivities are increased by crosslinking of the copolymer. The enhancing of permittivities of crosslinked samples has been observed in the weak-field measurements as mentioned earlier. The larger permittivities of crosslinked samples it allows to store more energy at the same electric field compared to the pristine. In discharging cycle, the changes of displacement upon releasing electric field are remained non-linear. However, all of the samples were not able to return to their original state

where no electric displacement found in the material. The relaxations of polarization in crosslinked samples are more rapid and tend to be more recoverable since after the electric fields were totally removed the measured displacements are very close to zero. This residue polarization is called remnant polarization. In contrast, the pristine seemed to have more residue charges that cannot be completely removed after the discharging cycle is done. Therefore the loss of the pristine is greater than the crosslinked ones.

A few important characteristics that can be drawn from the D-E hysteresis loops are summarized and presented in *Figure 34* to *Figure 36*, i.e., displacement at maximum load, remnant displacement and the ratio between these two displacements. Since the polarization is strongly depended on the applied electric field, each of these Figures is plotted as functions of the concentrations of Vulcup® and maximum applied electric fields. As an attempt to use D-E hysteresis loop for describing the ability to recover of the polarization, the ration of remnant displacement and the displacement at maximum applied electric field were calculated and presented.

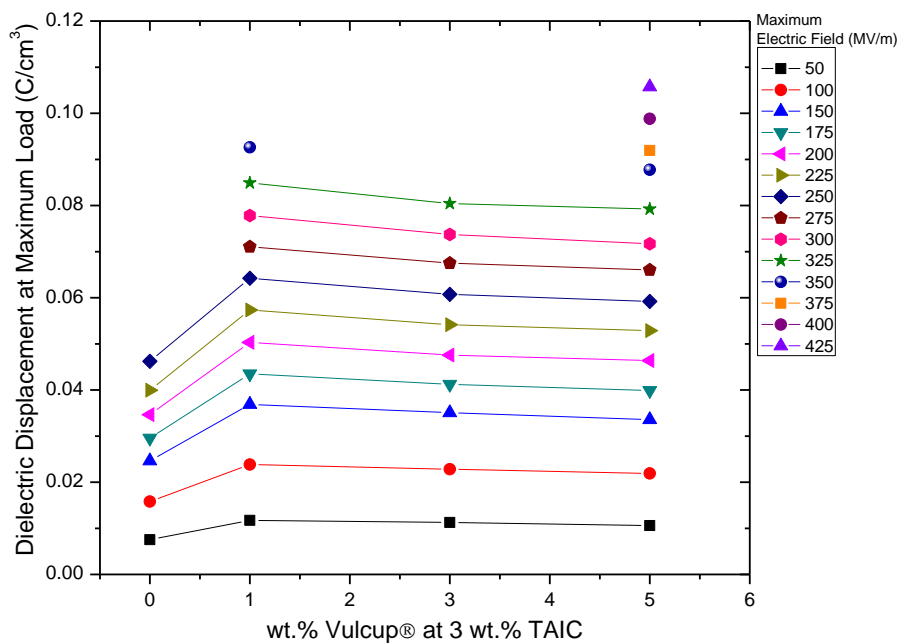


Figure 34 Dielectric displacement at maximum load versus concentration of Vulcup® at 3 wt.% TAIC.

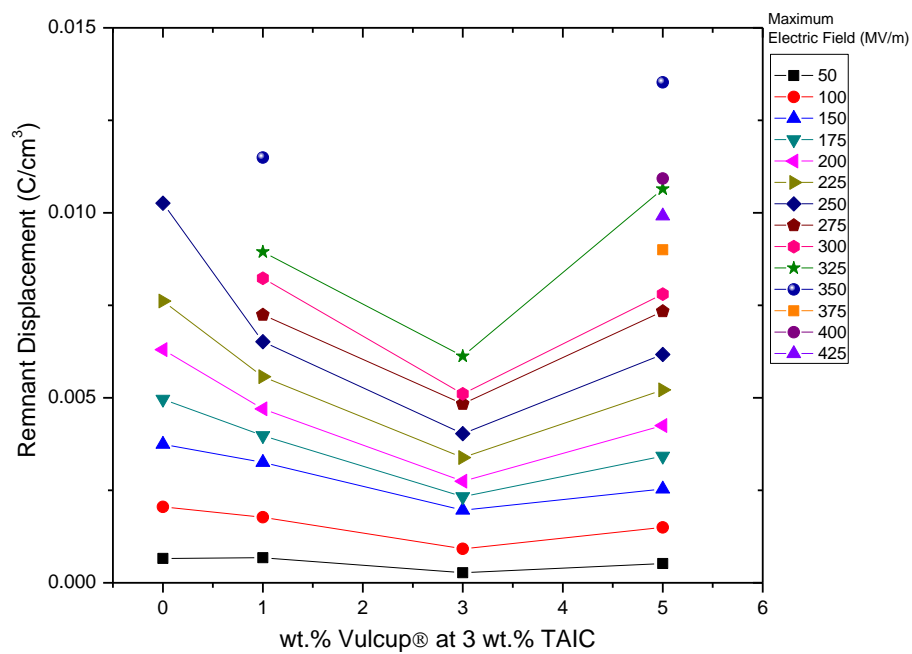


Figure 35 Remnant displacement versus concentration of Vulcup® at 3 wt.% TAIC.

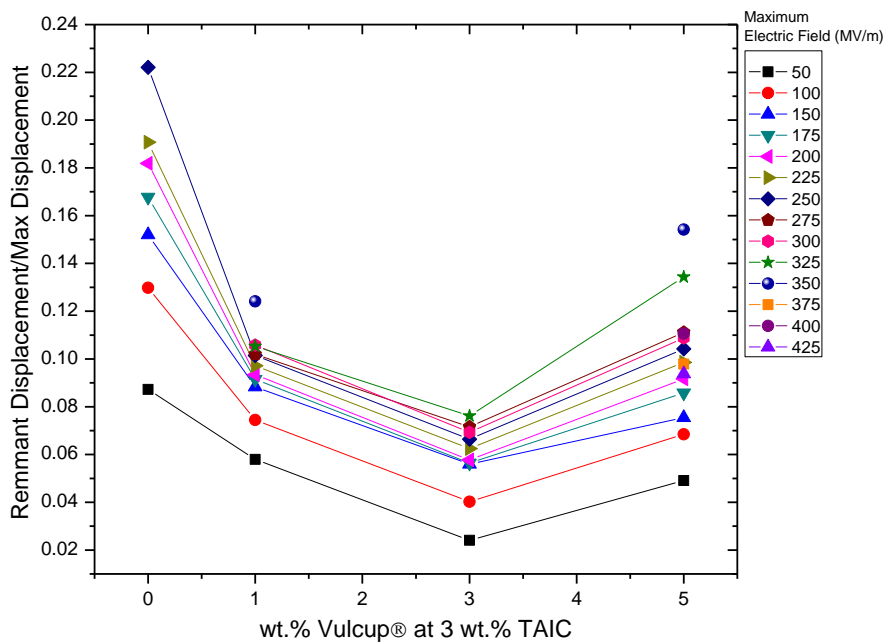


Figure 36 Ration between Remnant displacement and displacement at maximum load versus concentration of Vulcup® at 3 wt.% TAIC.

Dielectric displacements at maximum load, D_{\max} , of all crosslinked samples are higher than the pristine, see **Figure 34**. The 1 wt.% Vulcup® + 3 wt.% TAIC system has the strongest effect on enhancing this displacement value. Upon increasing of the maximum load this improvement of polarization is clearer, for example, at the maximum load of 250 MV/m, the crosslinked sample with 1 wt.% Vulcup® + 3 wt.% TAIC show 24% improvement of D_{\max} . However D_{\max} is decreased after further increase Vulcup® concentration. This reduction of D_{\max} is probably due to the higher crosslink densities of the samples with 3 wt.% and 5 wt.% Vulcup® may prohibit the orientation polarization in the crosslinked samples.

As clearly shown in **Figure 35**, the crosslinked sample with 3 wt.% Vulcup[®] + 3 wt.% TAIC shows a greatest reduction of the remnant displacement. The reduction of remnant displacement is clearer at elevated applied fields. At the electric field with the maximum load of 250 MV/m the remnant polarization was 61% decreased in the crosslinked sample with 3 wt.% Vulcup[®] + 3 wt.% TAIC compared to the pristine. This can be presumably conclude that the crosslink structure of the 3 wt.% Vulcup[®] + 3 wt.% TAIC system has an ability to return the polarization into its original state. To make this more clear the ratio of the remnant displacement and D_{\max} were calculated as presented in **Figure 36**. This ratio can reflect the recoverability after the material has been charged in the maximum loads. The crosslinked sample with 3 wt.% Vulcup[®] + 3 wt.% TAIC shows a greatest recoverability and the effect becomes stronger when the applied field exceeds 100 MV/m. It is also suggested by the result that the recoverability of the pristine strongly depends on the applied electric field but the crosslinked samples show gradual changes. This indicates that the polarization process in the pristine is getting more irreversible upon increasing of applied electric field. In contrast, the crosslink structure supports the recovering of the polarization process even at high field.

As mentioned earlier, the polarization deviation from the original state of the ending point is normally believed to be contributed to both polarization mechanisms and conduction of the leakage current. However, if the applied electric field is high enough it can lead to phase transformation process from the nonpolar phase to the polar ones. As the loops reach approximately 100 MV/m, it is believed that the majority of this loss is stemmed from ferroelectric phase switching losses in the material. The phase transformation leads to large increases in polarization but the transformation is difficult to

completely reverse when the field is removed resulting in a hysteresis of the polarization. General speaking, the phase transformation offers an increasing of storage energy upon charging cycle but, unfortunately, also prohibits the energy releasing process upon discharge cycle. This process creates loss in the ferroelectric based materials and is believed to be the major loss in P(VDF-CTFE). The results in *Figure 34* to *Figure 36* suggest that the crosslinking can concurrently increase the polarization and promote the recovery process.

The enhancing of polarization by crosslink structure maybe originated from two sources. The first source is the reduction of crystallite size. The smaller non polar crystal is easier to be induced and transformed in to polar phase. The polarization can also be influenced by crystal-amorphous interfacial structure, and because crosslinking induces formation of smaller crystal with barely decrease the total amount of the crystal content this interfacial region should be largely increased. Another source that may contribute to the increasing of polarization is that the crosslink site, TAIC, have polar groups in the chemical structure. These polar groups are readily to cause the orientational polarization in the materials resulting in increasing of polarization.

The crosslink structure is assumed to insist the recovery from phase transition process by providing a 3d network to the polymer chains. Since the transition from paraelectric phase to ferroelectric phase is the changes in the chain conformation. For instance, the TGTG' chain conformation in α -phase domain has to be rearranged into all-trans conformation of β -phase. The movements of polymer chain are time-consumed and often irreversible. Especially when the phase transformation originates or takes place at the amorphous/crystallite interfacial zone, this conformation switching can lead the chain

to delocalize in amorphous phase which is the free-volume filling process and it normally is an irreversible process above glass transition temperature. The crosslink sites, whose are located exclusively in the amorphous region, will act an elastic bridging between the polymer chains and therefore allow the phase transformation more reversible. However, this feature of crosslinking should be considered as a trade-off choice since it can adversely affect in reducing of the polarization if the crosslink density is too high.

Apparently, from the D-E loops, the crosslinked sample with 3 wt.% Vulcup[®] + 3 wt.% TAIC has performed the best result in term of loss reduction but suffered from lower breakdown strength. In contrast, the 1 wt.% Vulcup[®] + 3 wt.% TAIC system has performed the highest polarization but creates more loss. All of these parameters affect the energy density of the polymers. Electric field dependence of discharge energy density and energy loss of pristine and crosslinked P(VDF-CTFE) copolymers determine by D-E loops measurement are shown in *Figure 37*.

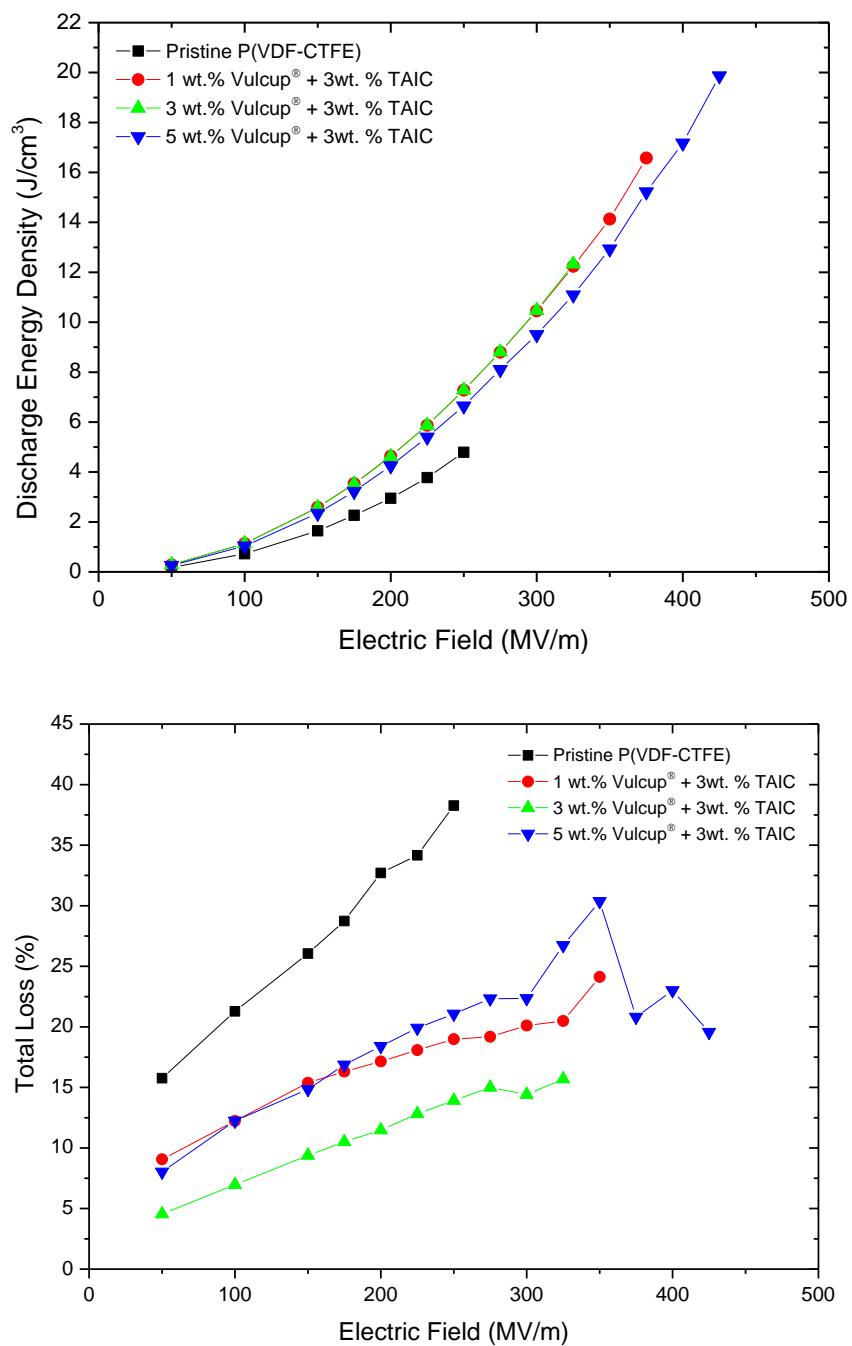


Figure 37 Electric field dependence of (top) discharge energy density and (bottom) energy loss of pristine and crosslinked P(VDF-CTFE) copolymers.

From *Figure 37*, all crosslinked samples showed significant increase in the maximum discharge energy. Due to the fact that the pristine cannot endure electric field higher than 250 MV/m, only 4.8 J/cm^3 of energy density was obtained. While the crosslinked sample with 3wt.% Vulcup[®] + 3wt.% TAIC has energy density of 7.3 J/cm^3 which is 52% increase compared to the pristine at the same electric field applied. The higher breakdown strength of crosslinked samples leads their energy density reached up to 19.9 J/cm^3 for the crosslinked with 5 wt.% Vulcup[®] + 3wt. % TAIC at 400 MV/m. It is also interesting to compare this result to the high quality thin film of the same copolymer made by extrusion-blow molding reported in ref. [21], the crosslinked sample by our approach shows a very impressive ~60% improvement in energy density at 400 MV/m. However, more than 25 J/cm^3 of energy density can be achieved from the blown film due to their higher breakdown strength.

As the field increases, the energy loss was observed in both pristine and crosslinked P(VDF-CTFE). However the field-induced developments of loss are different between the two systems. A steeper increasing of energy loss is observed in the pristine as the applied field increase above 100 MV/m compared to the crosslinked samples. As stated earlier, this rapid change is caused by the unrecoverable paraelectric to ferroelectric phase transition. While the increasing of losses is gentler in crosslinked samples as the field increases further, particularly above 175 MV/m. This behavior can be described by the effect of crosslink structures which comfort the destabilization of the polar phase generated upon increasing field. Thus the remarkable reduction of energy loss in the crosslinked samples can be clearly observed in entire range of electric field. At a field of 250 MV/m (breakdown field of the pristine) the energy loss of the

copolymer crosslinked by 3 wt.% Vulcup[®] + 3wt. % TAIC is only 13.92%, which is 64% less than that of the pristine.

In order to confirm that the crosslinked copolymers have better recoverability, the bipolar D-E loops measurements are performed. The Bipolar D-E hysteresis loops of pristine and 3 wt.% Vulcup[®] + 3 wt.% TAIC crosslinked (PVDF-CTFE) are presented in *Figure 38*.

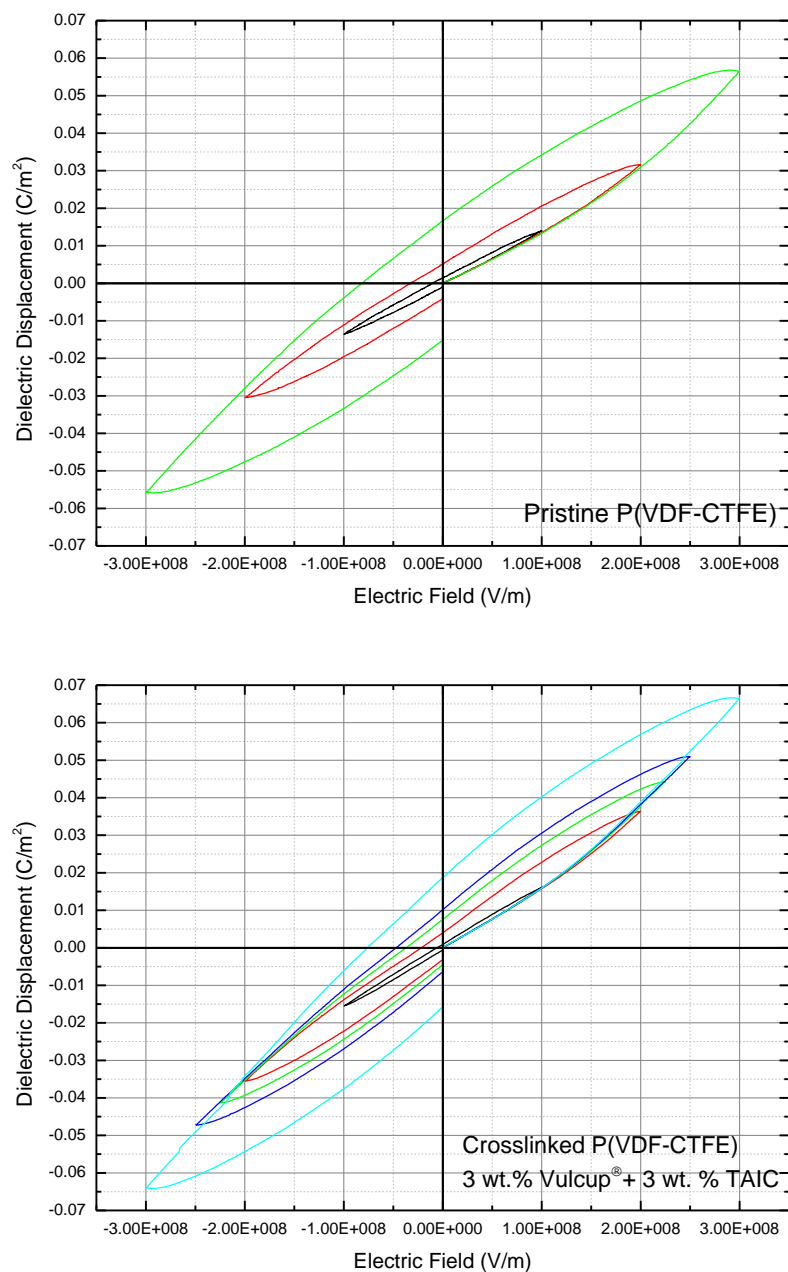


Figure 38 Bipolar D-E hysteresis loops of pristine and 3 wt.% Vulcup[®] + 3 wt.% TAIC crosslinked (PVDF-CTFE).

From these bipolar hysteresis loops, the coercive electric field can be extracted and summarized in **Figure 39**. The coercive field is basically a field that needed to apply

in the opposite direction of the charge-discharge process in order to force the residue polarization that left over back to zero. Apparently, the pristine requires more electric field to push the polarization back to the original state than the 3 wt.% Vulcup[®] + 3 wt.% TAIC crosslinked sample. This implied that it is more difficult in recovery of any polarization mechanism that occurred in the pristine than those in the crosslinked. The coercive results confirm the hypothesis that the crosslinking insist the recovery process.

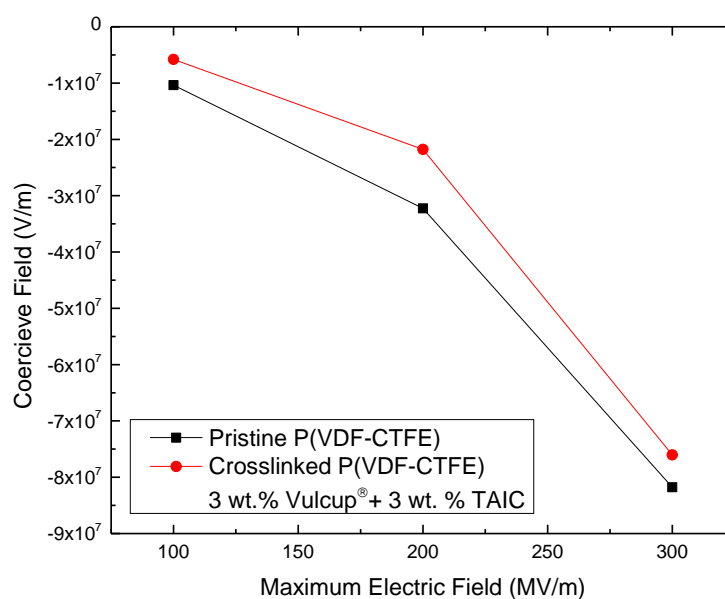


Figure 39 Coercive Field versus the maximum electric field of pristine and 3 wt.% Vulcup[®] + 3 wt.% TAIC crosslinked (PVDF-CTFE).

Capacitors always operate at elevated temperature due to the heat from surrounding devices and that generated themselves. From the weak-field dielectric spectra in **Figure 27**, the crosslinked samples have lower losses at the temperature ranging from 25 °C to 110 °C than the value of pristine sample. This reduction of losses

by crosslink is also expected in high field. Therefore the D-E loops measurements have been performed in elevated temperature environments in order to compare the characteristic of polarization during charging-discharging process. The electric field dependence of energy loss of the crosslinked P(VDF-CTFE) copolymers compared to the pristine at 50 °C and 70 °C are shown in **Figure 40**. The complete set of D-E hysteresis loops of all samples are shown in Appendix A.

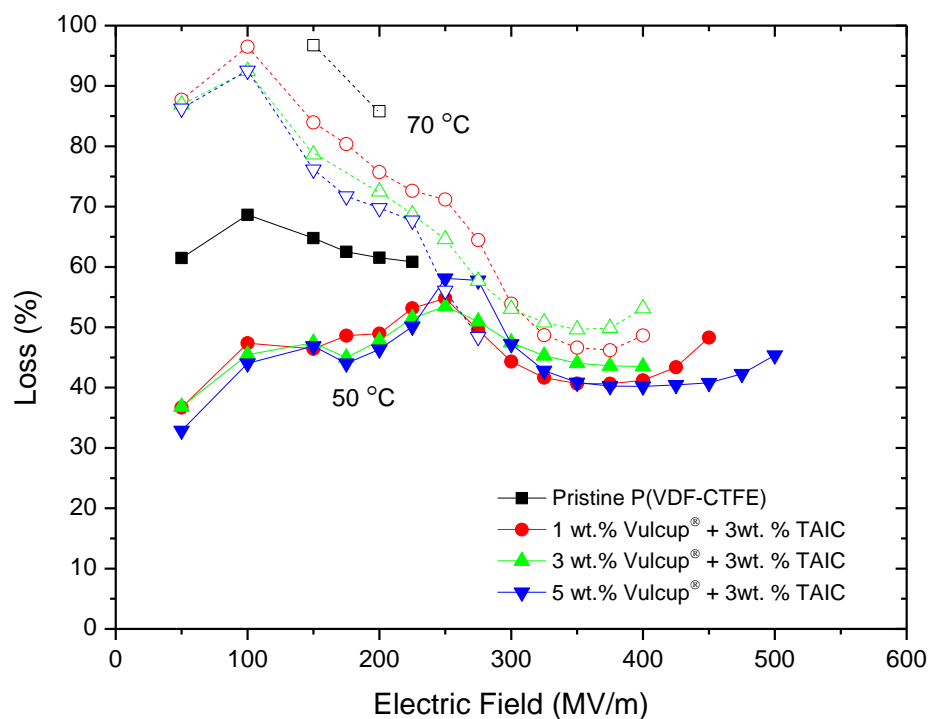


Figure 40 Energy loss of pristine and crosslinked P(VDF-CTFE) copolymers at 50°C and 70 °C .

2.6 Conductivity and Activation Energy

As stated earlier, the energy loss of P(VDF-CTFE) is comprised of dielectric loss, ferroelectric loss and conduction loss. Therefore it is worth to further investigate the conduction mechanism under high electric field to validate effect of crosslinking on the reduction of conduction loss.

It was believed by several research groups that the conduction mechanism of charge carriers in PVDF-based polymers is ionic conduction [43, 44]. Under an applied electric field, the ionic carriers drift from one electrode to another causing loss charge density. Another mechanism that is also possible is charge injection from the electrode and trap filling. In the presence of traps, increasing carrier injection will gradually fill the trap level until they are all filled. At this point further injected charges cannot be trapped and there will be a sudden increase in current. In the semicrystalline polymer, there are many traps with different energy levels due to the multiphase structure. Therefore the crosslinking method is believed to increase both number level of trap due to the defect generated. Indeed, as presented in XRD analysis section, the large reduction in crystallite size will lead massive increasing of interfacial region between amorphous and crystallite, thus the number of trap in crosslinked polymer should be increased. Another feature of this unique crosslinking approach is it allows us to insert a deep trap chemical structure into the polymer structure by a selection of co-agent. The co-agent will act as a crosslink site which bridging between polymer chains. In this research, TAIC is a well know radical trap that wildly used in a variety of chemical reaction. Although, to the author's knowledge, the mechanism of charge trapping conduction in the crosslinked structure of

TAIC is unknown this co-agent is very promising to be able to promote the level of trap in the copolymer.

In order to investigate the role of crosslinking to the conduction loss, a DC conductivity measurement has been performed. The time-dependence of DC conductivity for the crosslinked copolymers in comparison to the pristine is shown in **Figure 41**. The results have a strong confirmation that the crosslink structures inhibits charge transporting process since the conductivity is lowered almost by an order compared to the pristine.

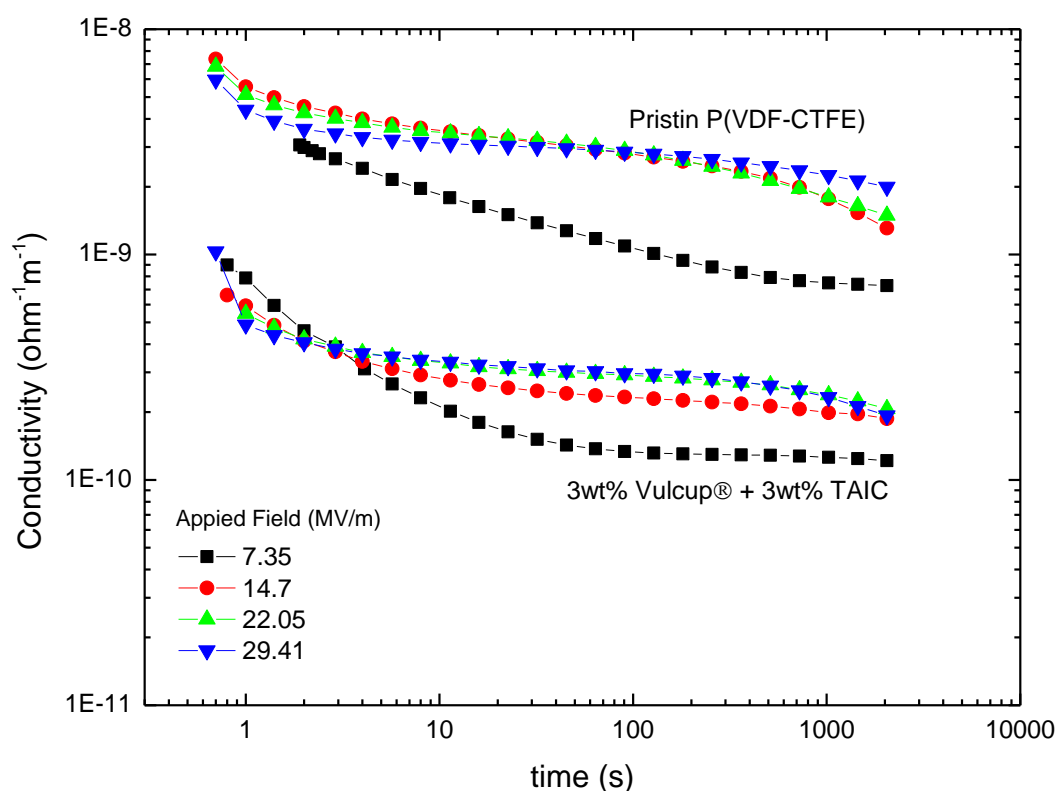


Figure 41 DC conductivity versus time of crosslinked and pristine P(VDF-CTFE) under different applied field at 25 °C.

The temperature-dependence of the conductivity of pristine and crosslinked copolymer was also performed to calculate the activation energy based on the Arrhenius plots. It was found that the activation energy has been increased from 1.273×10^{-19} J of the pristine to 1.602×10^{-19} J of the sample crosslinked by 3 wt.% Vulcup[®] + 3wt. % TAIC, confirming that conduction loss has been decreased by crosslinking.

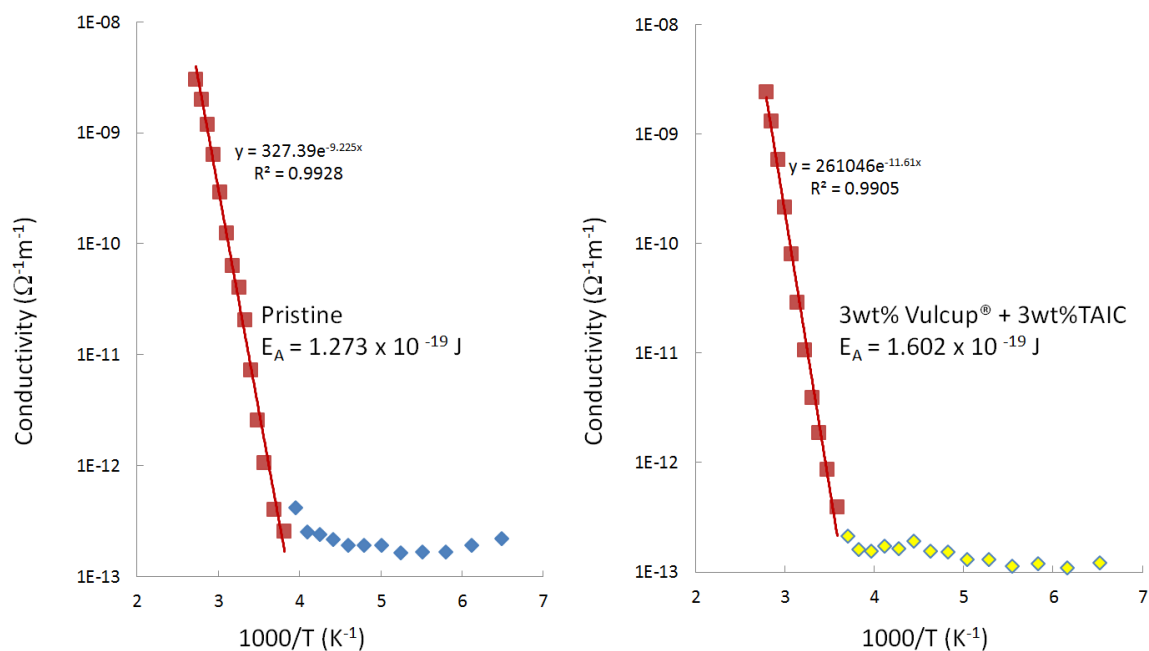


Figure 42 Arrhenius plots of pristine and 3 wt.% Vulcup[®] + 3 wt.% TAIC crosslinked (PVDF-CTFE).

2.7 Thermally stimulated depolarization current (TSDC)

From previous results, it is also suspected that the charge carriers have been blocked by traps generated by crosslinked structure in copolymer. In order to verify this hypothesis, the thermally stimulated discharge current (TSDC) measurement have been performed on both pristine and crosslinked samples. Thermally stimulated depolarization current (TSDC) measurements were carried out on pristine and 3 wt.% Vulcup[®] + 3 wt.% TAIC crosslinked (PVDF-CTFE). TSDC measurements were performed using a procedure illustrated in *Figure 43*. At first step, the samples were heated from room temperature to the poling temperature, under a poling electric field for a fixed poling time. Then the samples were quenched with liquid nitrogen to a lower temperature while maintaining polling field. After quenching the electric field was removed and sample temperature was raised with a constant heating rate. The depolarization currents were recorded upon raising temperature.

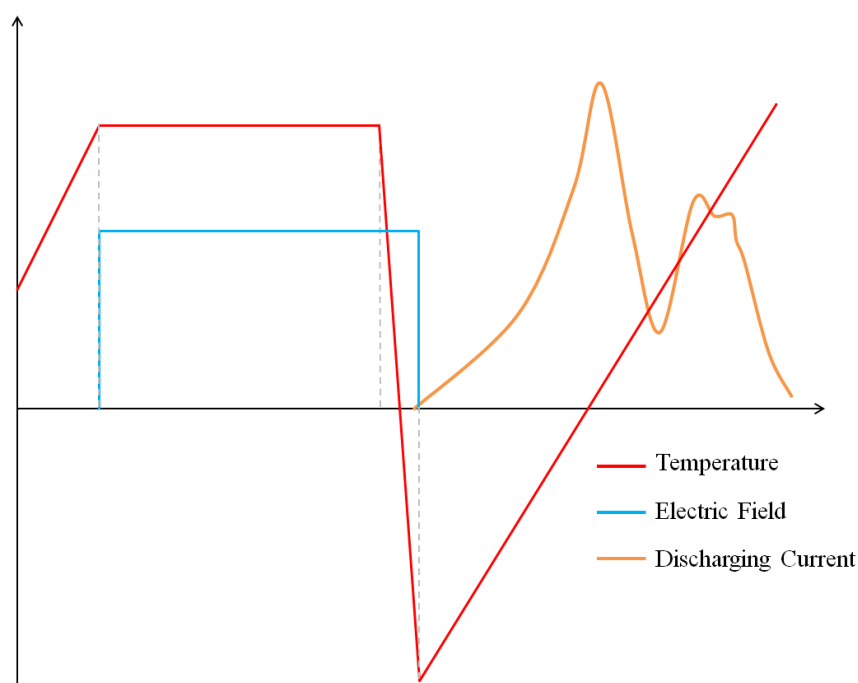


Figure 43 Schematic of TSDC measurement technique

The sample are first poled by a 10 MV/m field at elevated temperature ($\sim 100\text{ }^{\circ}\text{C}$) for 30 minutes and then quenched to liquid nitrogen temperature. The discharge currents are measured during a controlled heating ramp rate of $10\text{ }^{\circ}\text{C}/\text{min}$. The TSDC curve is then a plot between temperature and discharge current as shown in **Figure 44**. The β_c relaxation, which associated with the relaxation between the amorphous and crystallite, is shifted toward a higher temperature in crosslinked copolymer. This is an indicative of an increasing in activation energy which consistent with the result by Arrhenius plot. The γ_L and γ_H both are associated with the characteristics of trap formation. The upward shifting of these γ_L and γ_H relaxations suggests the formation of deeper traps in crosslinked copolymers and thus limits the loss caused by conduction.

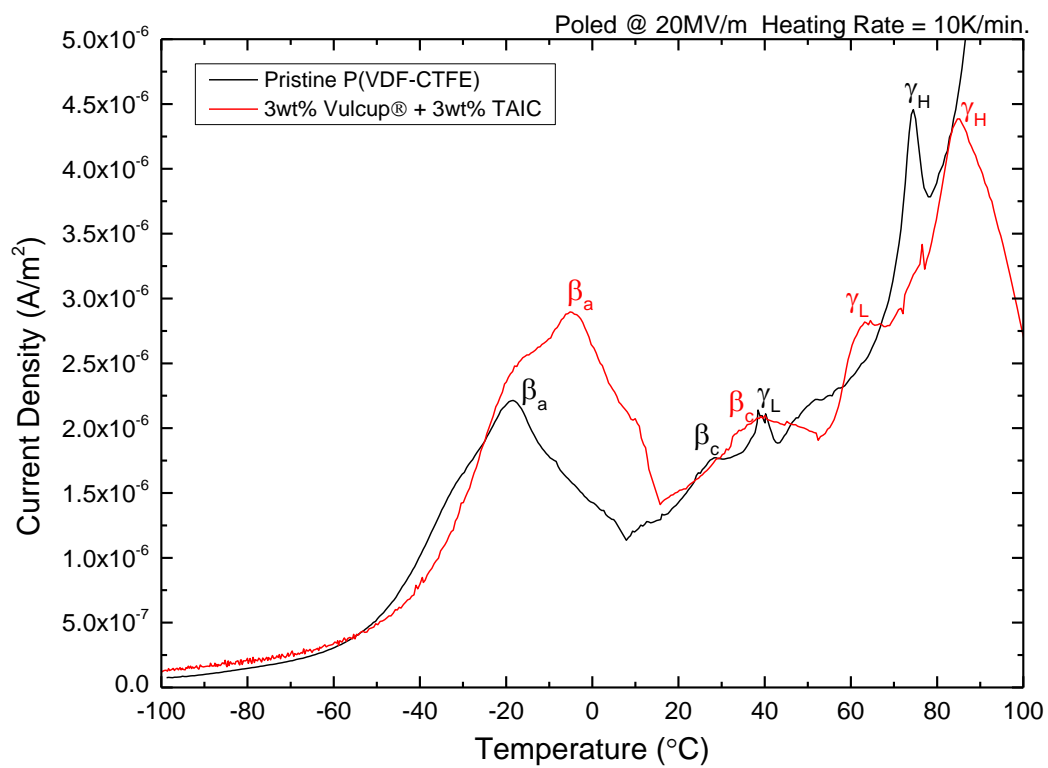


Figure 44 TSDC curves for pristine and 3 wt.% Vulcup[®] + 3wt. % TAIC crosslinked (PVDF-CTFE).

2.8 Electrical Breakdown Strength

Electrical breakdown is a complex phenomenon that occurs in insulating materials. As mentioned earlier, the electric breakdown strength gives a great influence in determining the energy density of a capacitor. In general, the dielectric breakdown of polymer insulators is used to describe process in which a considerable electric current increase as small voltage changes [45]. Breakdown process leads to formation of a conductive channel in solids. Along the conducting path there are broken chemical bonds and thermally degraded materials resulting from the large amount of energy that passes through a small cross sectional area. After the breakdown, capacitors perform more like a resistor since the conduction exists.

For defect-free polymer thin film under dc field, typically used in capacitor, there are two possible breakdown mechanisms, thermal breakdown and electromechanical breakdown. Thermal breakdown occurs upon unbalancing between the heat generated and removed from the insulation either macroscopically or, more usually, in small area. During the conduction taken place in materials it means that there is Joule heat (σE^2) being released within the dielectric. This serves to increase local temperature and hence the conductivity. The increase in the conductivity then leads to more Joule heating and further rises in the temperature and so on. If the temperature cannot be limited by thermal conduction then the thermal runaway condition is promptly to be occurred. The increasing due to the conduction leads to grow electric current until a discharge occurs then the material breaks down. Thermal breakdown is frequently found in the local regions where electrical conductivity is larger than the surrounding area. In this case if

the material has an insufficient thermal conductivity to dissipate heat, that generated by Joule's heating, this area becomes a hot spot where the local melting and physical and chemical erosion may take place. A conducting channel can be formed and eventually the device will be discharge.

Electromechanical breakdown is another breakdown mechanism believed to be common in polymeric materials since they are relatively soft and can encounter high electrostatic stresses at high electric fields. Electromechanical breakdown can be represented generally by the balancing equation between stresses that were generated electronically and mechanically.

$$\sigma_{EM} = \sigma_r$$

Equation 19 - Electromechanical stress balance. Where σ_{EM} is the electromechanical stress and σ_r is the repulsive stress.

Electromechanical breakdown occurs due to electrostatic attraction of the electrodes which decreases the thickness of the dielectric by an amount depending on the elastic modulus. If the applied voltage is maintained, the electric field ($E=V/d$) increased due to the decrease in thickness. This further leads to a greater compressive load, which also decrease thickness. At the breakdown field the stress induced by the applied field exceeds the yield stress of the film causing a rapid collapse and discharge between the electrodes. In addition, as mentioned earlier, the increase in E (by smaller d) causes more Joule heating in the dielectric. If the heat cannot be removed efficiently the temperature will be increased and hence lowers the elastic modulus, thereby accelerating the

breakdown mechanism. It is generally believed that certain thermoplastic polymers are governed by the electromechanical dielectric breakdown mechanism, especially at temperatures close to their softening temperatures. Electromechanical breakdown is common for rubbery materials above the glass transition temperature since a large drop in modulus is associated with this thermal transition making the rubbery polymers prone to deformation from the electromechanical stress [4].

Incorporation of the three dimensional networks in polymer structures has been well known as an effective way to increase mechanical properties such as modulus, yield strength, stress at breaks and the ultimate strength. As mentioned above, the better mechanical property lowers the possibility of the materials to break by the electromechanical mechanism. Therefore, the crosslinking method has been investigated in many polymer systems as an effective approach that can greatly improve the breakdown field. For example, in earlier works of Stark and Gordon on 1955, it has been demonstrated that electrical breakdown of linear polyethylene increases by crosslinking using high energy radiation, as shown in Figure 45 [46]. The results from their studies also confirmed that the crosslinked sample whose has superior Young's modulus performed a significant stability at high temperature. However this irradiation process has some drawbacks in terms of dielectric permittivity. As a matter of fact, the result in ref [47] shows a reduction of permittivity of polypropylene after high energy irradiation due to the formation of byproducts.

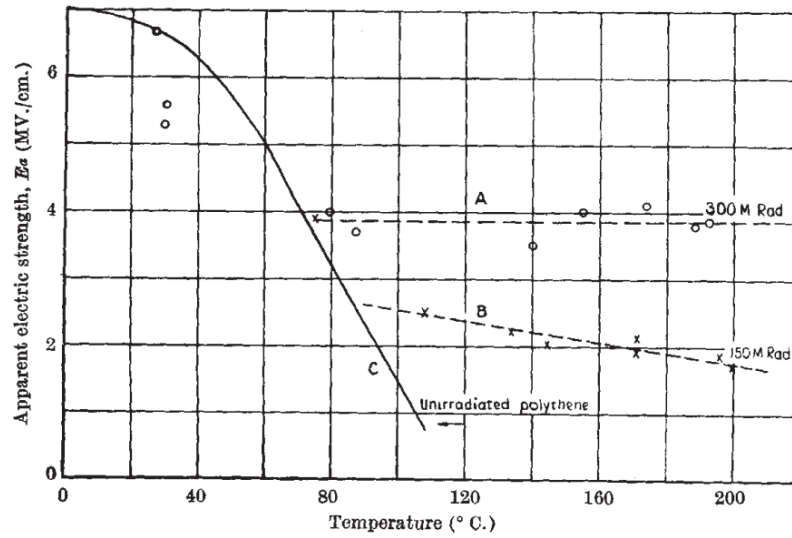


Figure 45 Dielectric breakdown of high energy radiation crosslinked polyethylene [46].

Enhancing breakdown strength of dielectric materials is very important for high voltage application. It is also a benefit of polymeric materials over the ceramic counterparts. It is also worth to mention that the higher breakdown strength also provides an additional ability for the device to operate at higher field with higher reliability when the dielectric materials are applied to a particular electric field.

The electrical breakdown strengths were characterize based on the Weibull failure probability function: $P=1-\exp[-(E/\alpha)^\beta]$, where P is the probability of failure at the applied field lower or equal to E . The α and β parameters define the scale and shape of the distribution. The Weibull equation may be transformed to: $\log_{10}[-\ln(1-P)] = \beta \log_{10}E - \beta \log_{10}\alpha$. A Plot of $\log_{10}[-\ln(1-P)]$ against $\log_{10}E$ is a straight line with a slope equal to β and the scale parameter α is equal to the field at the intercept with the abscissa (i.e. where $\log_{10}[-\ln(1-P)] = 0$, $P=0.632$ or 63%). In other words, α is the field strength which there is a 63% probability for the sample to breakdown, while β evaluates the scatter of data.

The Weibull analysis of breakdown strengths for the pristine and crosslinked P(VDF-CTFE) were demonstrated in **Figure 46** and the results are summarized in **Table 2**

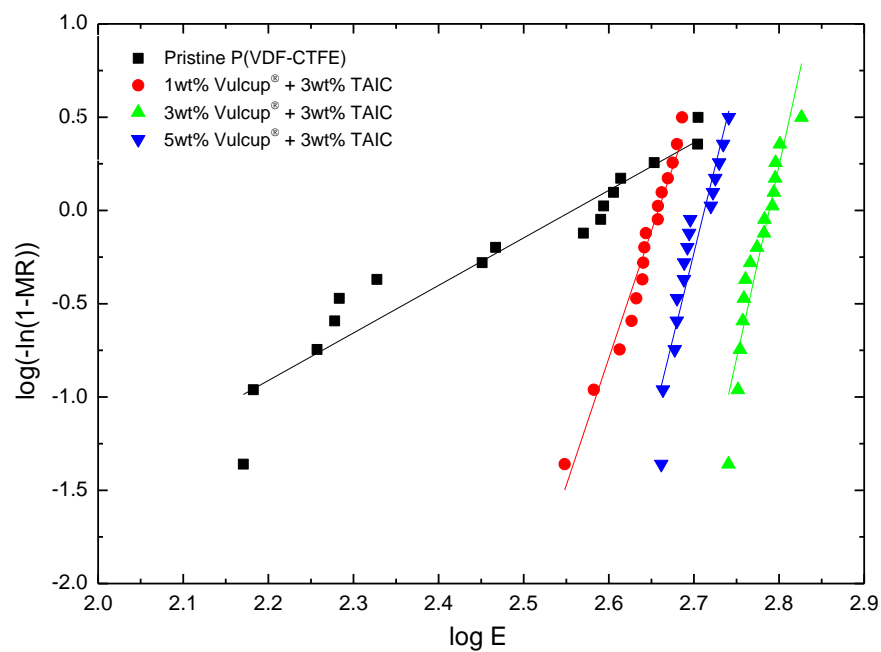


Figure 46 The Weibull analysis of breakdown strengths for the pristine and crosslinked P(VDF-CTFE).

Table 2 Weibull parameters of the pristine and crosslinked P(VDF-CTFE)

Polymer	α (MV/m)	β
Pristine P(VDF-CTFE)	361.11	2.55
1wt% Vulcup® + 3wt%TAIC	455.15	13.63
3wt% Vulcup® + 3wt%TAIC	614.37	20.68
5wt% Vulcup® + 3wt%TAIC	515.52	18.60

Figure 46 clearly demonstrates the improvement of the breakdown strength exhibited by crosslinked samples compared to the pristine. The sample with 3 wt.% Vulcup® + 3wt. % TAIC shows a marked improvement of 70%, the α increases from 361 MV/m for the pristine copolymer to 614 MV/m for the crosslinked sample. In addition, these crosslinked samples show an improvement in reliability compared to the pristine as reflected by the remarkable increase in β value. This improvement of breakdown strength by crosslinking can be originated by two reasons; first, the energy loss has been drastically decreased therefore the possibility of failure mechanism due to the electrical power dissipation by heat has been reduced; second, the presence of the crosslink structure in copolymer improves the mechanical properties of the copolymer thus reduced the possibility of electromechanical failure. Since we already showed the great improvement in reduction of the energy loss earlier, in order to verify the latter hypothesis of enhancing breakdown strength by improving of mechanical strength, the mechanical testing has been performed.

2.9 Mechanical Properties

It is believed that the electromechanical breakdown is the mechanism dominates in the failure of PVDF-based polymer at high electric field. This is because of the fact that the ferroelectric nature of these polymers leads to electrostrictive respond upon the application of electric field.

Garton and Stark [46] explain the breakdown behavior of various polymers such as polyethylene and polyisobutylene using electromechanical breakdown mechanism. In their works, the mechanical deformation caused by Maxwell stress due to the applied electrical field is considered as a major cause of the failure. The attraction of the charges on opposite electrodes from both sides causes mechanical stress by mutual Coulombic forces as the voltage is applied. The compressive stress is believed to cause a considerable reduction in thickness of the dielectric in the vicinity of breakdown field. The attractive force can be calculated by the differential of the storage energy in the system with respect to the electrode displacement at constant applied voltage as expressed by:

$$F = \left(\frac{\partial U}{\partial d} \right)_V = \frac{\partial}{\partial d} \left(\frac{1}{2} CV^2 \right)_V$$

Equation 20 – Compressive force govern by mutual Coulombic attraction. Where C is the capacitance, d is the thickness of dielectric and V is the voltage.

For a parallel-plate capacitor, we can express the compressive force per unit area:

$$\frac{F}{A} = -\frac{1}{2} \varepsilon_0 \varepsilon \left(\frac{V}{d} \right)^2$$

Equation 21 - Compressive force per unit area of a parallel-plate capacitor. Where A is the cross-sectional area, ε_0 is the permittivity of free space and ε is the relative permittivity of the dielectric.

As mentioned in *Equation 19*, at equilibrium, the compressive force is balanced by the elastic restoring force as expressed by

$$\frac{1}{2} \varepsilon_0 \varepsilon \left(\frac{V}{d} \right)^2 = Y \ln \frac{d_0}{d}$$

Equation 22 – Force balancing between electro-compressive force and elastic restoring force. Where Y is Young's modulus for the dielectric and d_0 is the original thickness of the dielectric.

In their paper, Stark and Garton define their failure criterion from an instability that occurs when the expression $d^2 \ln(d_0/d)$ has a maximum with respect to d when $d/d_0 = e^{-1/2} = 0.606$. This can be implied that there is no stable thickness smaller than $0.606d_0$ therefore the failure occurs due to mechanical collapse at this critical field.

$$E_b = \left(\frac{Y}{\varepsilon_0 \varepsilon} \right)^{\frac{1}{2}}$$

Equation 23 - Electromechanical breakdown equation.

Therefore, the effect of electromechanical breakdown strength of the dielectric can be determined from their relative permittivity and Young's modulus. In this equation, the breakdown field of the dielectrics is inversely proportional to the square root of the high field dielectric constant. For nonlinear dielectric materials, such as PVDF-based polymers, the dielectric constant at high electric field can be quite different from the weak field value. The high field dielectric constant can be calculated from the slope of the P-E loops. The electromechanical breakdown strength is also proportional to the square root mechanical modulus. Therefore the improvement of breakdown strength can be achieved by increasing the mechanical strength. To test this hypothesis the mechanical properties of pristine and crosslinked copolymers have been conducted using dynamic mechanical analysis (DMA).

The dynamically mechanical properties of the pristine and crosslinked copolymers were measured with DMA at low strain proportion. The samples were measured to a maximum strain of about 0.30% where the complex modulus was recorded. The complex modulus is represented by

$$G = G' + iG''$$

Equation 24 – Definition of complex modulus. Where G is the complex modulus, G' is the storage modulus, and G'' is the loss modulus.

The storage moduli, G' , of both pristine and 3 wt.% Vulcup[®] + 3 wt.% TAIC crosslinked (PVDF-CTFE) are decreased as the temperature was rising. Apparently, the modulus of the crosslinked sample is higher than the pristine almost the whole range of measured temperature (from -40 °C – 100 °C). It is obvious that improvement of the modulus increases the breakdown field of the crosslinked sample.

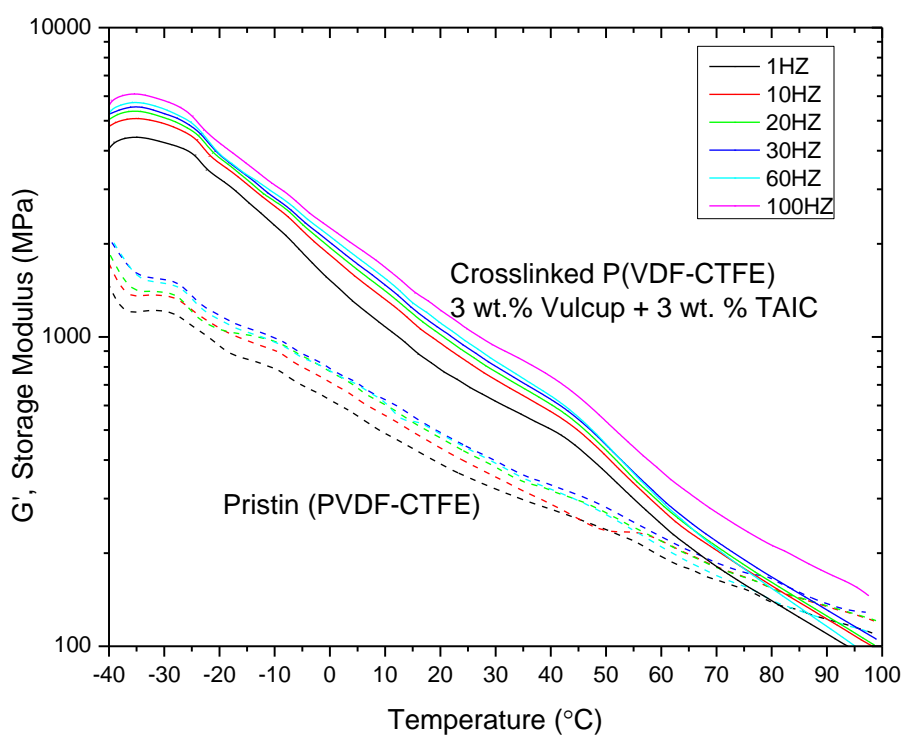


Figure 47 Storage moduli of the pristine and 3 wt.% Vulcup[®] + 3 wt.% TAIC crosslinked (PVDF-CTFE).

The predicted values of breakdown strength were calculated based on electromechanical model *Equation 23*. The summarized calculations are shown in **Table 3**. Obviously, the model fails to predict the breakdown strength. The failure of the

electromechanical model is stemmed from a numerous sources. The permittivity of both pristine and crosslinked (PVDF-CTFE) were extracted from the weak field measurement. These values are known to be not accurate since the permittivity of ferroelectric polymer depends on the applied electric field. The permittivity of the samples can possibly reach up to over one order of the weak field value. Also, the Young's moduli which is calculated based on the root mean square of storage modulus and loss modulus are not accurate in soft material such as polymers. The Stark-Gordon model has been modified to fit in many polymer systems. For example, the model was modified by replacing the Young's modulus with yield stress that can be archived by tensile measurement, this modified model has found to be more accurate. In some polymers the model has been unified to the thermal breakdown model to give a good prediction of their breakdown behavior. However, in this research there are no more attempts to clarify the accuracy of the model.

Table 3 Predicted breakdown strength values from electromechanical breakdown model and measured values of the pristine and 3 wt.% Vulcup[®] + 3 wt.% TAIC crosslinked (PVDF-CTFE)

Sample	ϵ	G' (MPa)	G'' (MPa)	Y(Calc.) (MPa)	E _b (Calc.) (MV/m)	E _b (measured) (MV/m)
Pristine	10.4	385.65	41.24	387.85	2031	316
3V3T	10.6	811.38	123.01	820.66	2927	614

Chapter 3

Thermally Processable crosslinking of P(VDF-CTFE)

Our previous studies have shown that the radical initiator of 1,4-bis(t-butyl peroxy) diisopropylbenzene (Vulcup[®]) and co-agent of triallylisocyanurate (TAIC) (*Figure 15*) are effective in producing highly crosslinked P(VDF-CTFE). The combinations of these two chemicals, however, limit some features for introducing the system into mass production, e.g., early crosslinking in compounding process and difficulty in thickness control.

In this chapter, we will develop series of crosslinking system which are thermally processable, i.e., thin films can be produced by melt extrusion. For this purpose, we will work with properly selected radical initiator, such as bicumene and photo-initiators, but remain our focus on TAIC co-agents. Consequently, these crosslink compound film can be produced by melt extrusion method and then crosslinked, which provides a low cost mass fabrication method of the capacitor thin films.

3.1 Introduction

Recently, demand and applications for electrically polymer dielectric have rapidly growth. For example, in 2005 global manufacturing of thin biaxial oriented polypropylene (currently one of the fastest growing polymers particularly for capacitors) was estimated at 6500 tons. With an average thickness of 7 μm , this amount of

polypropylene can make dielectric film to cover the area of the USA (c.a. 9000000 km²) [48]. In order to launch the thermo-chemical crosslink technique of VDF-based polymers into mass productions, it is necessary to seek effective polymer, initiator, and co-agent systems. In the needs of minimizing investment cost, the crosslink ingredients must provide industrial friendly that readily to adapt the formulae into the typical process. In this chapter, therefore, we seek some other initiators to replace peroxide in chapter 2.

From previous results in chapter 2, P(VDF-CTFE) can undergo free radical crosslinking reaction with 1,4-bis(t-butyl peroxy) diisopropylbenzene (Vulcup[®]) and co-agent of triallylisocyanurate (TAIC). It is obvious that this crosslinking system provide remarkable yields in both gel content and crosslink density. Moreover, the free radical crosslinking by the peroxide has no adverse effects in generating byproducts as observed in previous studies in high energy radiation crosslinking. However, in practical the system compositions are not suitable for mass production such as melt extrusion. It is required a system that allows to use in higher temperature to avoid any premature crosslinking or degrading of the components.

Generally, in order to process free radical crosslinkable polymer systems the polymer compound will follow three steps of increasing of process temperatures. In the first step, the temperature is increased to melt the polymer. For ensuring that only the desired crosslink reaction occurs, the melt processing temperature is kept as low as possible (still above the melting temperature) to avoid premature crosslinking. It is important to note that in some film fabrication methods, the melt processing may occur as a step to make a film preforms. The film after this step can be further modified, e.g., stretching or rolling, to provide polymer films with specific dimension or properties.

Then the crosslinking reaction can be performed in an additional processing of increasing temperature to the nominal crosslinking temperature or by other methods such as photocrosslinking. However, the crosslink film can be made by a single-step as well. For an example, the components were melt blended together at suitable melt processing and then directly extruded and crosslinked by a screw extruder. However, there are a number of additional parameters, such as viscosity and cooling rate, which are required to take in consideration for controlling the physical properties of the resulted films.

The second step of heating is to increase temperature from melt processing temperature to the crosslinking temperature. This temperature increasing step is varied by the difference between melting point of the polymer and the crosslinking temperature. Therefore, a change in the crosslink temperature with the choice of free radical inducing species typically requires a corresponding change in this temperature range.

Lastly, the temperature of the system has to be increased to meet the crosslinking temperature and preserved for certain amount of time to achieve a proper amount of crosslink state, i.e., gel content and crosslink density.

Accordingly, the need exists for an improved P(VDF-CTFE) compounding system. The improved components must permit a higher crosslinking temperature than presently achieved in chapter 2. It is worth to note that the increasing of crosslinking temperature also permits higher production rate. For instance, the higher extrusion screw rates are allowed without any appreciably negative impact upon premature crosslinking. In our study, since the P(VDF-CTFE) copolymer has the melting temperature in the range of 160-170 °C the melt processing temperatures above 220 °C are required to prohibit the premature crosslinking and to give a good quality film. Therefore we are introducing two

new crosslinkable P(VDF-CTFE) systems in this chapter. The first system proposed here is the system that replacing the initiator from 1,4-bis(t-butyl peroxy) diisopropylbenzene (Vulcup[®]) with (2,3-dimethyl-2,3-diphenylbutane)benzene, bicumene, (BC, $t_{1/2} = 1$ h at 260 °C). This system will allow crosslinking at higher temperature (above 250 °C).

3.2 Experimental Procedure

a. Materials Fabrication

Poly(vinylidene fluoride-co-chlorotrifluoroethylene), P(VDF-CTFE), is a random copolymer with 15wt.% CTFE monomer, in this study was supplied by Solvay (Solef 31508). The high thermal stability 2,3-dimethyl-2,3-diphenylbutane (bicumene, Perkadox-30, 95%, Akzo Nobel.) initiator was used as a high temperature crosslinking agent. A polyfunctional crosslinking agent, triallyl isocyanurate (TAIC) was purchased from Aldrich. All materials were used as received without purification. The crosslinking reaction mechanism is similar to those outlined in *Figure 15* except in the initiating step which instead of decomposing of the peroxide the bicumene is decomposed by a mechanism as shown in *Figure 48*. It is believed that the propagation and crosslinking mechanisms will be undergone by the same progress as induced by the Vulcup[®].

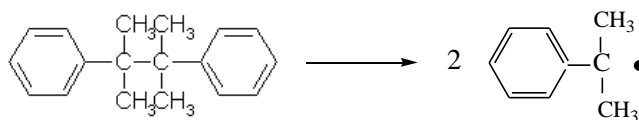


Figure 48 Decomposition mechanism of 2,3-dimethyl-2,3-diphenylbutane (bicumene)

Pristine and crosslinked copolymers were made by hot-pressing method. The mixture compounds were prepared by vigorously shaking in controlled cryogenic atmosphere. The compounds were then hot-pressed using temperature and pressure as shown in *Figure 49*. At the beginning, the powder compound was placed into rapid heating and pressing to reach 160 °C under 6000 psi within 10 minutes. The temperature and pressure of the process were then held constantly for 60 minutes. The polymer film was further heated rapidly to 260 °C in 30 minutes. Finally, the polymer film was kept in high pressure and high temperature for 330 minutes to make sure the reaction is completed. The heat has then been cut off while pressure was maintained until the sample cooled down to room temperature. The resultant films were then peeled off and dried in vacuum oven at 135 °C for 72 hours to remove any trace amount of impurities and by-products. This step was also used as an annealing process to the copolymer at the same time. The copolymer films with thickness around 12-15 μm were obtained.

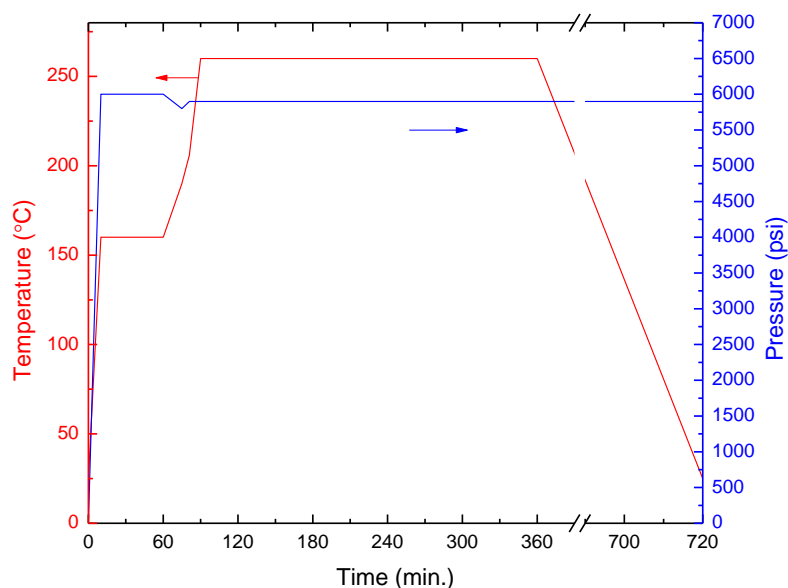


Figure 49 Hot-pressing process conditions for fabricating crosslinked P(VDF-CTFE) films using 1,4-bis(t-butyl peroxy) diisopropylbenzene (Vulcup[®]) triallylisocyanurate (TAIC)

b. Characterization

The gel contents and crosslink densities were examined using the ASTM D2765-01 standard procedure. Wide-angle X-ray diffraction (WAXD) studies were conducted using a Scintag Cu-KR diffractometer with an X-ray wavelength of 1.54 Å. All data were deconvoluted using “Peakfit” software with a Gaussian-Lorentz superposition fitting functions. Fourier transform infrared spectroscopy (FT-IR) was carried out on Varian Digilab FTS-8010 spectrometer in room temperature. Spectrums were obtained in the attenuated total reflectance (ATR) mode using ZnSe crystal as a contact to the samples. Polarization hysteresis loops at room temperature were collected using a

modified Sawyer-Tower circuit. The copolymer samples were subjected to a triangular unipolar wave with a frequency of 10 Hz. Dielectric properties were acquired using an Agilent LCR meter (E4980A) with 1.0 V bias. Dielectric breakdown strength measurements were performed using the electrostatic pull-down method, with a 500 V/s ramp. Gold electrodes of 2.6 mm diameter and typical thickness of 60 nm were sputtered on both sides of the samples for the electrical measurements.

3.3 Structural Analysis

a. Sol-gel analysis

The sol-gel analysis was performed using ASTM D2765 as described in section 2.4. The average molecular weight between two adjacent crosslinked sites was calculated using Flory-Rehner swelling theories (*Equation 17*). **Figure 50** demonstrates the influence of bicumene and TAIC concentration on the gel contents and M_c . It appears that the gel contents of all compounds are very high even with 1 % bicumene and 1 % TAIC. The results suggest that of the bicumene is very effective for using as a reaction initiator. It is clear to observe that the TAIC plays a strong influence in M_c . By increasing of TAIC contents the crosslink density is remarkably increased.

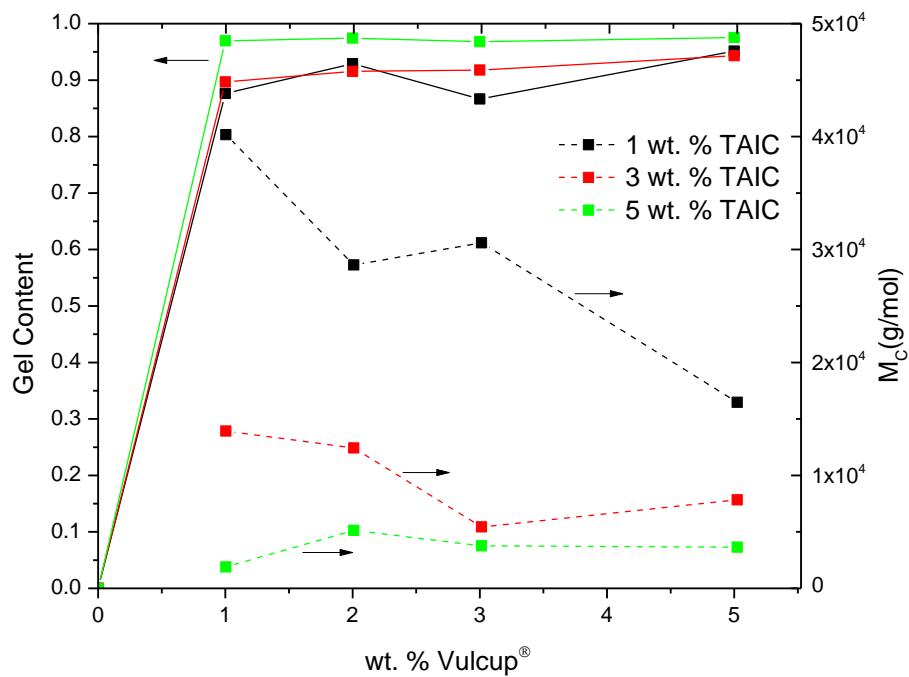


Figure 50 Gel contents and average molecular between crosslinking sites as determined using Flory-Rehner swelling theories versus bicumene concentration with 1 wt. % TAIC (black), 3wt. % TAIC (red), and 5 wt.% TAIC (green).

b. Fourier Transform Infrared Spectroscopy Analysis

FTIR spectra of the melt pressed copolymer samples of pristine and crosslinked with various bicumene concentrations with 3wt.% TAIC are shown in **Figure 51**

The peak at wave number 1685 cm^{-1} is assigned as the carbonyl group contained in TAIC that increased with the concentration of the bicumene feeding. The increasing of this peak reflects the higher crosslink density in the copolymers which is agreed to the result from gel analysis.

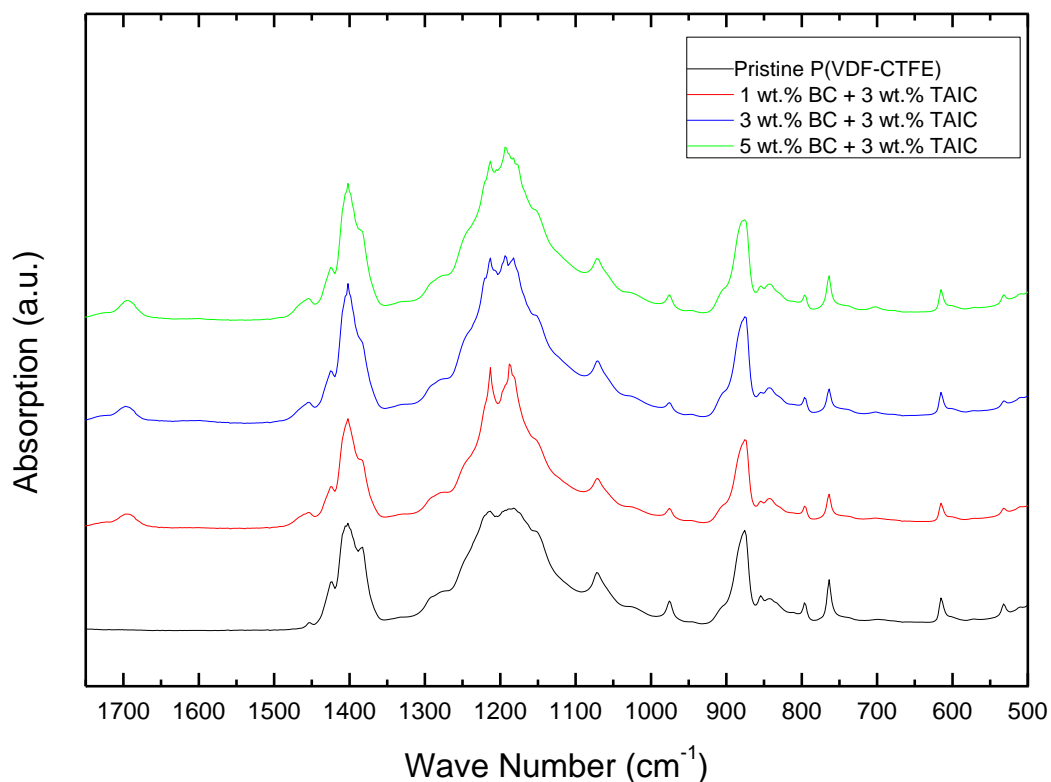


Figure 51 ATR-FTIR spectra of pristine and crosslinked P(VDF-CTFE) with different bicumene concentration (3wt.% TAIC).

c. X-rays diffraction analysis

The XRD patterns of pristine melt pressed and crosslinked copolymers are shown in *Figure 52*. The patterns are characteristics of four α -phase crystallographic planes with very a small peak intensity of (110,200) β -phase. Especially for the sample with 5 wt. % bicumene + 3 wt % TAIC, the peak of (110,200) β -phase is considerably disappeared. The crosslink structure seems capable to inhibit the formation of polar phase even though the samples were cooling from molten under high pressure. The Peak fitting of the diffraction patterns showed clear changes in peak intensity. The crystallinity of the samples can be calculated by integrations of the areas under each peak. As may be seen in *Figure 53*, the introduction of crosslinked network into polymer structure with this approach decreases the overall crystallinity. For instance, crystallinity of crosslinked sample with 5 wt.% bicumene was decreased to 19 % which is 42 % reduction when compared to the pristine. On the contrary, the crosslink densities of the crosslinked sample by bicumene are much higher than the value form Vulcup[®] system. For this reason, the formation of crystallite is restricted to very short chain section resulting in very low crystallinity. Therefore this crosslink process is not suitable for maintaining crystal content in the copolymer.

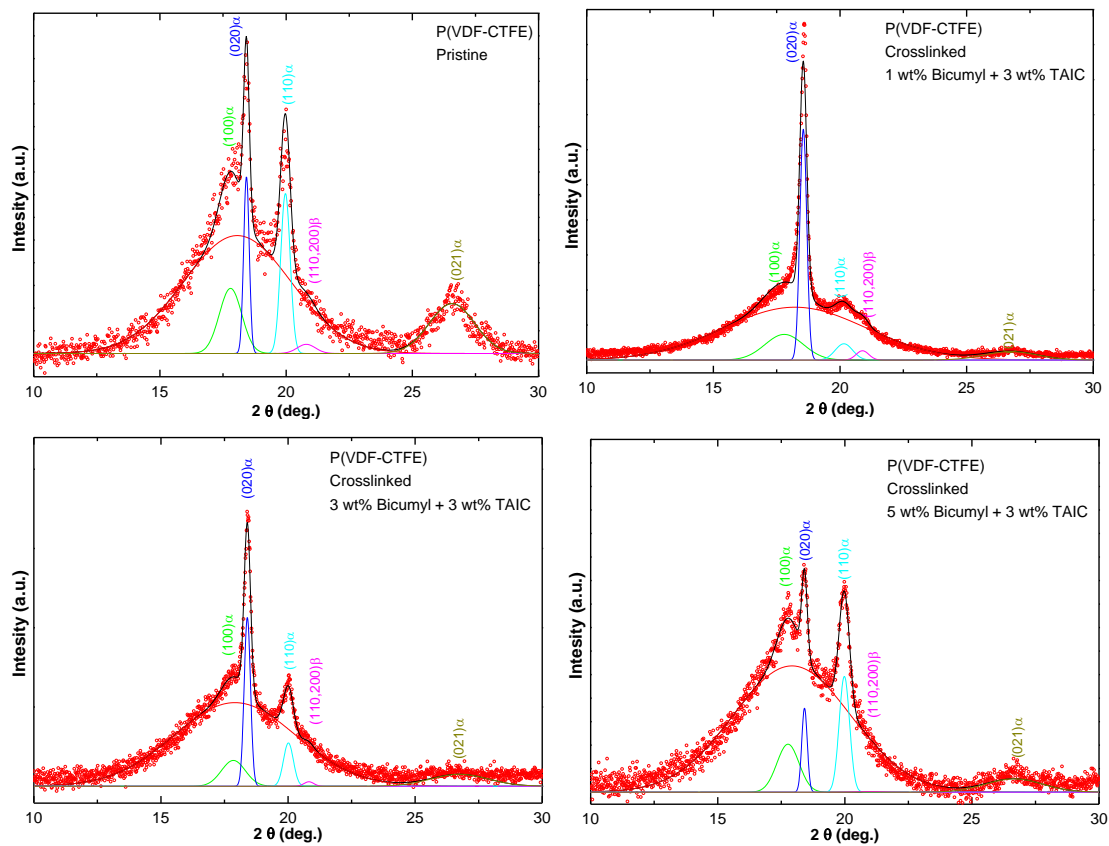


Figure 52 XRD patterns of pristine and crosslinked P(VDF-CTFE) using bicumene at 3 % wt. TAIC.

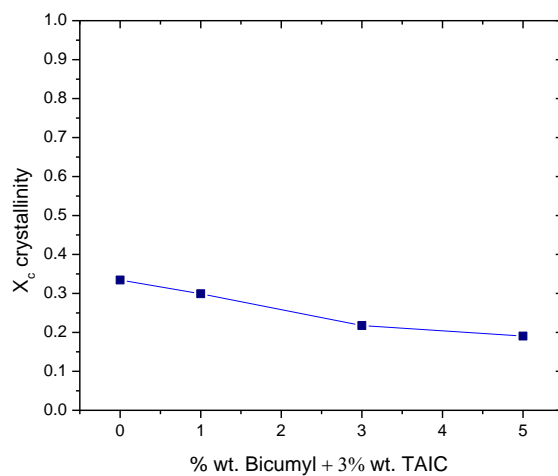


Figure 53 Crystallinity versus bicumene concentration at 3 % wt. TAIC.

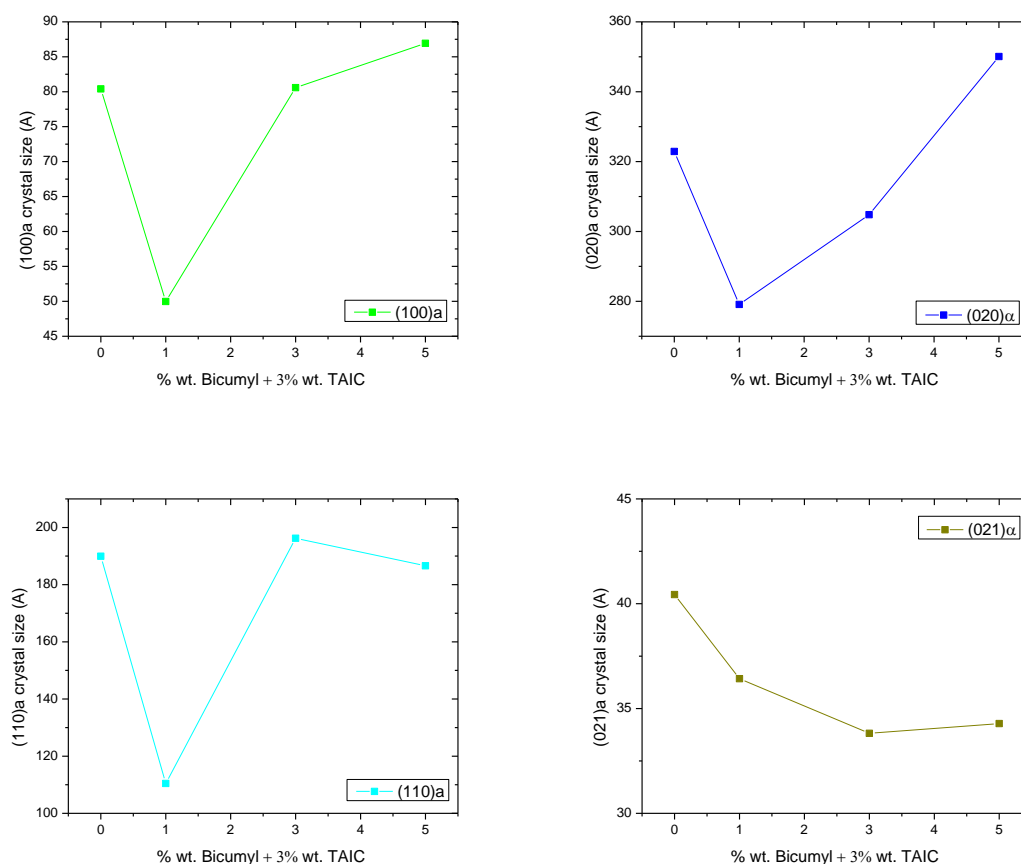


Figure 54 Crystal sizes of α phase crystals in all four crystallographic planes versus the bicumene concentration at 3 % wt. TAIC.

The indirect information of crystallite size was calculated by using Scherrer's equation the crystallite size can be computed based on the assumption that there is no-strain in crystal. The crosslinking system with 1 wt.% bicumene + 3wt.% TAIC shows a remarkable decreased in crystal size. As the introduction of crosslinked structure, shorter chain section between crosslink sites is achieved, therefore an enormous reduction in crystallite size has been observed in this composition system. However, as the bicumene

content increased the crystal size in (100), (020), and (110) crystallographic planes are increased. The increasing of crystal size is surprising yet unexplainable in this current stage. According to the XRD results this crosslinkable system fails to reduce the crystal size with maintaining the level of crystallinity.

3.4 Weak-Field Dielectric Properties

The frequency dependence of the permittivity (ϵ') and of the dielectric losses ($\tan(\delta) = \epsilon''/\epsilon'$) for pristine and crosslinked P(VDF-CTFE) by bicumene and TIAC are shown *Figure 55*. The measurements were measured at 25 °C under an electric field approximately of 0.05 MV/m with the heating ramp of 10 °C/min. All crosslinked copolymers show a similar permittivity for entire range of frequency from 20 Hz to 1MHz, with significantly lower than the data from the pristine. This is probably affected by the crosslink network retards the polarization upon applying electric field. It is also believed that this permittivity decreasing is due to the reduction of crystalline phase. The losses of crosslinked copolymers are lower for the whole range of frequency compared to the pristine. This result suggests that the crosslink structure probably immobilizes the charge transportation and inhibits space charge formation.

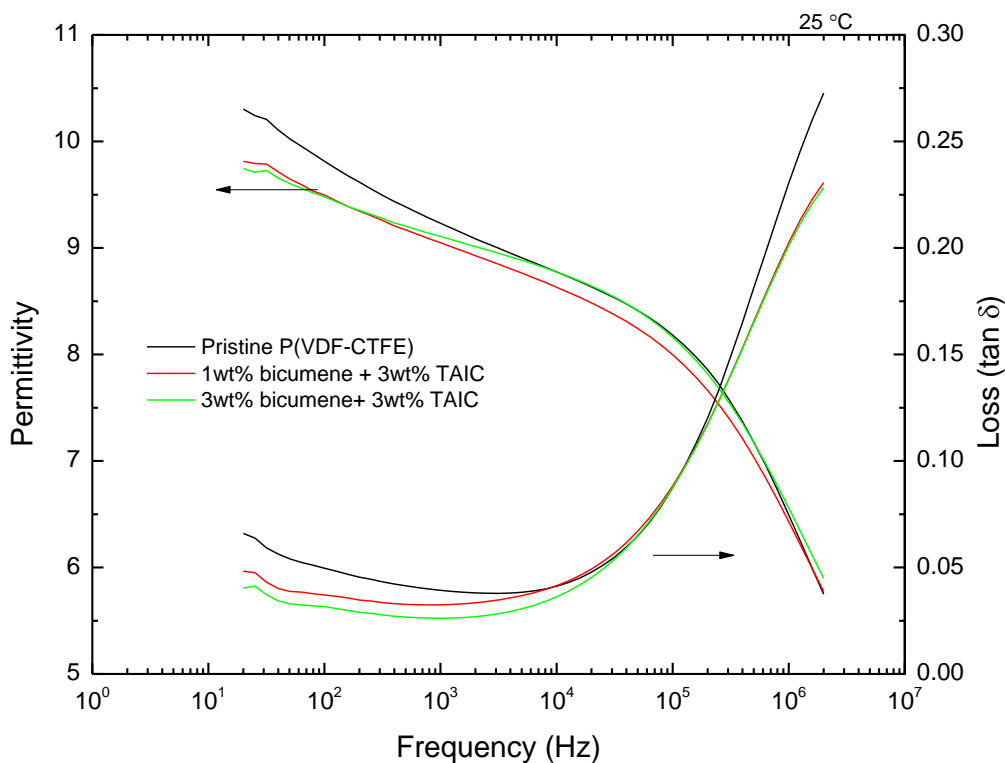


Figure 55 Permittivity and dielectric losses ($\tan(\delta)$) versus frequency measured at 25 °C for pristine and crosslinked P(VDF-CTFE) by bicumene and TAIC.

3.5 High Field Electric Displacement

The high field performances of crosslinked and pristine P(VDF-CTFE) were examined by measuring a series of displacement-electric field loops (D-E loops). The electric displacement hysteresis loops bicumene crosslinked P(VDF-CTFE) are shown in **Figure 56** to **Figure 58** where the comparison of D-E filed loops of pristine and crosslinked P(VDF-CTFE) with the maximum electric field of 250 MV/m. is shown in **Figure 59**.

It is clear that the crosslinked samples show reductions in polarization. The polarization levels are decreased with increasing bicumene. This marked declining of polarization is consistent with the result from weak field analyses that showed the downward shifting of permittivity in crosslinked samples. The origin of these reductions of displacement can be described by the increasing of crosslink density which restricts the dipole orientation. However, it can be clearly seen that the D-E loops of crosslinked samples are much slimmer than the pristine. Also the remnant polarizations are greatly decreased, for instance, 5 wt.% bicumene[®] + 3wt. % TAIC sample showed the lowest remnant displacement which is only 35% of the value from the pristine. It is also worth to mention that the breakdown fields of crosslinked samples are greatly improved compared to the pristine (loops are shown in *Figure 29*) because the crosslinked sample were able to endure the repeat charge-discharge cycles at higher field.

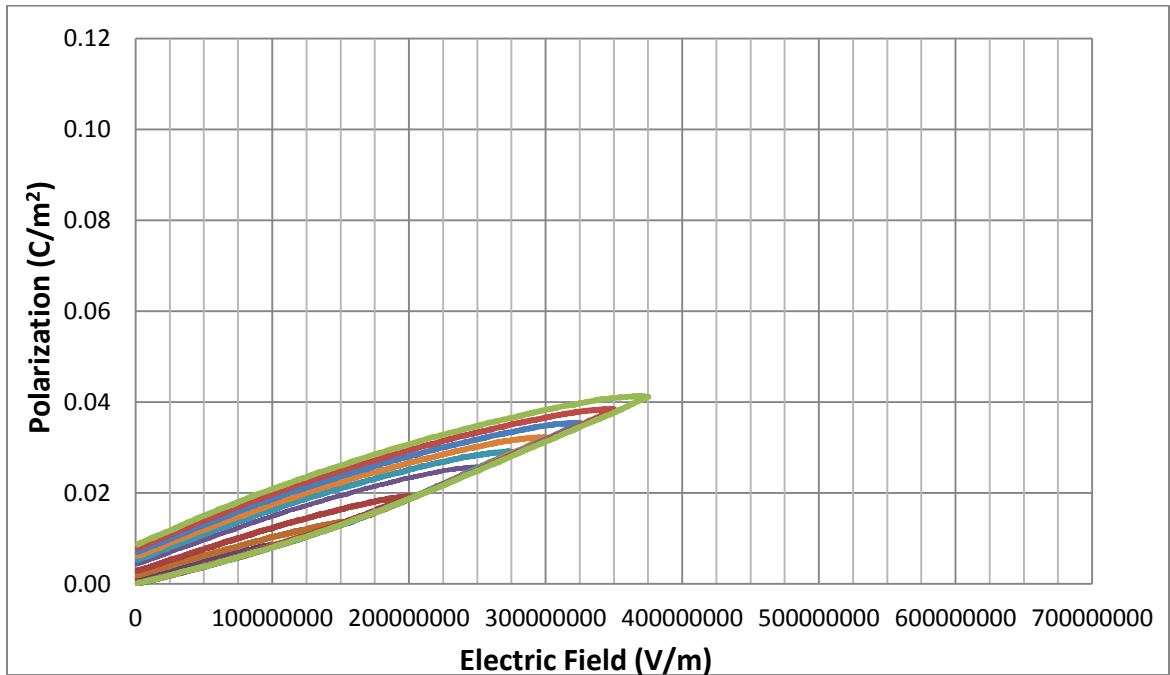


Figure 56 Electric displacement in crosslinked P(VDF-CTFE) using 1 wt. % Bicumyl + 3 wt.% TAIC at 10 Hz.

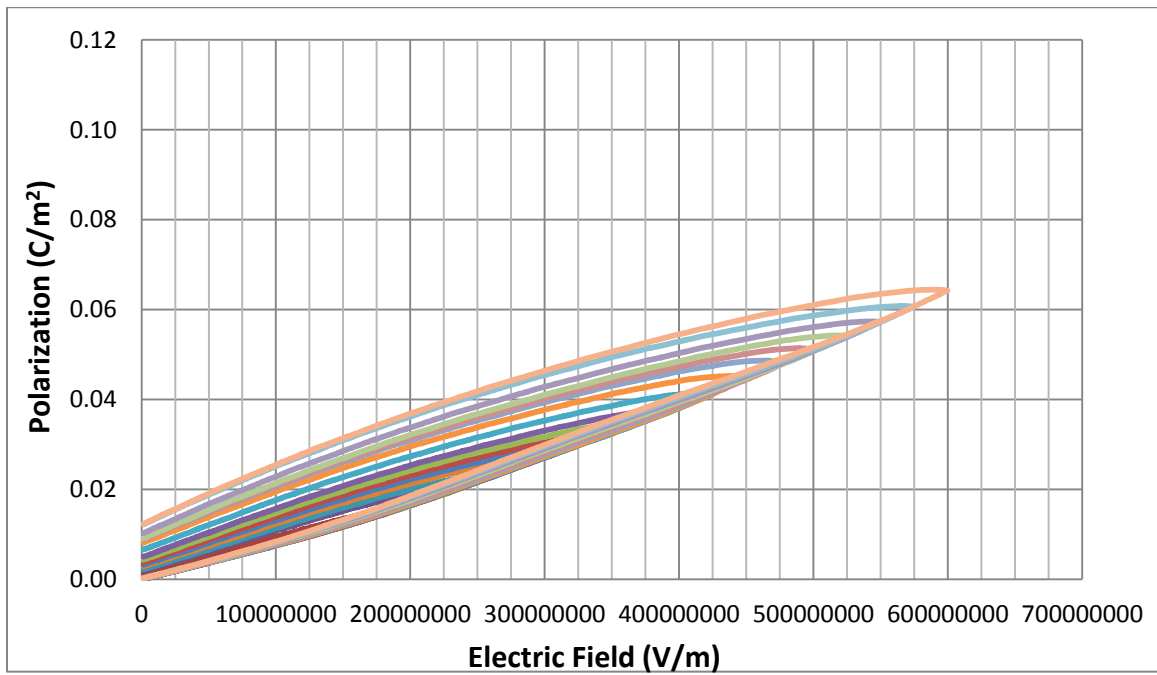


Figure 57 Electric displacement in crosslinked P(VDF-CTFE) using 3 wt. % Bicumene + 3 wt.% TAIC at 10 Hz.

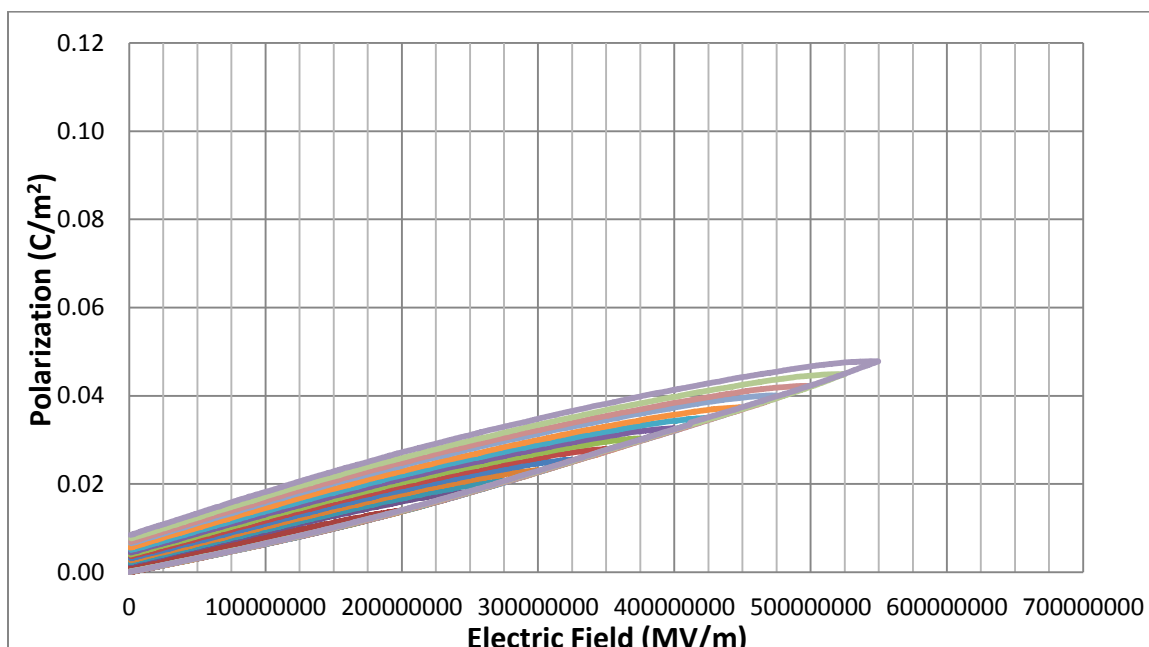


Figure 58 Electric displacement in crosslinked P(VDF-CTFE) using 5 wt. % Bicumene + 3 wt.% TAIC at 10 Hz.

Hysteresis loops of all samples have a similar shape. In charging cycle, the changes of displacement versus the applied electric field are more linearly in crosslinked samples. The slopes of D-E loops of crosslinked sample are clearly lower than the pristine. This reflects that the effective permittivities are decreased by crosslinking of the copolymer. The suppressing of permittivities of crosslinked samples has been observed in the weak-field measurements as mentioned earlier. The smaller permittivities of crosslinked samples limit the storage energy at the same electric field compared to the pristine. In discharging cycle, the changes of displacement upon releasing electric field are remained non-linear. However, all of the samples were not able to return to their original state. The pristine seemed to have more residue charges that cannot be

completely removed after the discharging cycle is done. Therefore the loss of the pristine is greater than the crosslinked samples.

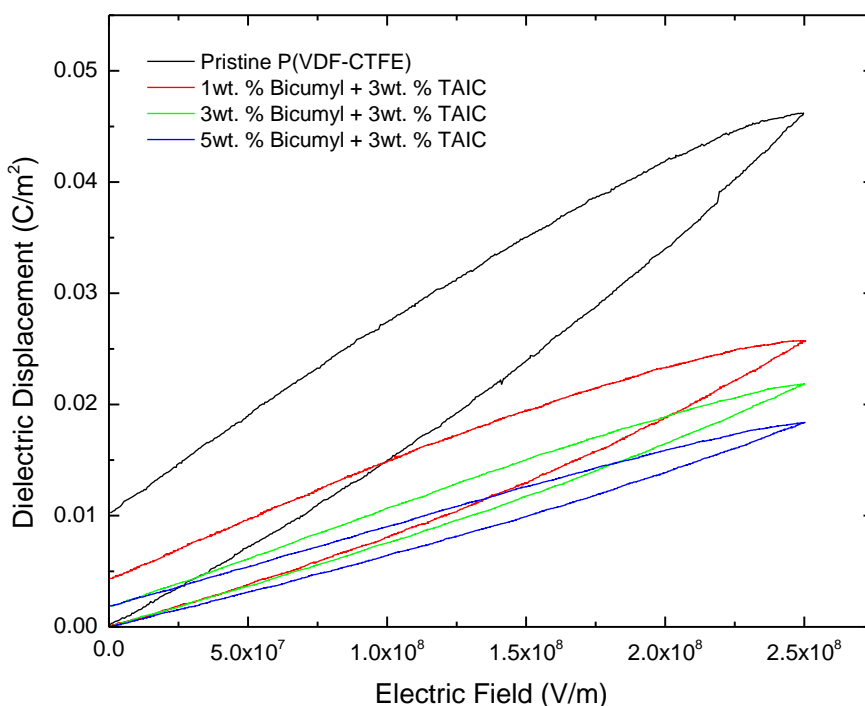


Figure 59 A comparison of displacement-electric field loops of pristine and bicumene crosslinked P(VDF-CTFE). The measurement was taken at 25 °C with a 10 Hz triangular unipolar signal with the maximum electric field of 250 MV/m.

The displacement at maximum load and remnant can be drawn from the D-E hysteresis loops and are summarized and presented in **Figure 60** and **Figure 61** respectively. Since the polarization is strongly dependent on the applied electric field, each of these Figures is plotted as functions of the concentrations of bicumene and maximum applied electric fields.

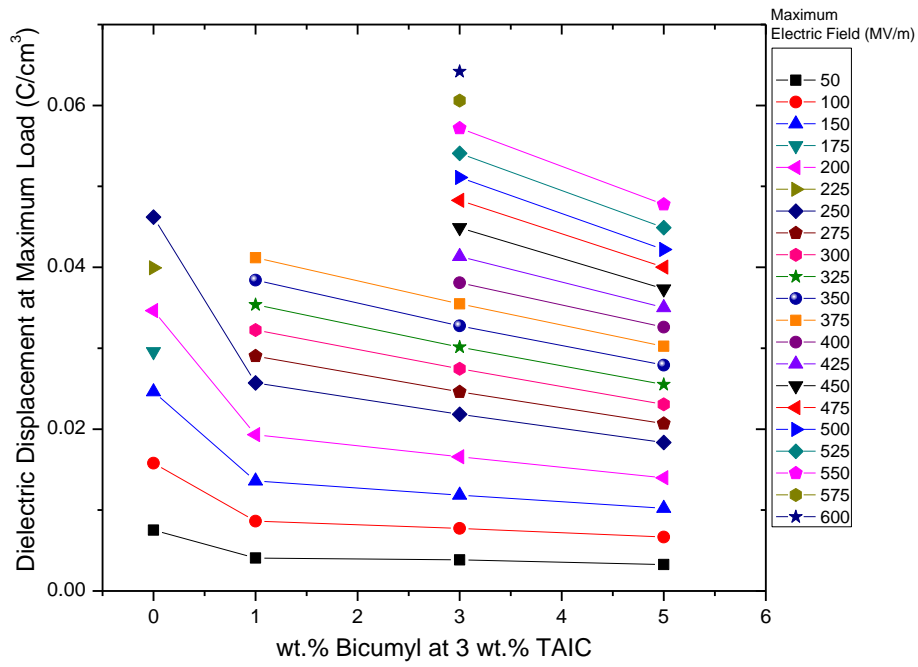


Figure 60 Dielectric displacement at maximum load versus concentration of bicumene at 3 wt.% TAIC.

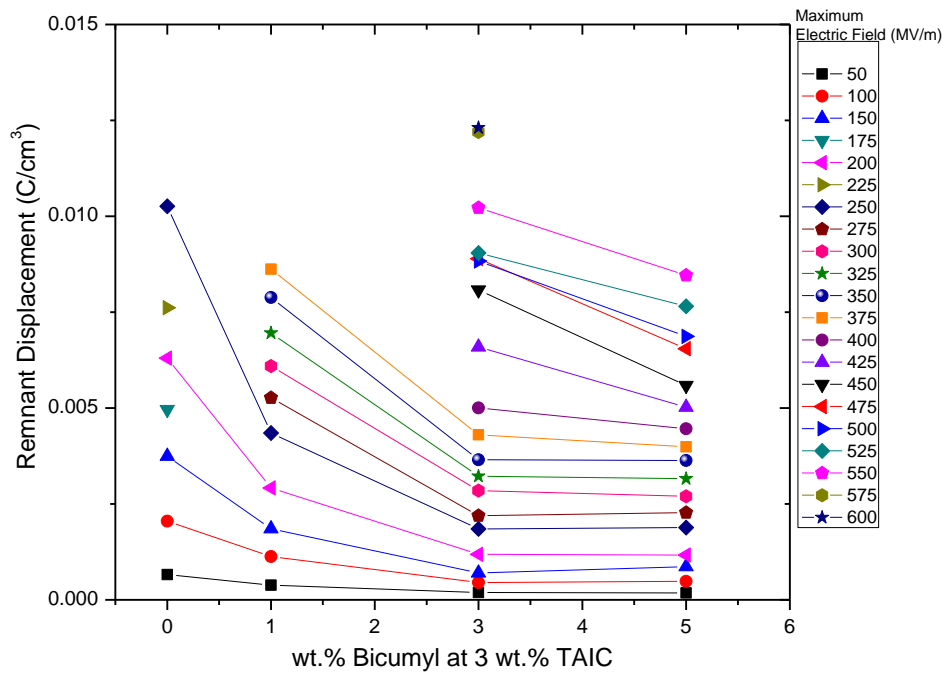


Figure 61 Remnant displacement versus concentration of bicumene at 3 wt.% TAIC.

From **Figure 60**, at the same maximum electric field dielectric displacements, D_{\max} , of all crosslinked samples are lower than the pristine. This effect of crosslinking becomes stronger upon increasing of the maximum, for example, at the maximum load of 250 MV/m, the crosslinked sample with 5 wt.% bicumene + 3 wt.% TAIC show 60% reduction of D_{\max} . This reduction of D_{\max} is probably due to the higher crosslink densities of the samples may prohibit the orientation polarization in the crosslinked samples.

As clearly shown in **Figure 61**, the crosslinked samples show great reduction of the remnant displacement. Again, the reduction of remnant displacement is clearer at elevated applied fields. At the electric field with the maximum load of 250 MV/m the remnant polarization was 81% decreased in the crosslinked sample with 5 wt.% bicumene + 3 wt.% TAIC compared to the pristine. This can be presumably concluded that the crosslink structure insists the recovery of the polarization into its original state. All of these parameters affect the energy density of the polymers. Electric field dependence of discharge energy density and energy loss of pristine and crosslinked P(VDF-CTFE) copolymers determined by D-E loops measurement are shown in **Figure 62** and **Figure 63**, respectively.

All crosslinked samples show significant increase in the maximum discharge energy. Due to the fact that the pristine cannot endure electric field higher than 250 MV/m, only 4.8 J/cm^3 of energy density was obtained. While the higher breakdown strength of crosslinked samples leads their energy density reached up to 12.2 J/cm^3 with 3wt.% bicumene + 3wt.% TAIC at the electric field of 600 MV/m applied.

From **Figure 63**, as the field increases, the energy loss was observed in both pristine and crosslinked P(VDF-CTFE). However the field-induced developments of loss in crosslinked samples with 3 wt. % and 5 wt. bicumene are much lower than the pristine. As stated earlier, this behavior can be described by the effect of crosslink structures which comfort the destabilization of the polar phase generated upon increasing field. At a field of 250 MV/m (breakdown field of the pristine) the energy loss of the crosslinked copolymer by 3 wt. % bicumene + 3wt. % TAIC is only 20.8%, which is 45% less than that of the pristine.

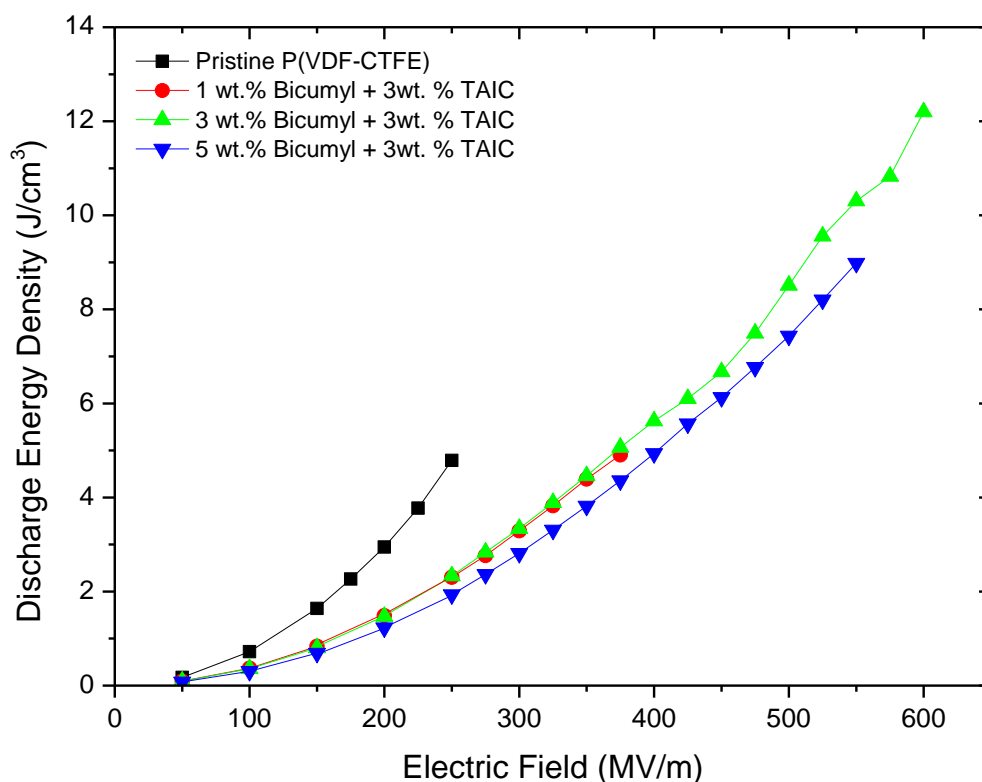


Figure 62 Electric field dependence of discharge energy density and of pristine and bicumene crosslinked P(VDF-CTFE) copolymers.

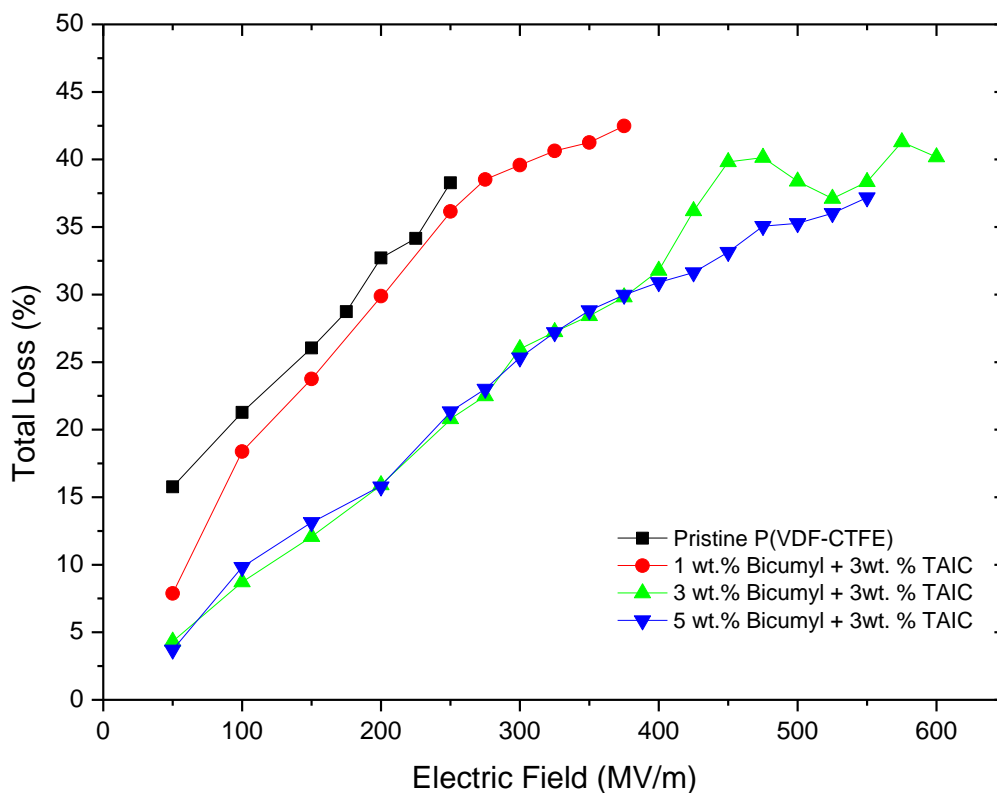


Figure 63 Energy loss of pristine and bicumene crosslinked P(VDF-CTFE) copolymers.

In summary, this study shows evidence that bicumene crosslinking system can successfully create crosslinks in P(VDF-CTFE) that, in turn, reduces the amount of the polar β -phase and thus reduces ferroelectric losses and improves energy storage efficiency. While this method may not be practical for capacitor applications due to defects introduced from the bicumene crosslinking causing a reduction in total amount of crystalline phase. However, the breakdown strength of the copolymer after crosslinked with this approach are seemed to be much higher than that of the pristine, the further study of breakdown strength is demonstrated in next section.

3.6 Electrical Breakdown Strength

The Weibull analysis of breakdown strengths for the pristine and crosslinked P(VDF-CTFE) were demonstrated in **Figure 64** and the results are summarized in **Table 4**. The Weibull analysis of breakdown strengths clearly demonstrates the improvement of the breakdown strength exhibited by bicumene crosslinked samples compared to the pristine. The sample with 3 wt.% bicumene + 3wt. % TAIC shows a marked improvement of 67.5%, the α value increases from 361 MV/m for the pristine copolymer to 603.75 MV/m for the crosslinked sample. In addition, these bicumene crosslinked samples show an improvement in reliability compared to the pristine as reflected by the remarkable increase in β value.

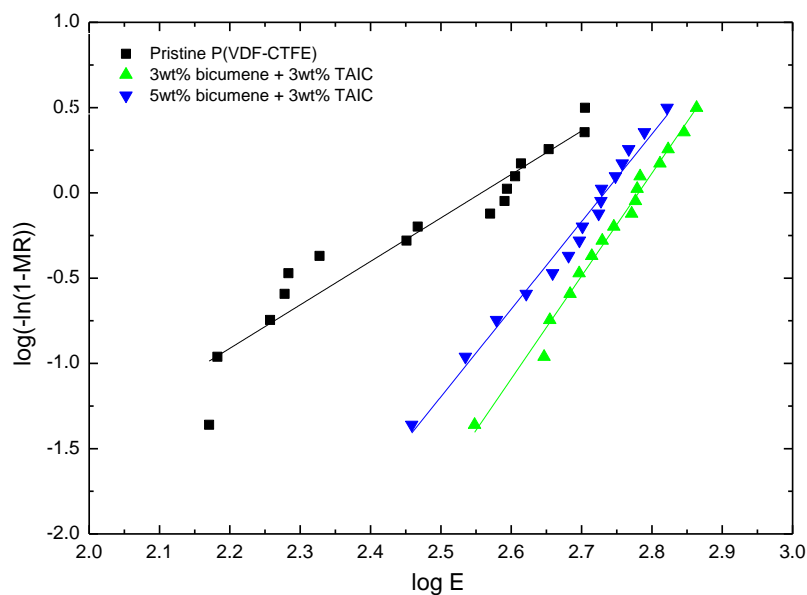


Figure 64 The Weibull analysis of breakdown strengths for the pristine and bicumene crosslinked P(VDF-CTFE).

Table 4 Weibull parameters of the pristine and bicumene crosslinked P(VDF-CTFE)

Polymer	α (MV/m)	β
Pristine P(VDF-CTFE)	361.11	2.55
3wt% bicumene + 3wt%TAIC	603.75	6.03
5wt% bicumene + 3wt%TAIC	507.20	5.13

Chapter 4

Conclusions and Future Work

This dissertation demonstrates an approach for enhancing the electrical energy storage capabilities of poly(vinylidene chlorotrifluoroethylene) [(PVDF-CTFE)] copolymer through chemically crosslinking techniques. The work in this study is mainly focused on how the modification in molecular level is going to affect the energy storage performances. In order to do this, a carefully investigating of relationships between the modified microscopic structures and their changes in macroscopic properties is critical and therefore share a majority part as a scientific tool for acquiring new knowledge.

We have successfully modified P(VDF-CTFE) copolymer using chemically crosslinking method. In chapter 2, we demonstrates that the crosslink structures is effectively obtained by 1,4-bis(t-butyl peroxy) diisopropylbenzene (Vulcup[®]) free radical reactions. With the incorporation of 3 wt. % triallyl isocyanurate (TAIC) radical trap, the gel content of the resulted crosslinked copolymer can reach 95 % by adding only 3 wt. % of the peroxide. We also discover that the crosslink density can be directly controlled by changing the feeding amount of the initiator.

The analysis of XRD and DSC results suggests that the crosslink structures favor the formation of non-polar α phase crystal since the increasing of non-polar phase fraction is observed. In order to understand the original of this non-polar phase favorable, FTIR analysis has been used to investigate the role of crosslinks that affect chain conformations. The results from FTIR indicate the reduction of all-trans

conformation upon increasing Vulcup[®] concentration. This is due to these crosslinked network structures act as defects preventing the polymer chains to arrange in all-trans conformation. Therefore the crystallization mechanism is limited to the non-polar α phase. This technique is also effective in reducing crystallite size with slightly sacrifice total crystallinity. This is analogous to that observed in introducing of defects such as CTFE and CFE comonomer into the PVDF homopolymer. However, the effects caused by crosslinks may greater than the introduction of bulky side groups due to the covalently bonding between chains restricts the mobility of the chain section even in molten state and limits their incorporation in crystallite structure. Thus the crystal structures presumably prefer taking place in shorter chain sections between crosslink sites.

The most challenging aspect in this dissertation is to improve energy density of P(VDF-CTFE) by concurrently minimize loss, optimize polarization level, and maximize breakdown strength. Smaller crystallites are hypothesized as one of the sources of reduction in energy loss since it simultaneously decreases ferroelectric domains. The polarization mechanisms upon applied electric field in a confined domain are more comfortable to return into their original state since the chain rotations are located in short sections. Moreover, the crosslinks are believed to act as an elastic junction that helps the recovery from the polarizations. From our results, the reduction of loss by peroxide crosslinking has been verified by the dielectric measurements in both weak and high electric fields. The peroxide crosslinking approach has potential in reducing both ferroelectric loss and conduction loss. Among all crosslinked systems, the sample containing 3 wt. % Vulcup[®] + 3 wt.% TAIC performs the best result in loss reduction. For instance, at a field of 250 MV/m the total energy loss of the copolymer crosslinked

by 3 wt. % Vulcup[®] + 3wt. % TAIC is only 13.92%, which is 64% less than that of the pristine. By carefully analyze D-E loops, conductivity, and TSDC data, we can demonstrate that crosslinking decrease both ferroelectric loss and conduction loss. The reduction of ferroelectric loss is central to the increasing of recoverability from the non-polar to phase transition while the reduction of conduction loss is due to the introduction of energy traps and the increasing of activation energy of the crosslinked copolymer.

Dielectric displacement of crosslinked copolymer by this method is markedly enhanced. For instance, at the maximum load of 250 MV/m, the crosslinked sample with 1 wt.% Vulcup[®] + 3 wt.% TAIC show 24% improvement of polarization level at the maximum field. The enhancing of polarization level by crosslink structure maybe originated from two sources. The first source is the reduction of crystallite size. The smaller non polar crystal is easier to be induced and transformed in to polar phase. The polarization can also be influenced by crystal-amorphous interfacial structure, and because crosslinking induces formation of smaller crystal with barely decrease the total amount of the crystal content this interfacial region should be largely increased. Another source that may contribute to the increasing of polarization is that the crosslink site, TAIC, have polar groups in the chemical structure. These polar groups are readily to respond to the applied field and cause the orientational polarization in the materials resulting in increasing of polarization.

The electrical breakdown has been greatly improved by crosslinking. The sample with 3 wt.% Vulcup[®] + 3wt. % TAIC shows a marked improvement of 70%, the α value which is increased from 361 MV/m for the pristine to 614 MV/m for the crosslinked sample. In addition, these crosslinked samples show and improvement in reliability

compared to the pristine as reflected by the remarkable increased in β value. This improvement of breakdown strength by crosslinking can be originated by two reasons; first, the energy loss has been drastically decreased therefore the possibility of failure mechanism due to the electrical power dissipation by heat has been reduced; second, the presence of the crosslink structure in copolymer improves the mechanical properties of the copolymer thus reduced the possibility of electromechanical failure.

All of above improvements have been synergized and consequently greatly enhance the energy density. All crosslinked samples showed significant increase in the maximum discharge energy. The crosslinked sample with 3wt.% Vulcup[®] + 3wt.% TAIC has energy density of 7.3 J/cm^3 which is 52% increase compared to the pristine at the same 250 MV/m electric field applied. The higher breakdown strength of crosslinked samples leads their energy density reached up to 19.9 J/cm^3 for the crosslinked with 5 wt.% Vulcup[®] + 3wt. % TAIC at 400 MV/m. This is a greatly improvement with 315 % increasing in energy density compared to the pristine. It is clearly that the peroxide crosslinking method performs an excellent improve of electrical energy density.

In chapter 3, we demonstrate alternative crosslinking systems in hope to allow the system to be thermally processable. The high thermal stability 2,3-dimethyl-2,3-diphenylbutane (bicumene) initiator was used to permit the crosslinking reaction in high temperature (260 °C). This bicumene crosslinking system is very effective with high yield of gel content and crosslink density. The 45 % reduction of loss at 250 MV/m and 67.5 % increased of breakdown strength can be obtained. However, the negative issue with this approach is that the crosslinking inhibits the crystallization process and therefore resulting in reduction of polarization level. For instance, at the maximum load

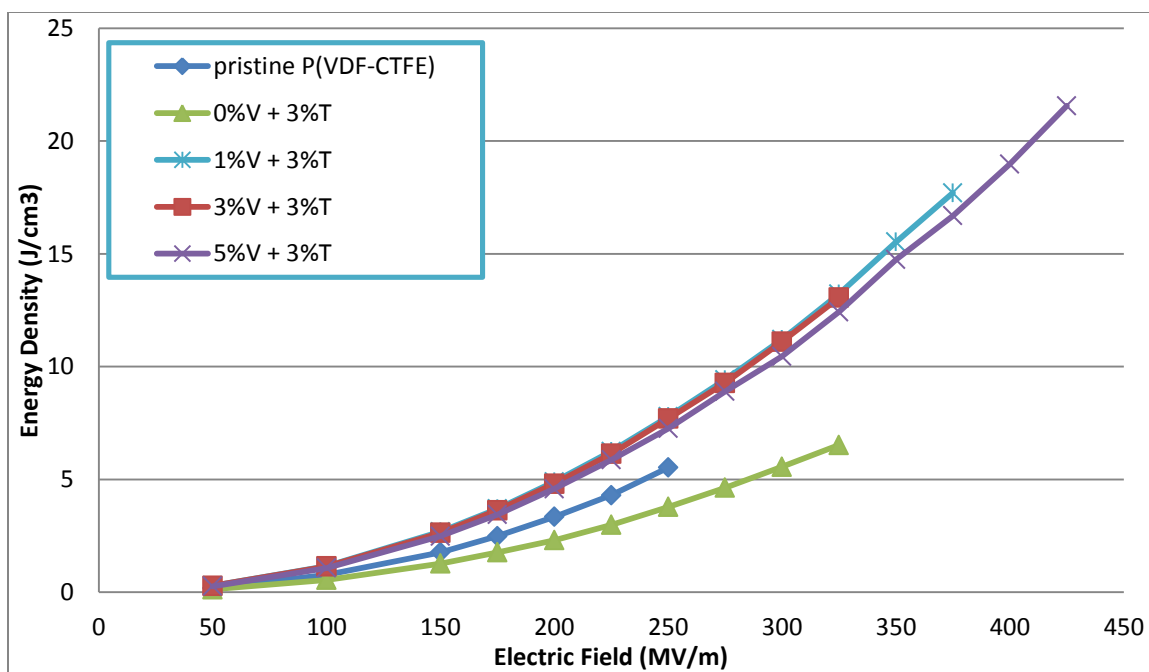
of 250 MV/m, the crosslinked sample with 5 wt.% bicumene + 3 wt.% TAIC show 60% reduction of maximum polarization level. While this method may not be practical for improving polarization level, the crosslinked samples with 3wt. % bicumene + 3wt.% TAIC shows the energy density reached up to 12.2 J/cm^3 at the electric field of 600 MV/m applied which is 154 % increased.

In this study, the crosslinking approaches for the enhancing of energy density in P(VDF-CTFE) have been validated. The methods are quite simple and ready to upscale them in to manufacturing process. However, there are some questions that remain to be answered. For example, there is no direct evidence of phase switching rather than the non-linear behavior observed in hysteresis loops. More in-depth studies of phase switching under applied electric field should be carried out to confirm the phenomena. In this case we might consider the time of flight x-ray diffractions with samples under electric field.

On the processability point of view, the polymer films in this study are thicker than those typically use in commercial. The limitation of lab-scale process may inhibit the intrinsic properties of the materials since thicker materials usually have more possibilities to include unwanted structures such as defects, pinholes, inclusion and impurities. Development of an appropriate process may increase the overall energy density of the polymers.

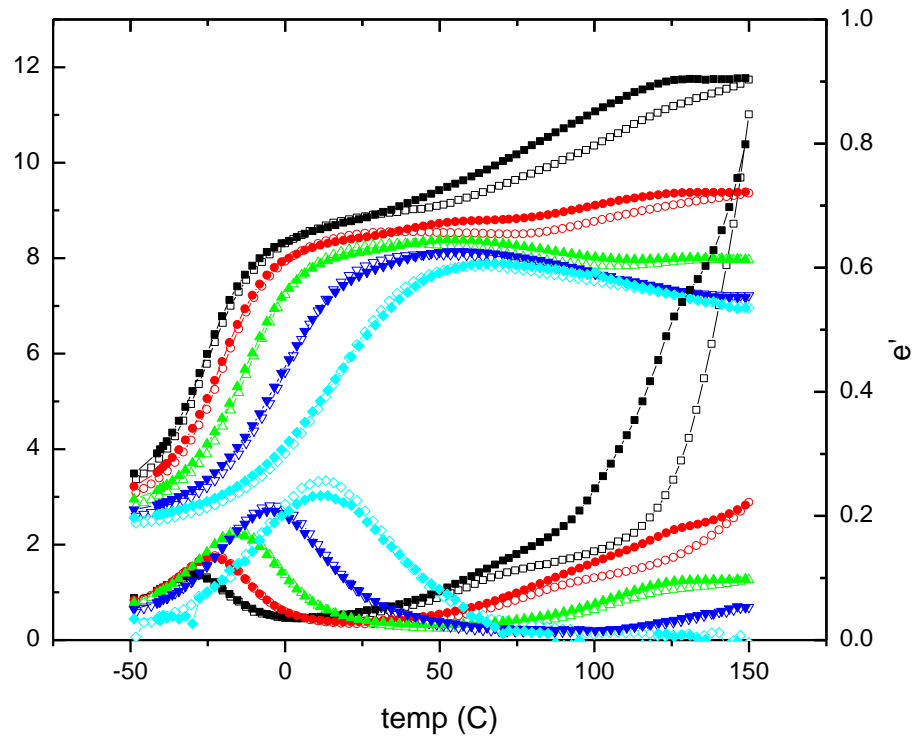
Appendix A

Storage Energy Density of Pristine and crosslinked P(VDF-CTFE) copolymer



Energy storage of pristine and crosslinked P(VDF-CTFE) as a function of applied field.

Appendix B
Dielectric spectra of Pristine and crosslinked P(VDF-CTFE) copolymer



REFERENCES

1. Christen, T. and M.W. Carlen, *Theory of Ragone plots*. Journal of Power Sources, 2000. **91**(2): p. 210-216.
2. Livingston, J.D., *Electronic properties of engineering materials*. MIT series in materials science and engineering. 1999: Wiley.
3. Kao, K.-C., *Dielectric phenomena in solids: with emphasis on physical concepts of electronic processes*. 2004: Academic Press.
4. Blythe, A.R. and D. Bloor, *Electrical properties of polymers* 2nd ed. 2005: Cambridge ; New York : Cambridge University Press.
5. Kremer, F. and A. Schönhal, *Broadband dielectric spectroscopy*. 2003: Springer.
6. Naber, R.C.G., et al., *High-performance solution-processed polymer ferroelectric field-effect transistors*. Nature Materials, 2005. **4**(3): p. 243-248.
7. Chu, B.J., et al., *A dielectric polymer with high electric energy density and fast discharge speed*. Science, 2006. **313**(5785): p. 334-336.
8. Cao, Y., P.C. Irwin, and K. Younsi, *The future of nanodielectrics in the electrical power industry*. Ieee Transactions on Dielectrics and Electrical Insulation, 2004. **11**(5): p. 797-807.
9. Kim, C., A. Facchetti, and T.J. Marks, *Polymer gate dielectric surface viscoelasticity modulates pentacene transistor performance*. Science, 2007. **318**(5847): p. 76-80.
10. Laghari, J.R. and A.N. Hammoud, *A BRIEF SURVEY OF RADIATION EFFECTS ON POLYMER DIELECTRICS*. Ieee Transactions on Nuclear Science, 1990. **37**(2): p. 1076-1083.
11. Banhegyi, G., *Dielectric relaxation and dielectric strength of polypropylene and its composites*, in *Polypropylene An A-Z reference*, J. Karger-Kocsis, Editor. 1999, Kluwer academic Publishers.

12. Lovinger, A.J., *Poly(vinylidene fluoride)*, in *Developments in Crystalline Polymers - I*, D.C. Bassett, Editor. 1982, Applied Science Publishers: London and New Jersey. p. 197-273.
13. Mandelkern, L., *The crystalline state*, in *Physical properties of polymers*, J.E. Mark, Editor. 2003, Cambridge University Press: Cambridge.
14. D. T. Clark, W.J.F., D. Kilcast, W. K. R. Musgrave,
<http://www3.interscience.wiley.com/cgi-bin/fulltext/104052501/PDFSTART>.
Journal of Polymer Science: Polymer Chemistry Edition, 1973. **11**(2): p. 389 - 411.
15. A. Torres, J.J., B. Vega and J. A. De Saja, *Thermally stimulated depolarization currents in PVDF- α : a dipolar interaction approach to β and γ transitions*. Journal of Materials Science, 1987. **22**(5): p. 1623-1629.
16. Kochervinskii, V.V., *Ferroelectricity of polymers based on vinylidene fluoride*. Russian Chemical Reviews, 1999. **68**(10): p. 821 - 857
17. Welch, G.J., *Solution properties and unperturbed dimensions of poly(vinylidene fluoride)*. Polymer, 1974. **15**(7): p. 429-432.
18. Furukawa, T., M. Date, and E. Fukada, *Hysteresis phenomena in polyvinylidene fluoride under high electric field*. Journal of Applied Physics, 1980. **51**(2): p. 1135-1141.
19. Lovinger, A.J., *FERROELECTRIC POLYMERS*. Science, 1983. **220**(4602): p. 1115-1121.
20. Black, C.T., C. Farrell, and T.J. Licata, *Suppression of ferroelectric polarization by an adjustable depolarization field*. Applied Physics Letters, 1997. **71**(14): p. 2041-2043.
21. Zhou, X., et al., *Electrical energy density and discharge characteristics of a poly(vinylidene fluoride-chlorotrifluoroethylene) copolymer*. Ieee Transactions on Dielectrics and Electrical Insulation, 2007. **14**(5): p. 1133-1138.
22. Date, M., T. Furukawa, and E. Fukada, *DIPOLAR ORIENTATION AND HYSTERESIS IN POLYVINYLIDENE FLUORIDE*. Journal of Applied Physics, 1980. **51**(7): p. 3830-3833.

23. Daudin, B., M. Dubus, and J.F. Legrand, *EFFECTS OF ELECTRON-IRRADIATION AND ANNEALING ON FERROELECTRIC VINYLIDENE FLUORIDE-TRIFLUOROETHYLENE COPOLYMERS*. Journal of Applied Physics, 1987. **62**(3): p. 994-997.
24. Lovinger, A.J., *POLYMORPHIC TRANSFORMATIONS IN FERROELECTRIC COPOLYMERS OF VINYLIDENE FLUORIDE INDUCED BY ELECTRON-IRRADIATION*. Macromolecules, 1985. **18**(5): p. 910-918.
25. Zhang, Q.M., V. Bharti, and X. Zhao, *Giant electrostriction and relaxor ferroelectric behavior in electron-irradiated poly(vinylidene fluoride-trifluoroethylene) copolymer*. Science, 1998. **280**(5372): p. 2101-2104.
26. Ameduri, B., *From Vinylidene Fluoride (VDF) to the Applications of VDF-Containing Polymers and Copolymers: Recent Developments and Future Trends*. Chemical Reviews, 2009. **109**(12): p. 6632-6686.
27. Taguet, A., B. Ameduri, and B. Boutevin, *Crosslinking of vinylidene fluoride-containing fluoropolymers*, in *Crosslinking in Materials Science*, B. Ameduri, Editor. 2005, Springer-Verlag Berlin: Berlin. p. 127-211.
28. Logothetis, A.L., *CHEMISTRY OF FLUOROCARBON ELASTOMERS*. Progress in Polymer Science, 1989. **14**(2): p. 251-296.
29. Schmiegel, W.W. and A.L. Logothetis, *CURING OF VINYLIDENE FLUORIDE-BASED FLUOROELASTOMERS*. Abstracts of Papers of the American Chemical Society, 1983. **186**(AUG): p. 49-MACR.
30. Pruett, R.L., et al., *REACTIONS OF POLYFLUORO OLEFINS .2. REACTIONS WITH PRIMARY AND SECONDARY AMINES*. Journal of the American Chemical Society, 1950. **72**(8): p. 3646-3650.
31. Paciorek, K.L., L.C. Mitchell, and C.T. Lenk, *MECHANISM OF AMINE CROSSLINKING OF FLUOROELASTOMERS .1. SOLUTION STUDIES*. Journal of Polymer Science, 1960. **45**(146): p. 405-413.
32. Kojima, G. and H. Wachi, *VULCANIZATION OF A FLUOROELASTOMER DERIVED FROM TETRAFLUOROETHYLENE AND PROPYLENE*. Rubber Chemistry and Technology, 1978. **51**(5): p. 940-947.

33. Finlay, J.B., A. Hallenbeck, and J.D. Maclachlan, *PEROXIDE-CURABLE FLUOROELASTOMERS*. Journal of Elastomers and Plastics, 1978. **10**(1): p. 3-16.
34. Ameduri, B., et al., *Synthesis and polymerization of fluorinated monomers bearing a reactive lateral group. 9. Bulk copolymerization of vinylidene fluoride with 4,5,5-trifluoro-4-ene pentyl acetate*. Macromolecules, 1999. **32**(14): p. 4544-4550.
35. Lovinger, A.J., *RADIATION EFFECTS ON THE STRUCTURE AND PROPERTIES OF POLY(VINYLLIDENE FLUORIDE) AND ITS FERROELECTRIC COPOLYMERS*. Acs Symposium Series, 1991. **475**: p. 84-100.
36. Wang, T.T., *PROPERTIES OF PIEZOELECTRIC POLY (VINYLLIDENE FLUORIDE) FILMS IRRADIATED BY GAMMA-RAYS*. Ferroelectrics, 1982. **41**(1-4): p. 347-357.
37. Dargaville, T.R., M. Celina, and R.L. Clough, *Evaluation of vinylidene fluoride polymers for use in space environments: Comparison of radiation sensitivities*. Radiation Physics and Chemistry, 2006. **75**(3): p. 432-442.
38. Buckley, G.S. and C.M. Roland, *Network structure in poly(vinylidene fluoride-trifluoroethylene) electrostrictive films*. Applied Physics Letters, 2001. **78**(5): p. 622-624.
39. Flory, P.J. and J. Rehner, *Statistical mechanics of cross-linked polymer networks II Swelling*. Journal of Chemical Physics, 1943. **11**(11): p. 521-526.
40. Gregorio, R. and M. Cestari, *EFFECT OF CRYSTALLIZATION TEMPERATURE ON THE CRYSTALLINE PHASE CONTENT AND MORPHOLOGY OF POLY(VINYLLIDENE FLUORIDE)*. Journal of Polymer Science Part B-Polymer Physics, 1994. **32**(5): p. 859-870.
41. Sobhani, H., M. Razavi-Nouri, and A.A. Yousefi, *Effect of flow history on poly(vinylidene fluoride) crystalline phase transformation*. Journal of Applied Polymer Science, 2007. **104**(1): p. 89-94.

42. Kim, K.J., et al., *CURIE TRANSITION, FERROELECTRIC CRYSTAL-STRUCTURE, AND FERROELECTRICITY OF A VDF/TRFE(75/25) COPOLYMER .1. THE EFFECT OF THE CONSECUTIVE ANNEALING IN THE FERROELECTRIC STATE ON CURIE TRANSITION AND FERROELECTRIC CRYSTAL-STRUCTURE*. Journal of Polymer Science Part B-Polymer Physics, 1994. **32**(15): p. 2435-2444.
43. Eberle, G., H. Schmidt, and W. Eisenmenger, *Piezoelectric polymer electrets*. Dielectrics and Electrical Insulation, IEEE Transactions on, 1996. **3**(5): p. 624-646.
44. Xia, F. and Q.M. Zhang, *Schottky emission at the metal polymer interface and its effect on the polarization switching of ferroelectric poly(vinylidene fluoride-trifluoroethylene) copolymer thin films*. Applied Physics Letters, 2004. **85**(10): p. 1719-1721.
45. Fothergill, L.A.D.a.J.C., *Electrical degradation and breakdown in polymers*. 1992.
46. Stark, K.H. and C.G. Garton, *ELECTRIC STRENGTH OF IRRADIATED POLYTHENE*. Nature, 1955. **176**(4495): p. 1225-1226.
47. Benderly, A.A. and Bernstei.Bs, *RADIATION-CROSSLINKED POLYPROPYLENE - PHYSICAL AND DIELECTRIC PROPERTIES*. Journal of Applied Polymer Science, 1969. **13**(3): p. 505-&.
48. Jacobs, F. (2005) *PP for Film Capacitors: Origin, Manufacturing and Processing*.

VITA

Paisan Khanchaitit

Paisan Khanchaitit was raised in Chaing Mail, Thailand. He moved to Bangkok, to attend Kasetsart University where he graduated with his B.Eng (Chemical Engineering) in 1995. Upon graduation he decided to continue his study on his beloved field, polymer science, at the Chulalongkorn University in Bangkok. In 2001 he received a scholarship from Japanese government to joined the Short Term Exchange Program (STEP) to do a research in electroluminescence property of semiconductor polymers. He received his MS in 2004. In 2006 he again received a national scholarship to pursue his PhD study in United States. He then joined the Materials Science and Engineering department, graduate school at the Pennsylvania State University in University Park. He completed his PhD in spring semester 2012, during the tragic story on Joe Paterno. After his marathon studying, he plans on joining the National Nanotechnology Center in Thailand.